

**THREE DEGREE OF FREEDOM WHEELCHAIR MOUNTED ROBOTIC ARM  
EXOSKELETON**

---

A Thesis

Presented to the

Faculty of

San Diego State University

---

In Partial Fulfillment

of the Requirements for the Degree

Master of Science

in

Mechanical Engineering

---

by

Allen Goltiao Tan

Summer 2015

# **SAN DIEGO STATE UNIVERSITY**

The Undersigned Faculty Committee Approves the  
Thesis of Allen Goltiao Tan:

Three Degree of Freedom Wheelchair Mounted Robotic Arm Exoskeleton

---

Kee Moon, Chair  
Department of Mechanical Engineering

---

Samuel Kassegne  
Department of Mechanical Engineering

---

Yusef Ozturk  
Department of Electrical Engineering

---

Approval Date

Copyright © 2015

by

Allen Goltiao Tan

## **DEDICATION**

This thesis is dedicated to my parents, whose love and hard work have catapulted me to  
unforeseen heights.

## ABSTRACT OF THE THESIS

Three Degree of Freedom Wheelchair Mounted Robotic Arm Exoskeleton  
by  
Allen Goltiao Tan  
Master of Science in Mechanical Engineering  
San Diego State University, 2015

Wearable robots are devices that can improve the quality of life for its users. The particular wearable robot covered in this thesis is an orthotic robot in the form of an upper-limb exoskeleton that will be mounted onto a wheelchair. The robot consists of three ROBOTIS Dynamixel actuators, which have a built-in microcontroller. The microcontroller allows for position feedback, load information, and an inbuilt proportional-integral-derivative (PID) controller. The motivation for the research is to design a lightweight robotic arm. The possibility of such a device is explored with the inclusion of a constant force spring to compensate for gravity. In addition, with the motor's ability to provide load information, this thesis will explore how well the built-in features of the actuator help determine user intent.

## TABLE OF CONTENTS

	PAGE
ABSTRACT .....	v
LIST OF TABLES.....	x
LIST OF FIGURES .....	xi
ACKNOWLEDGMENTS .....	xv
<b>CHAPTER</b>	
1 INTRODUCTION .....	1
2 BACKGROUND AND LITERATURE REVIEW .....	3
2.1 Robots .....	3
2.1.1 Definition of Robot .....	3
2.1.2 History of Robots .....	3
2.2 Wearable Robots .....	5
2.2.1 Example of Empowering Robotic Exoskeleton: HAL .....	5
2.2.2 Example of Orthotic Robot: ARMin .....	6
2.2.3 Example of Prosthetic Robot: DEKA Arm.....	8
3 THEORY .....	10
3.1 Matrix Transformation.....	10
3.1.1 Translation .....	11
3.1.2 Rotation .....	11
3.1.3 Multiple Transformations .....	12
3.2 Forward Kinematics.....	12
3.2.1 Denavit-Hartenberg.....	12
3.2.2 Modified Denavit-Hartenberg .....	14
3.3 Inverse Kinematics .....	17
3.4 Trajectory Planning .....	17
3.4.1 Definition of Trajectory .....	17
3.4.2 Joint-Space.....	18
3.4.3 Cartesian-Space.....	19
3.4.4 Difference Between Joint-Space and Cartesian-Space.....	20

3.5	Robot Jacobian .....	20
3.5.1	Types of Joints .....	20
3.5.2	Velocity for a Single Joint.....	20
3.5.3	Velocity for Two Joints .....	21
3.5.4	Linear Velocity Jacobian .....	21
3.5.5	Angular Velocity Jacobian .....	23
3.5.6	Inverting the Jacobian .....	23
3.5.7	Singularities.....	23
3.6	Static Force .....	23
3.7	Dynamics .....	25
3.8	Lagrangian.....	25
3.8.1	Mass Matrix.....	26
3.8.2	Centrifugal and Coriolis Forces.....	28
3.8.3	Gravity Forces .....	30
4	EQUIPMENT .....	31
4.1	Dynamixel Motor .....	31
4.1.1	Description.....	31
4.1.2	Wiring .....	32
4.1.3	Limitations .....	34
4.2	Delsys Trigno.....	36
5	DESIGN .....	39
5.1	Robotic Arm Exoskeleton Frame.....	39
5.1.1	Base .....	40
5.1.2	Link 1 .....	40
5.1.3	Link 2 .....	43
5.1.4	Link 3 .....	45
5.1.5	Hysteresis .....	47
5.2	Safety .....	49
5.3	Upper-Limb Motion.....	51
6	KINEMATIC MODELING .....	54
6.1	Modified Denavit-Hartenberg .....	54
6.1.1	Link 1 .....	54

6.1.2	Link 2 .....	55
6.1.3	Link 3 .....	56
6.1.4	End-Effector .....	57
6.2	Workspace .....	57
7	DYNAMIC MODELING .....	59
7.1	Truncated Notation .....	59
7.2	Location of Center of Mass .....	59
7.2.1	Velocity at Link Center of Mass .....	59
7.3	Kinetic Energy .....	60
7.3.1	Joint 1 .....	60
7.3.2	Joint 2 .....	62
7.3.3	Joint 3 .....	65
7.3.4	Total Kinetic Energy .....	69
7.4	Potential Energy .....	69
7.5	Lagrangian .....	70
7.6	General Joint Torque .....	70
7.7	Joint 1 Torque .....	71
7.8	Joint 2 Torque .....	73
7.9	Joint 3 Torque .....	74
8	PID CONTROLLER .....	77
8.1	Linearization and State-Space .....	77
8.2	Verification of Linear Model .....	79
8.2.1	Joint 2 Released from Non-Equilibrium Position .....	79
8.2.2	Joint 3 Released from Non-Equilibrium Position .....	81
8.3	Individual PID Controller .....	82
9	GRAVITY COMPENSATION .....	88
9.1	No Compensation .....	88
9.2	Constant Force Spring .....	90
10	DETERMINATION OF USER INTENT .....	94
10.1	Torque Feedback .....	94
10.2	Electromyography Feedback .....	100
11	CONCLUSION .....	106

12 FUTURE WORK .....	107
REFERENCES .....	108

## LIST OF TABLES

	PAGE
Table 4.1. MX-64R Specs.....	32
Table 4.2. Delsys Trigno Features .....	37
Table 5.1. Bill of Materials and Weight Comparison for Link 1 .....	41
Table 5.2. Center of Mass for Link 1 .....	42
Table 5.3. Moment of Inertia Tensor About Axis of Rotation for Link 1.....	43
Table 5.4. Bill of Materials and Weight Comparison for Link 2 .....	43
Table 5.5. Center of Mass for Link 2 .....	45
Table 5.6. Moment of Inertia Tensor About Axis of Rotation for Link 2.....	45
Table 5.7. Bill of Materials and Weight Comparison for Link 3 .....	45
Table 5.8. Center of Mass for Link 3 .....	47
Table 5.9. Moment of Inertia Tensor About Axis of Rotation for Link 3.....	47
Table 5.10. Physical Range of Joints .....	51
Table 6.1. Modified DH Link Parameters for Robotic Arm .....	54
Table 8.1. Characteristics of Motor 1 Response .....	84
Table 8.2. Characteristics of Motor 2 Response .....	85
Table 8.3. Characteristics of Motor 3 Response .....	86
Table 9.1. Properties of Upper Arm .....	89
Table 9.2. Properties of Forearm and Hand .....	89
Table 10.1. Center of Mass of Link 2 for 2DOF Configuration.....	97

## LIST OF FIGURES

	PAGE
Figure 2.1. Three different paths between point 'A' and point 'B'.....	4
Figure 2.2. The items of a cam mechanism. ....	5
Figure 2.3. Unimate in General Motors factory. ....	6
Figure 2.4. Orthotic vs prosthetic robots: top left - upper-limb orthotic; top right - upper-limb prosthetic; bottom left - lower-limb orthotic; bottom right - lower-limb prosthetic. ....	7
Figure 2.5. Dr. Sankai with HAL. ....	8
Figure 2.6. User in wheelchair with ARMin II. ....	9
Figure 2.7. Man using DEKA arm to drink water. ....	9
Figure 3.1. Vector in 3D coordinate system. ....	10
Figure 3.2. Denavit-Hartenberg parameters. ....	13
Figure 3.3. Modified Denavit-Hartenberg parameters. ....	15
Figure 3.4. First link in modified Denavit-Hartenberg notation. ....	16
Figure 3.5. Depiction of a revolute and a prismatic joint. ....	20
Figure 3.6. Virtual work principal for a manipulator. ....	24
Figure 3.7. Kinetic energy of link $i$ . ....	26
Figure 4.1. MX-64R actuator. ....	31
Figure 4.2. Daisy-chain link of Dynamixel motors connected to a controller. ....	33
Figure 4.3. Two sets of 4-Pin connectors on MX-64 motor. ....	33
Figure 4.4. Matching pins on multiple MX-64 motors. ....	34
Figure 4.5. Error in position due to gear backlash. ....	35
Figure 4.6. Delsys Trigno wireless EMG system. ....	36
Figure 4.7. Trigno sensor placement. ....	37
Figure 4.8. Trigno EMG detection. ....	38
Figure 5.1. Annotated robotic arm CAD model. ....	39
Figure 5.2. CAD model of base. ....	40
Figure 5.3. CAD model of link 1. ....	41
Figure 5.4. X-Y axes for link 1. ....	42

Figure 5.5. X-Z axes for link 1.....	42
Figure 5.6. CAD model of link 2. ....	44
Figure 5.7. X-Y axes for link 2. ....	44
Figure 5.8. X-Z axes for link 2.....	44
Figure 5.9. CAD model of link 3. ....	46
Figure 5.10. X-Y axes for link 3. ....	46
Figure 5.11. X-Z axes for link 3. ....	46
Figure 5.12. Hysteresis of position error for motor 2. ....	48
Figure 5.13. Hysteresis of position error for motor 3. ....	49
Figure 5.14. Robotic arm attached to wheelchair with user. ....	50
Figure 5.15. Arm motion due to motor 1: shoulder horizontal extension and shoulder horizontal flexion.....	51
Figure 5.16. Arm motion due to motor 2: shoulder vertical extension and shoulder vertical flexion.....	52
Figure 5.17. Arm motion due to motor 3: elbow extension and elbow flexion. ....	53
Figure 6.1. Joint 1 angle.....	54
Figure 6.2. Joint 2 and joint 3 angles. ....	54
Figure 6.3. End-effector workspace in XY plane. ....	58
Figure 6.4. End-effector workspace in XZ plane.....	58
Figure 8.1. Response of joint 1 due to a non-equilibrium initial joint 2 angle of 5 degrees.	79
Figure 8.2. Response of joint 1 due to a non-equilibrium initial joint 2 angle of 10 degrees.....	79
Figure 8.3. Response of joint 2 due to a non-equilibrium initial joint 2 angle of 5 degrees.	80
Figure 8.4. Response of joint 2 due to a non-equilibrium initial joint 2 angle of 10 degrees.....	80
Figure 8.5. Response of joint 3 due to a non-equilibrium initial joint 2 angle of 5 degrees.	80
Figure 8.6. Response of joint 3 due to a non-equilibrium initial joint 2 angle of 10 degrees.....	80
Figure 8.7. Response of joint 1 due to a non-equilibrium initial joint 3 angle of 5 degrees.	81
Figure 8.8. Response of joint 1 due to a non-equilibrium initial joint 3 angle of 10 degrees.....	81
Figure 8.9. Response of joint 2 due to a non-equilibrium initial joint 3 angle of 5 degrees.	82
Figure 8.10. Response of joint 2 due to a non-equilibrium initial joint 3 angle of 10 degrees.....	82

Figure 8.11. Response of joint 3 due to a non-equilibrium initial joint 3 angle of 5 degrees. ....	82
Figure 8.12. Response of joint 3 due to a non-equilibrium initial joint 3 angle of 10 degrees. ....	82
Figure 8.13. Block diagram of PID controller. ....	83
Figure 8.14. Comparison of theoretical response and actual response for motor 1. ....	84
Figure 8.15. Comparison of theoretical response and actual response for motor 2. ....	85
Figure 8.16. Comparison of theoretical response and actual response for motor 3. ....	86
Figure 9.1. Free body diagram about joint 2 for a static position. ....	88
Figure 9.2. Static joint 2 torque with no limb. Area highlighted in yellow shows recommended torque range for motor. ....	90
Figure 9.3. Side view and front view of robotic arm with constant force spring attached. ....	90
Figure 9.4. Free body diagram about joint 2 for a static position with a constant force spring applied along link 2. ....	91
Figure 9.5. Static joint 2 torque with no limb for various constant force springs. Area highlighted in yellow shows recommended torque range for motor. ....	92
Figure 9.6. Static joint 2 torque with limb for joint 3 angle fixed at zero. Area highlighted in yellow shows recommended torque range for motor. ....	93
Figure 9.7. Static joint 2 torque with limb for joint 2 angle fixed at zero. Area highlighted in yellow shows recommended torque range for motor. ....	93
Figure 10.1. Torque sensor calibration. ....	94
Figure 10.2. Model of 2DOF system. ....	95
Figure 10.3. Comparison of theoretical joint torque and actual joint torque for motor 1. ....	98
Figure 10.4. Comparison of theoretical joint torque and actual joint torque for motor 2. ....	99
Figure 10.5. Load information compared to position error for motor 1. ....	99
Figure 10.6. Load information compared to position error for motor 2. ....	100
Figure 10.7. Wrist flexion. ....	101
Figure 10.8. Wrist extension. ....	101
Figure 10.9. Electrode placement for flexor carpi ulnaris. ....	102
Figure 10.10. Electrode placement for extensor carpi ulnaris. ....	102
Figure 10.11. Raw EMG of flexor carpi ulnaris and extensor carpi ulnaris muscles during wrist flexion. Area highlighted in yellow is when wrist flexion takes place. ....	103

Figure 10.12. Squared EMG of flexor carpi ulnaris and extensor carpi ulnaris muscles during wrist flexion. Area highlighted in yellow is when wrist flexion takes place. ....	103
Figure 10.13. Raw EMG of flexor carpi ulnaris and extensor carpi ulnaris muscles during wrist extension. Area highlighted in yellow is when wrist extension takes place. ....	105
Figure 10.14. Squared EMG of flexor carpi ulnaris and extensor carpi ulnaris muscles during wrist extension. Area highlighted in yellow is when wrist extension takes place. ....	105

## ACKNOWLEDGMENTS

I would like to thank Dr. Kee Moon for giving me this opportunity to work under his tutelage. I have learned a lot about robotics, and I hope to continue to work in the field in the future.

I would like to also like to thank Dr. Samuel Kassegne and Dr. Yusef Ozturk for helping me along the way, as well as participating in my work by agreeing to be a part of my thesis committee.

I want to thank Dr. Peiman Naseradinmousavi for being patient with me as he went to great lengths to help me understand the Lagrangian, as well as to assist me in deriving the Lagrangian by hand.

I want to thank Dr. Harsimran Baweja for his help with the paper for the 2015 IEEE/RSJ International Conference on Intelligent Robots and Systems. His suggestions and criticisms helped to improve the quality of my thesis.

I would like to thank Mike Lester and Uriel de Luna for taking the time to help machine the components of the robotic arm. Although they were busy, they still found the time to create a quality product.

Finally, I would like to thank Julian Espinoza for his assistance in control theory. Although he was busy with priorities of his own, he always took the time to clarify items I did not understand.

The research was partially funded by grants from the Korea Institute for Advancement of Technology (KIAT) and the Center for Sensorimotor Neural Engineering (CSNE) that is an NSF Engineering Research Center.

## **CHAPTER 1**

### **INTRODUCTION**

Robots have increasingly become ubiquitous throughout society as new applications are found for them. Robots are mainly utilized as a way to improve human lives, where they can be used to reduce the time or effort needed to perform a task, or be used to perform tasks that extend beyond the limits of humans. These tasks include mundane tasks such as vacuuming, to tasks outside the human capability such as lifting heavy objects or exploring new planets. One field in which robotics is gaining traction is healthcare. For the healthcare field, robots fill the need for more healthcare personnel, as well as improve the quality of life for the geriatric, the injured, and the disabled [1].

One way that robots can improve a person's quality of life is to restore functionality to a user's limb, or take the place of a user's missing limb. Robots that fall into this designation can be further classified as either an exoskeleton or as a prosthetic. An exoskeleton is more for users who still have their limb attached, but are unable to make complete use of it due to injury or disease. These circumstances include patients who have experienced stroke, have an injury to their spinal cord, or have muscle dystrophies [2]. A prosthetic on the other hand is for those who are missing limbs, especially amputees. Robotic prosthetics can take a variety of forms, including robotic arms, robotic hands, and robotic feet [3].

This thesis will specifically focus on an orthotic robotic arm exoskeleton that will be attached to an electric wheelchair. The robot is to restore functionality in the user's upper-limb to help that person control the joystick used to move the electric wheelchair. The robotic arm consists of three Robotis Dynamixel actuators, which are capable of providing load information of each individual motor. The goal of the research is to create a lightweight device that is portable such that it can remain attached to the wheelchair at all times, and not be a hindrance to the user. One aspect of creating a lightweight device is the ability to control the robotic arm by using the load information of the motors to determine the user's intended upper-limb motions. This will allow for a portable system that does not require wires or electrodes that run to parts of the user's body. And because there are no straps or harnesses required to secure the user's arm into the device, the user can easily slip in and out of the device, and the user can use the device immediately if need be.

The following is an overview of the thesis, with a brief description of the items covered in each particular chapter:

- Chapter 1 is the introduction to the thesis, and an overview of the importance of the research;
- Chapter 2 is the background and literature review, which will go over the background of robotics and provide examples of wearable robots;
- Chapter 3 goes over theory of robotics mechanics, especially kinematics and dynamics;
- Chapter 4 will explain the equipment, especially the actuators and electromyography system;
- Chapter 5 consists of the design of the robotic arm, going more into depth on the properties of each link, as well as safety consideration and limitations of the robot itself;
- Chapter 6 provides the kinematic modeling of the system;
- Chapter 7 will go into the hand derivation of the Lagrangian, which is used to obtain equations for individual joint torque;
- Chapter 8 will go into the individual PID control of each actuator, and a comparison of the results between the theoretical and the actual response;
- Chapter 9 will go into the results of gravity compensation using a constant force spring;
- Chapter 10 will go over the results determining user intent based on the load information of the motor, and through electromyography biosignals;
- Chapter 11 will be the conclusion, where the results are summarized, and suggestions are made for refinement;
- Chapter 12, the final chapter is where future work is discussed. This includes ways to improve the robot.

## CHAPTER 2

### BACKGROUND AND LITERATURE REVIEW

#### 2.1 ROBOTS

##### 2.1.1 Definition of Robot

**Robot** is a term first introduced in 1920 by Karel Čapek, a Czech writer, in his play *Rossum's Universal Robots (R.U.R.)*. The origin of the word robot comes from the Czech word *robota*, which translates to “serf labor.” In his play, robots are artificial human-like creatures, whose purpose is to serve humans. Today, the definition of a robot goes beyond Čapek’s original intention of the word; a robot is a reprogrammable machine that is able to perform jobs autonomously. For Shimon Nof, these jobs should fall into what he calls the *Three Laws of Robotics Applications* [4]:

1. Jobs that are dangerous should be performed by robots instead of humans;
2. Jobs that humans do not desire to complete should be performed by robots instead of humans;
3. Jobs that can be performed more economically by robots should be performed by robots instead of humans.

These laws illustrate how robots can take on many forms and assist in many ways.

##### 2.1.2 History of Robots

Although the term robot was introduced less than a century ago, the idea of robots have existed much longer. Ancient Greek poet Homer mentions robot-like creatures in the epic *Iliad*, which is estimated to be written around 710-760 BC [5]. In the epic, Homer describes two mechanical handmaidens that are made out of gold. They assist the Greek god of fire, Hephaestus, who is also a master craftsman. Because he has weak legs, Hephaestus relies on the assistance of the handmaidens as he works.

Robots along the vein of Homer’s handmaidens would not be possible for about another 2800 years. Instead, man tried to create autonomous machines in the form of **automatons**. Automatons are similar to robots in that they are autonomous machines, but automatons are much more limited in their performance and function. This is the result of automatons lacking the ability to be reprogrammed. Therefore, each task completed by an automaton has been performed in a certain order or in a particular manner.

Take for example the different paths of an arm attached to an android (automated human) as presented in Figure 2.1.

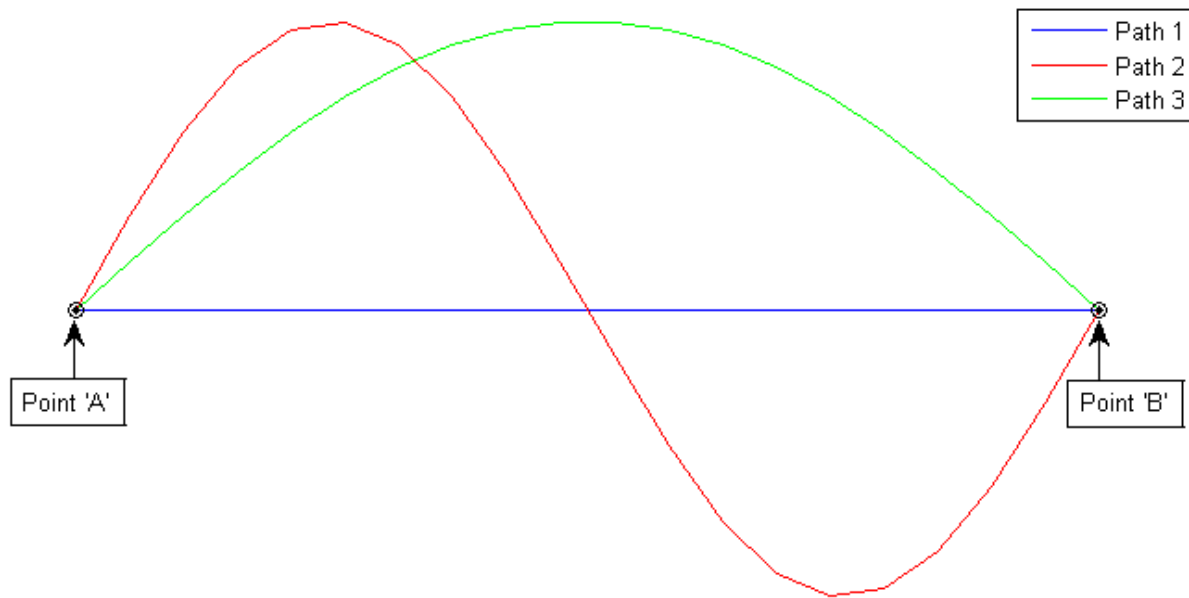


**Figure 2.1. Three different paths between point 'A' and point 'B'.**

A robotic arm could be reprogrammed to traverse between point 'A' and point 'B' through any of the three paths. In fact, there are infinite possibilities in which the robotic arm could travel between those two points. An automaton arm on the other hand, will be designed to travel along a single path between point 'A' and point 'B,' and it will follow along that path only. This is done through the use of *cam mechanisms*, which can be thought of as a mechanical version of computer programming [6]. The following two items make up a cam mechanism:

- cam - contoured device that rotates about a fixed point;
- follower - device (usually a rod) that moves to different positions as it follows the profile of the cam.

The diagram shown in Figure 2.2 shows the cam in red, and the follower in blue. The green circle is the axis of rotation for the cam. As the cam rotates about its axis of rotation, the follower will move up and down as it follows the profile of the cam.

The cam mechanism has provided autonomous movement for many automatons throughout history. Unlike robots, most of the automatons were not very useful as far as performing dangerous tasks, performing dull tasks, or performing tasks more efficiently than humans. Instead, automatons served mainly as entertainment.

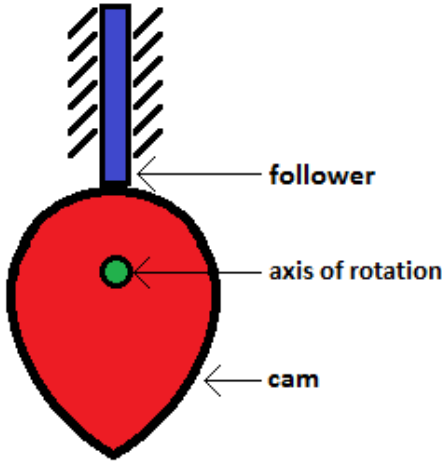


**Figure 2.2. The items of a cam mechanism.**

Robots would not truly exist until the twentieth century. This is the result of three advancements in technology, most of which took place around World War II [7]: servo mechanisms theory, digital computation, and solid state electronics. The first programmable robot was the *Unimate*. It was first used in 1961, in a General Motors plant to handle die castings and weld parts together for automobiles. Figure 2.3 below shows the robot in a General Motors factory. The Unimate follows the first law of robotics applications, in which it is performing a task a little too "dangerous" for humans.

## 2.2 WEARABLE ROBOTS

The primary purpose of wearable robots is to improve the user's abilities, and help the user go beyond what he or she is currently capable of. This could be for healthy users looking to exceed the capabilities of a normal human being, users who have lost function in their limb, or users who have lost their limb completely. This puts wearable robotics into three distinct categories [8]:

- **Empowering Robotic Exoskeletons** where the device serves to go beyond one's physical aptitude;
- **Orthotic Robots** where the device serves to restore function of one's limb;
- **Prosthetic Robots** where the device serves to replace one's limb.

Figure 2.4 demonstrates the difference between an orthotic wearable robot and a prosthetic robot in an upper-limb setting, as well as in a lower-limb setting.

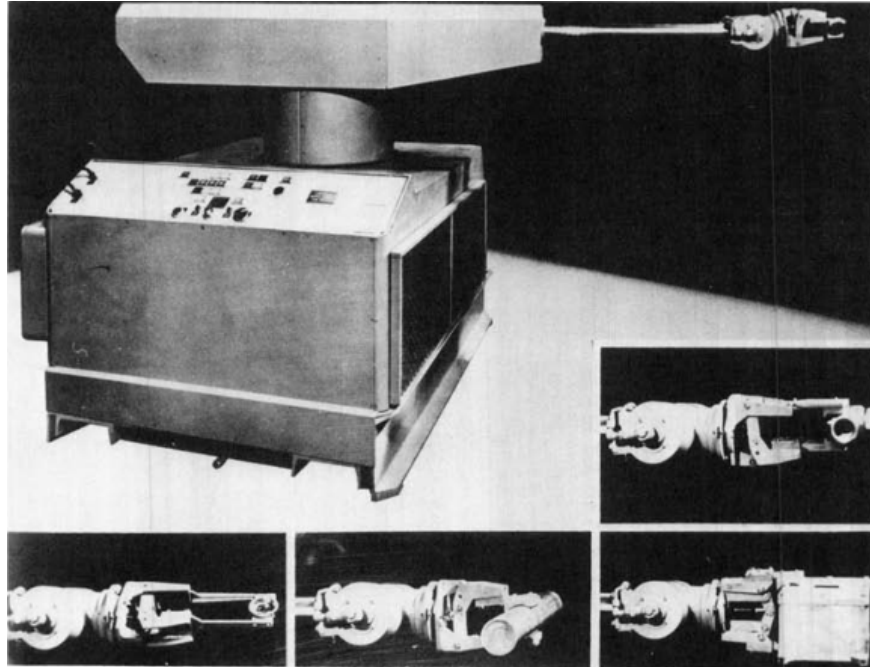


**Figure 2.3. Unimate in General Motors factory.** Source: Engelberger, Joseph F. “Historical Perspective of Industrial Robotics.” In *Handbook of Industrial Robots*, edited by Shimon F. Nof, xvii-xviii. New York: John Wiley & Sons, 1985.

### 2.2.1 Example of Empowering Robotic Exoskeleton: HAL

The HAL-5 is a full-body exoskeleton, which assists the user’s upper extremities, as well as the user’s lower extremities. Figure 2.5 is an image of HAL next to Dr. Yoshiyuki Sankai, the one who originally came up with the idea. He founded the company Cyberdyne, based in Japan.

Depending on the application, the HAL-5 can be classified as either an empowering robotic exoskeleton, or an orthotic robot. The HAL-5 is mainly used to improve the quality of lives for those with reduced functionality in their limbs, in which the exoskeleton can be used to increase mobility, or as a rehabilitation tool [9]. One application of the HAL used as an empowering robotic exoskeleton is to help farmers perform strenuous tasks in the field, such as “uprooting crops, tilling the soil and pruning trees” [3:424]. To control the HAL system, sensors are placed on the user’s skin, in which biosignals are used as input [10].

### 2.2.2 Example of Orthotic Robot: ARMin

ARMin is the creation of the Sensory-Motor Sensors Lab based in Switzerland. The ARMin functions as an orthotic robot as it is used for rehabilitation of the upper extremities for stroke patients. Figure 2.6 is an image of a person sitting in a wheelchair with their right



**Figure 2.4. Orthotic vs prosthetic robots:** top left - upper-limb orthotic; top right - upper-limb prosthetic; bottom left - lower-limb orthotic; bottom right - lower-limb prosthetic. Source: Pons, J.L., Ceres R., and L. Calderon. *Introduction to Wearable Robotics: Biomechatronic Exoskeletons*, edited by J.L. Pons, 1-16. Madrid: John Wiley & Sons, Ltd, 2008.



**Figure 2.5. Dr. Sankai with HAL.** Source: Sankai, Yoshiyuki. “Leading Edge of Cybernics: Robot Suit HAL.” Paper presented at the 2006 SICE-ICASE International Joint Conference, Busan, South Korea, October 18-21, 2006.

upper-limb using the ARMin II. In an older iteration of the ARMin, the exoskeleton was mounted onto a wall, and the user would sit underneath it [11, 12]. Although the ARMin II can be attached to a wheelchair, it is rather bulky for use outside of a lab.

The ARMin hopes to improve the quality of lives for stroke patients. In a study conducted in 1994, 18% of stroke patients with severe weakness in their arm were able to regain function completely [13]. The input for the ARMin II from the user is based on a force/torque sensor. One way that the ARMin II is used for rehabilitation is by giving the user tasks to complete in a virtual environment. These include games, such catching a ball, as well as having the user place an object onto a table in the virtual world using a virtual hand [13].

### 2.2.3 Example of Prosthetic Robot: DEKA Arm

Dean Kamen of DEKA Research and Development Corporation, which is based in New Hampshire, created the DEKA Arm to be a prosthetic robot. The goal of the project was to create a device that could replace functionality of a missing upper-limb for amputees. It is able to handle delicate items such as grapes, as well as items that require more strength and grip, such as a hand drill [14]. The DEKA Arm incorporates multiple input sources, including inertial measurement units (IMUs) placed on the foot, and electromyogram signals read from the user’s skin [15]. Figure 2.7 shows a man using the DEKA Arm to drink from a bottle of water.



**Figure 2.6. User in wheelchair with ARMin II.**  
Source: T. Nef et al., “ARMin - Exoskeleton for Arm Therapy in Stroke Patients.” Paper presented at the 10th International Conference on Rehabilitation Robotics, Noordwijk, Netherlands, June 13-15, 2007.



**Figure 2.7. Man using DEKA arm to drink water.** Source: DEKA Research and Development Corporation. “The DEKA Arm.” Accessed April 7, 2015. [http://www.dekaresearch.com/deka\\_arm.shtml](http://www.dekaresearch.com/deka_arm.shtml).

## CHAPTER 3

### THEORY

#### 3.1 MATRIX TRANSFORMATION

A general vector in 3d space will have x, y, and z components. Figure 3.1 shows a general vector  $\vec{p}$  going from the origin to a point in space.

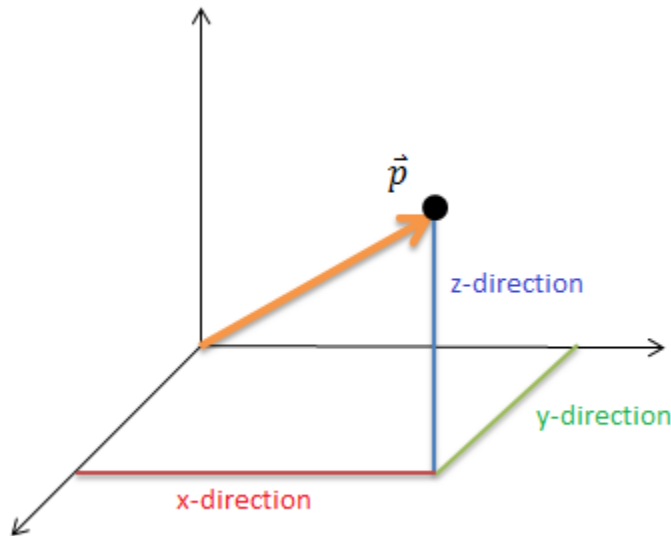


**Figure 3.1. Vector in 3D coordinate system.**

Vector  $\vec{p}$  can be expressed as follows:

$$\vec{p} = p_x \mathbf{i} + p_y \mathbf{j} + p_z \mathbf{k} = \begin{Bmatrix} p_x \\ p_y \\ p_z \end{Bmatrix}. \quad (3.1)$$

Furthermore, a fourth row may be added using term  $w$  for the scale factor:

$$\vec{p} = \begin{Bmatrix} p_x \\ p_y \\ p_z \\ w \end{Bmatrix}. \quad (3.2)$$

### 3.1.1 Translation

If we want to move the vector to another point in the same coordinate system, we can multiply the  $\vec{p}$  vector by a transformation matrix to find the new vector. The transformation matrix that we will use is the **Translation Transformation Matrix**:

$$\text{Translation Transformation Matrix} = [T] = \begin{bmatrix} 1 & 0 & 0 & d_x \\ 0 & 1 & 0 & d_y \\ 0 & 0 & 1 & d_z \\ 0 & 0 & 0 & 1 \end{bmatrix}. \quad (3.3)$$

The first three rows and columns of the matrix are a 3x3 Identity Matrix. The last column of the Translation Transformation Matrix is the value that the vector will shift in the x, y and z directions.

Applying the Translation Transformation Matrix to vector  $\vec{p}$  (with a scale factor  $w = 1$ ) to find vector  $\vec{p}_{new}$  will result in the following:

$$\vec{p}_{new} = [T]\vec{p} = \begin{bmatrix} 1 & 0 & 0 & d_x \\ 0 & 1 & 0 & d_y \\ 0 & 0 & 1 & d_z \\ 0 & 0 & 0 & 1 \end{bmatrix} \begin{Bmatrix} p_x \\ p_y \\ p_z \\ 1 \end{Bmatrix} = \begin{Bmatrix} p_x + d_x \\ p_y + d_y \\ p_z + d_z \\ 1 \end{Bmatrix}. \quad (3.4)$$

### 3.1.2 Rotation

Similarly, for rotations there are **Rotation Transformation Matrices**. However, because rotation can occur about three different axes, there are three different equations in the x, y and z direction:

$$\text{Rotation Transformation Matrix about } x\text{-axis} = [R_x] = \begin{bmatrix} 1 & 0 & 0 & 0 \\ 0 & \cos \theta & -\sin \theta & 0 \\ 0 & \sin \theta & \cos \theta & 0 \\ 0 & 0 & 0 & 1 \end{bmatrix}, \quad (3.5)$$

$$\text{Rotation Transformation Matrix about } y\text{-axis} = [R_y] = \begin{bmatrix} \cos \theta & 0 & \sin \theta & 0 \\ 0 & 1 & 0 & 0 \\ -\sin \theta & 0 & \cos \theta & 0 \\ 0 & 0 & 0 & 1 \end{bmatrix}, \quad (3.6)$$

$$\text{Rotation Transformation Matrix about } z\text{-axis} = [R_z] = \begin{bmatrix} \cos \theta & -\sin \theta & 0 & 0 \\ \sin \theta & \cos \theta & 0 & 0 \\ 0 & 0 & 1 & 0 \\ 0 & 0 & 0 & 1 \end{bmatrix}. \quad (3.7)$$

A general form of using the Rotation Transformation Matrix is as follows:

$$\vec{p}_{new} = [R]\vec{p}. \quad (3.8)$$

### 3.1.3 Multiple Transformations

If multiple transformations take place for vector, then the order of Matrix Multiplication goes from right to left:

$$\vec{p}_{new} = [\text{Transformation n}][\text{Transformation n-1}] \dots [\text{Transformation 1}] \vec{p}. \quad (3.9)$$

This is because the first transformation will be applied to the vector, changing it to a new one. The second transformation will then be applied to that modified vector, and so on.

## 3.2 FORWARD KINEMATICS

**Kinematics** allows us to relate the joint positions with the position and orientation of the end-effector [16]. **Forward kinematics**, or direct kinematics, is used to solve for the position of the end-effector by knowing the properties of the robot's joints. A **joint** refers to a degree-of-freedom (DOF) in a robot, which is usually a motor. Joints are connected by rigid segments called **links**. The **end-effector** is the tool necessary for a robot to complete its task and it is placed on the final link, or *end*, of a robot [17]. Another way to think of how forward kinematics works is to look at how it applies to a complete robot configuration: you start from the base, and you continue *forward* until you reach the end-effector.

### 3.2.1 Denavit-Hartenberg

The **Denavit-Hartenberg (DH)** matrix transformation is one way to do forward kinematics. It takes the joint parameters between two links to find the position of the second link relative to the first link. The link parameters used in Denavit-Hartenberg are as follows [17]:

- $\alpha_i$  - angle of rotation needed about the  $x_i$ -axis to make the  $z_{i-1}$ -axis parallel to the  $z_i$ -axis;
- $a_i$  - displacement along the  $x_i$ -axis between the  $z_{i-1}$  and  $z_i$ -axes;

- $\theta_i$  - angle of rotation needed about the  $z_{i-1}$ -axis to make the  $x_{i-1}$ -axis parallel to the  $x_i$ -axis;
- $d_i$  - displacement along the  $z_{i-1}$ -axis between the  $x_{i-1}$  and  $x_i$ -axes.

Figure 3.2 shows the parameters in relation to two different joints connected by a link.

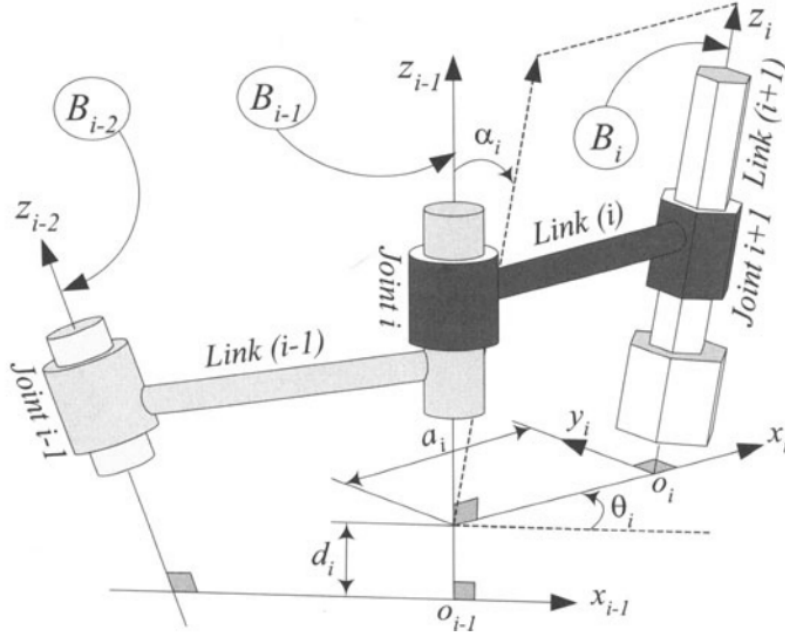


**Figure 3.2. Denavit-Hartenberg parameters. Source: Jazar, Reza. *Theory of Applied Robotics: Kinematics, Dynamics and Control*. New York: Springer, 2010.**

There are four steps to move the second joint's coordinate system to the first joint:

1. Use matrix transformation  $R_{x_{i-1},\alpha_i}$  to do a rotation about the  $x_i$ -axis to make  $z_i$ -axis parallel to  $z_{i-1}$ -axis:

$$R_{x_{i-1},\alpha_i} = \begin{bmatrix} 1 & 0 & 0 & 0 \\ 0 & \cos \alpha_i & -\sin \alpha_i & 0 \\ 0 & \sin \alpha_i & \cos \alpha_i & 0 \\ 0 & 0 & 0 & 1 \end{bmatrix}. \quad (3.10)$$

2. Use matrix transformation  $D_{x_{i-1},a_i}$  to do a translation about the  $x_i$ -axis to make  $z_i$ -axis collinear with  $z_{i-1}$ -axis:

$$D_{x_{i-1},a_i} = \begin{bmatrix} 1 & 0 & 0 & a_i \\ 0 & 1 & 0 & 0 \\ 0 & 0 & 1 & 0 \\ 0 & 0 & 0 & 1 \end{bmatrix}. \quad (3.11)$$

3. Use matrix transformation  $R_{z_{i-1},\theta_i}$  to do a rotation about the  $z_i$ -axis to make  $x_i$ -axis parallel to  $x_{i-1}$ -axis:

$$R_{z_{i-1},\theta_i} = \begin{bmatrix} \cos \theta_i & -\sin \theta_i & 0 & 0 \\ \sin \theta_i & \cos \theta_i & 0 & 0 \\ 0 & 0 & 1 & 0 \\ 0 & 0 & 0 & 1 \end{bmatrix}. \quad (3.12)$$

4. Use matrix transformation  $D_{x_{i-1},d_i}$  to do a translation about the  $z_i$ -axis to make  $x_i$ -axis collinear with  $x_{i-1}$ -axis:

$$D_{x_{i-1},a_i} = \begin{bmatrix} 1 & 0 & 0 & 0 \\ 0 & 1 & 0 & 0 \\ 0 & 0 & 1 & d_i \\ 0 & 0 & 0 & 1 \end{bmatrix}. \quad (3.13)$$

Putting all the matrices for the four steps together yields the following equation [17]:

$${}^{i-1}T_i = D_{x_{i-1},d_i} R_{z_{i-1},\theta_i} D_{x_{i-1},a_i} R_{x_{i-1},\alpha_i} = \begin{bmatrix} \cos \theta_i & -\sin \theta_i \cos \alpha_i & \sin \theta_i \sin \alpha_i & a_i \cos \theta_i \\ \sin \theta_i & \cos \theta_i \cos \alpha_i & -\cos \theta_i \sin \alpha_i & a_i \sin \theta_i \\ 0 & \sin \alpha_i & \cos \alpha_i & d_i \\ 0 & 0 & 0 & 1 \end{bmatrix}. \quad (3.14)$$

In general, to find the position vector of a point on a rigid body relative to the global, or base, coordinate system, the equation is as follows [17]:

$${}^0r_p = {}^0T_B {}^n r_p. \quad (3.15)$$

${}^0T_B$  can also be expanded if there are multiple links and joints [17]:

$${}^0T_B = {}^0T_1(q_1) {}^1T_2(q_2) {}^2T_3(q_3) \dots {}^{n-1}T_n(q_n). \quad (3.16)$$

### 3.2.2 Modified Denavit-Hartenberg

The **Modified Denavit-Hartenberg** is another method for computing forward kinematics. The link parameters used in the Modified Denavit-Hartenberg are as follows:

- $\alpha_i$  - angle of rotation needed about the  $x_i$ -axis to make the  $z_i$ -axis parallel to the  $z_{i+1}$ -axis;
- $a_i$  - displacement along the  $x_i$ -axis between the  $z_i$  and  $z_{i+1}$ -axes;
- $\theta_i$  - angle of rotation needed about the  $z_i$ -axis to make the  $x_{i-1}$ -axis parallel to the  $x_i$ -axis;
- $d_i$  - displacement along the  $z_i$ -axis between the  $x_{i-1}$  and  $x_i$ -axes.

Figure 3.3 shows the parameters in relation to two different joints connected by a link for the Modified Denavit-Hartenberg notation.

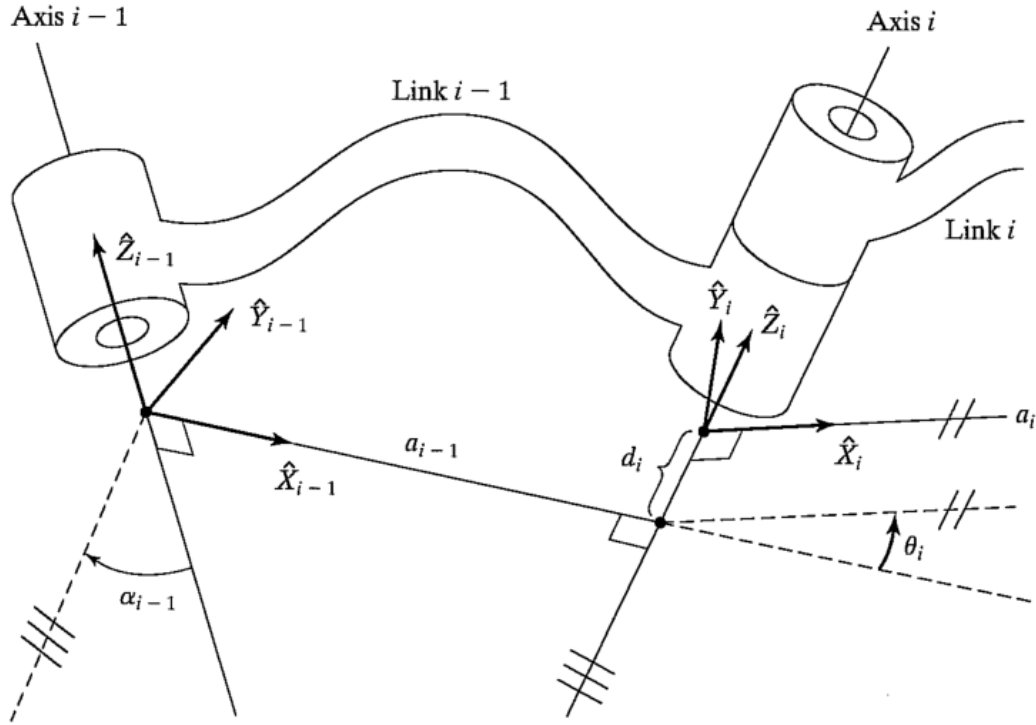


**Figure 3.3. Modified Denavit-Hartenberg parameters.** Source: Craig, John J. *Introduction to Robotics: Mechanics and Control*. 3rd ed. Upper Saddle River: Prentice Hall, 2004.

Further explanation of the Modified Denavit-Hartenberg can be found in John J. Craig's *Introduction to Robotics: Mechanics and Control* [18]. The  ${}^{i-1}T_i$  notation for the Modified Denavit-Hartenberg can be written in the following form [18]:

$${}^{i-1}T_i = R_{x_i, \alpha_{i-1}} D_{x_i, a_{i-1}} R_{z_i, \theta_i} D_{z_i, d_i} = \begin{bmatrix} \cos \theta_i & -\sin \theta_i & 0 & a_{i-1} \\ \sin \theta_i \cos \alpha_{i-1} & \cos \theta_i \cos \alpha_{i-1} & -\sin \alpha_{i-1} & -\sin \alpha_{i-1} d_i \\ \sin \theta_i \sin \alpha_{i-1} & \cos \theta_i \sin \alpha_{i-1} & \cos \alpha_{i-1} & \cos \alpha_{i-1} d_i \\ 0 & 0 & 0 & 1 \end{bmatrix}. \quad (3.17)$$

As with the original Denavit-Hartenberg method, Equations (3.15) and (3.16) are still applicable to the Modified Denavit-Hartenberg method.

### 3.2.2.1 DIFFERENCES BETWEEN ORIGINAL AND MODIFIED DENAVIT-HARTENBERG

The main differences between the two forward kinematic notations are the locations of the axes' coordinate systems, or frames. For the Original Denavit-Hartenberg, there exists only one frame at the first joint, and that frame is fixed. This frame is often referred to as the global frame (*frame 0*). The subsequent joints are the locations of the remaining frames, where the final frame exists at the end-effector. In other words, joint  $i$  will have frame  $i-1$ .

For the Modified Denavit-Hartenberg however, two frames exist at the first joint: the fixed global frame (*frame 0*), and a frame corresponding to the movement of the joint (*frame 1*). Figure 3.4 shows the first link in this notation for a revolute and a prismatic joint. For more information on joints, please refer to section 3.5.1.

### First Link

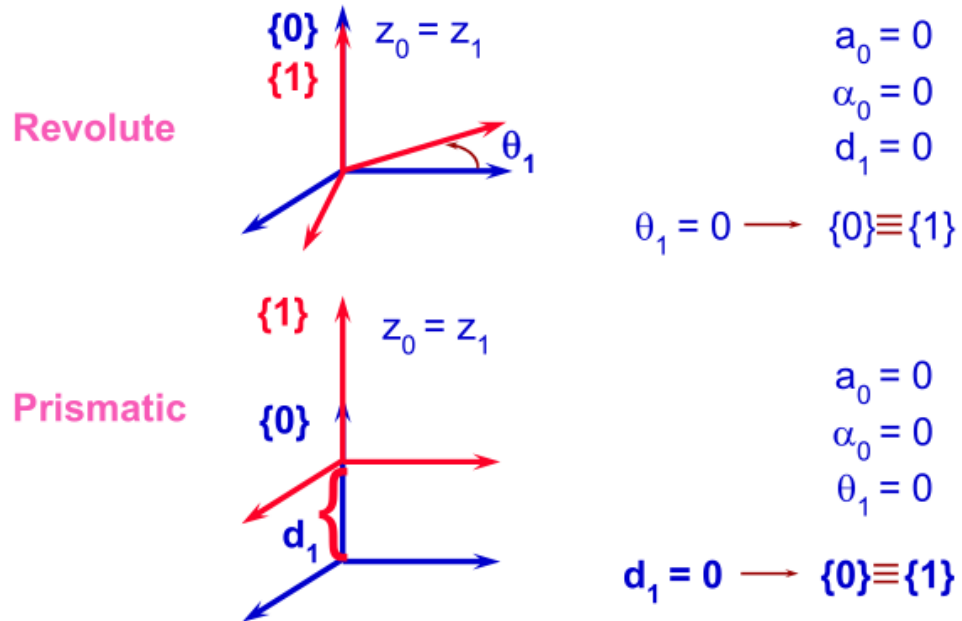


**Figure 3.4. First link in modified Denavit-Hartenberg notation.** Source: Khatib, Oussama. “Forward Kinematics 1.” Accessed July 1, 2014. [http://cs.stanford.edu/groups/manips/images/stories/teaching/cs223a/handouts/kinematics-2\\_2014.pdf](http://cs.stanford.edu/groups/manips/images/stories/teaching/cs223a/handouts/kinematics-2_2014.pdf).

The origins of *frame 0* and *frame 1* are at the same location, simplifying a few of the parameters to zero [19]. For the Modified Denavit-Hartenberg, there is no frame at the end-effector, as the last frame exists at the location of the last joint. Here, joint  $i$  will have

frame  $i$ . For the remainder of the theory chapter, the equations will be solved using the Modified Denavit-Hartenberg notation in mind.

### 3.3 INVERSE KINEMATICS

**Inverse kinematics** is used to solve for the joint variables with a given end-effector position. Solving an inverse kinematics problem is not as simple as a forward kinematics problem however because of the following reasons [16]:

1. There is not always a *closed-form solution*;
2. There may be *multiple solutions*;
3. There may be *infinite solutions*.

For a six DOF robot, the  ${}^0T_B$  matrix multiplication will become  ${}^0T_6$ , which can be expanded as follows [17]:

$${}^0T_6 = {}^0T_1^{-1} {}^1T_2 {}^2T_3 {}^3T_4 {}^4T_5 {}^5T_6 = \begin{bmatrix} r_{11} & r_{12} & r_{13} & r_{14} \\ r_{21} & r_{22} & r_{23} & r_{24} \\ r_{31} & r_{32} & r_{33} & r_{34} \\ r_{41} & r_{42} & r_{43} & r_{44} \end{bmatrix}. \quad (3.18)$$

The  $r_{ij}$  variables represent unknown elements. To find the joint variables, you slowly eliminate unknowns within  ${}^0T_6$  by performing the following [17]:

$${}^1T_6 = {}^0T_1^{-1} {}^0T_6 \quad (3.19)$$

$${}^2T_6 = {}^1T_2^{-1} {}^1T_1^{-1} {}^0T_6 \quad (3.20)$$

$${}^3T_6 = {}^2T_3^{-1} {}^1T_2^{-1} {}^1T_1^{-1} {}^0T_6 \quad (3.21)$$

$${}^4T_6 = {}^3T_4^{-1} {}^2T_3^{-1} {}^1T_2^{-1} {}^1T_1^{-1} {}^0T_6 \quad (3.22)$$

$${}^5T_6 = {}^4T_5^{-1} {}^3T_4^{-1} {}^2T_3^{-1} {}^1T_2^{-1} {}^1T_1^{-1} {}^0T_6 \quad (3.23)$$

$$I = {}^5T_6^{-1} {}^4T_5^{-1} {}^3T_4^{-1} {}^2T_3^{-1} {}^1T_2^{-1} {}^1T_1^{-1} {}^0T_6 \quad (3.24)$$

### 3.4 TRAJECTORY PLANNING

#### 3.4.1 Definition of Trajectory

In robotics, trajectory planning involves working with a path and a trajectory. A **path** is a collection of all the configurations of a robot as it moves from an initial position to a final position, without any concern for timing [20]. A **trajectory** is also a collection of all the configurations of a robot as it moves from an initial position to a final position, except the timing of each configuration along the path is important.

### 3.4.2 Joint-Space

**Joint-space** relates the robot's motion to its joint values [20]. In other words, the joint values are what drive the position and movement of the robot.

#### 3.4.2.1 THIRD-ORDER POLYNOMIAL

For a third-order polynomial, the known values are the initial location, initial velocity, final position and final velocity. In other words, we know where we are starting and we know where we want to end up. We can use the inverse kinematic equations to find the joint angles of the final position and orientation. Since trajectory is based on time, we have an initial time  $t_i$  for when the joint is at its initial angle  $\theta_i$ . We also have a final time  $t_f$  for when the joint is at its final angle  $\theta_f$ . The joint angle in relation to time can be placed in the following form:

$$\theta(t) = c_0 + c_1 t + c_2 t^2 + c_3 t^3. \quad (3.25)$$

The derivative of the third-order polynomial for the joint angle is

$$\dot{\theta}(t) = c_1 + 2c_2 t + 3c_3 t^2. \quad (3.26)$$

Plugging in the initial time  $t_i$  and final time  $t_f$  yields

$$\theta(t_i) = c_0 + c_1 t_i + c_2 t_i^2 + c_3 t_i^3 \quad (3.27)$$

$$\dot{\theta}(t_i) = c_1 + 2c_2 t_i + 3c_3 t_i^2 \quad (3.28)$$

$$\theta(t_f) = c_0 + c_1 t_f + c_2 t_f^2 + c_3 t_f^3 \quad (3.29)$$

$$\dot{\theta}(t_f) = c_1 + 2c_2 t_f + 3c_3 t_f^2 \quad (3.30)$$

whose matrix form is

$$\begin{Bmatrix} \theta_i \\ \dot{\theta}_i \\ \theta_f \\ \dot{\theta}_f \end{Bmatrix} = \begin{bmatrix} 1 & t_i & t_i^2 & t_i^3 \\ 0 & 1 & 2t_i & 3t_i^2 \\ 1 & t_f & t_f^2 & t_f^3 \\ 0 & 1 & 2t_f & 3t_f^2 \end{bmatrix} \begin{Bmatrix} c_0 \\ c_1 \\ c_2 \\ c_3 \end{Bmatrix} \quad (3.31)$$

#### 3.4.2.2 FIFTH-ORDER POLYNOMIAL

Expanding upon the third-order polynomial, known values also include an initial acceleration and a final acceleration. For a fifth-order polynomial, the joint angle in relation to time can be placed in the following form:

$$\theta(t) = c_0 + c_1 t + c_2 t^2 + c_3 t^3 + c_4 t^4 + c_5 t^5. \quad (3.32)$$

The derivative of the fifth-order polynomial for the joint angle is

$$\dot{\theta}(t) = c_1 + 2c_2t + 3c_3t^2 + 4c_4t^3 + 5c_5t^4. \quad (3.33)$$

The second derivative of the fifth-order polynomial for the joint angle is

$$\ddot{\theta}(t) = 2c_2 + 6c_3t + 12c_4t^2 + 20c_5t^3. \quad (3.34)$$

Plugging in the initial time  $t_i$  and final time  $t_f$  yields:

$$\theta(t_i) = c_0 + c_1t_i + c_2t_i^2 + c_3t_i^3 + c_4t_i^4 + c_5t_i^5 \quad (3.35)$$

$$\dot{\theta}(t_i) = c_1 + 2c_2t_i + 3c_3t_i^2 + 4c_4t_i^3 + 5c_5t_i^4 \quad (3.36)$$

$$\ddot{\theta}(t_i) = 2c_2 + 6c_3t_i + 12c_4t_i^2 + 20c_5t_i^3 \quad (3.37)$$

$$\theta(t_f) = c_0 + c_1t_f + c_2t_f^2 + c_3t_f^3 + c_4t_f^4 + c_5t_f^5 \quad (3.38)$$

$$\dot{\theta}(t_f) = c_1 + 2c_2t_f + 3c_3t_f^2 + 4c_4t_f^3 + 5c_5t_f^4 \quad (3.39)$$

$$\ddot{\theta}(t_f) = 2c_2 + 6c_3t_f + 12c_4t_f^2 + 20c_5t_f^3 \quad (3.40)$$

whose matrix form is

$$\begin{Bmatrix} \theta_i \\ \dot{\theta}_i \\ \ddot{\theta}_i \\ \theta_f \\ \dot{\theta}_f \\ \ddot{\theta}_f \end{Bmatrix} = \begin{bmatrix} 1 & t_i & t_i^2 & t_i^3 & t_i^4 & t_i^5 \\ 0 & 1 & 2t_i & 3t_i^2 & 4t_i^3 & 5t_i^4 \\ 0 & 0 & 2 & 6t_i & 12t_i^2 & 20t_i^3 \\ 1 & t_f & t_f^2 & t_f^3 & t_f^4 & t_f^5 \\ 0 & 1 & 2t_f & 3t_f^2 & 4t_f^3 & 5t_f^4 \\ 0 & 0 & 2 & 6t_f & 12t_f^2 & 20t_f^3 \end{bmatrix} \begin{Bmatrix} c_0 \\ c_1 \\ c_2 \\ c_3 \\ c_4 \\ c_5 \end{Bmatrix}. \quad (3.41)$$

### 3.4.3 Cartesian-Space

Cartesian-space trajectories are planned using the position and orientation of the robot relative to the Cartesian reference frame. Cartesian-space trajectories allow for movements along a straight line. To move in a straight line, the end-effector must travel a path that is divided into small segments between the initial position to the final position. The steps necessary for moving the robot using Cartesian-Space are as follows:

- The robot's inverse kinematic equations are solved for a closed form solution;
- The joint variables are found from the closed form solution;
- The controller is sent commands to move the robot's joints to those calculated variables.

The biggest problem with using a Cartesian-space trajectory is that it requires more computer resources. An advantage to using Cartesian-space trajectory however, is that it "yields a controlled and known path" [20:179]. In other words, we always know the position of the joints and the end-effector.

### 3.4.4 Difference Between Joint-Space and Cartesian-Space

The difference between joint-space and Cartesian-space is how each method solves for the joint values. Joint-space uses polynomial equations to find the joint variables; Cartesian-space on the other hand finds the joint variables through inverse kinematics. In other words, Cartesian-space involves finding a point along a straight line between the initial and final positions, and solving the inverse kinematic equations to find the joint variables necessary to get to that point.

## 3.5 ROBOT JACOBIAN

The Jacobian is a useful tool in robotics for analyzing velocity kinematics and static force. The robot Jacobian, which is a function of joint position, allows us to find a linear relationship between the joint velocity and the end-effector velocity [21].

### 3.5.1 Types of Joints

For robotics, there are mainly two types of joints: **prismatic** and **revolute**. Figure 3.5 provides an illustration of a prismatic and revolute joint.

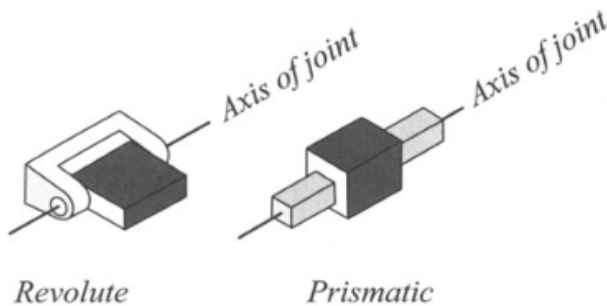


**Figure 3.5. Depiction of a revolute and a prismatic joint.** Source: Jazar, Reza. *Theory of Applied Robotics: Kinematics, Dynamics and Control*. New York: Springer, 2010.

### 3.5.2 Velocity for a Single Joint

#### 3.5.2.1 PRISMATIC JOINT

The linear velocity  $v$  can be defined as follows for a prismatic joint:

$$v = \dot{q}\hat{k}. \quad (3.42)$$

The angular velocity  $\omega$  can be defined as follows for a prismatic joint:

$$\omega = 0. \quad (3.43)$$

### 3.5.2.2 REVOLUTE JOINT

The linear velocity  $v$  can be defined as follows for a revolute joint:

$$v = \dot{q}\hat{k} \times r. \quad (3.44)$$

The angular velocity  $\omega$  can be defined as follows for a revolute joint:

$$\omega = \dot{q}\hat{k}. \quad (3.45)$$

### 3.5.3 Velocity for Two Joints

Using the Jacobian notation in place of  $f(\dot{q}_q, \dot{q}_2, q_1, q_2)$  for  $\begin{Bmatrix} v \\ \omega \end{Bmatrix}$  we get

$$\begin{Bmatrix} v \\ \omega \end{Bmatrix} = J(q_1, q_2) \begin{Bmatrix} \dot{q}_1 \\ \dot{q}_2 \end{Bmatrix} \quad (3.46)$$

where  $J(q_1, q_2)$  is the Jacobian Matrix. The Jacobian can be split into a linear velocity component, and also a angular velocity component.

### 3.5.4 Linear Velocity Jacobian

The term for the linear velocity Jacobian is  $J_v$ , in which the velocity  $v$  can be related to the joint velocity  $\dot{q}$  as follows:

$$v = J_v \dot{q}. \quad (3.47)$$

In general, the linear velocity Jacobian can be thought of as the partial derivation of the end-effector position ( $p_e$ ) with respect to *joint i* as follows:

$$J_v = \left[ \frac{\partial p_e}{\partial q_1} \quad \frac{\partial p_e}{\partial q_2} \quad \dots \quad \frac{\partial p_e}{\partial q_i} \right]. \quad (3.48)$$

The linear Jacobian will be a  $3 \times n$  matrix, in which there are  $n$  columns for  $n$  joints. The full linear Jacobian is then

$$J_v = \begin{bmatrix} J_{v_1} & J_{v_2} & \dots & J_{v_n} \end{bmatrix}. \quad (3.49)$$

### 3.5.4.1 PRISMATIC JOINTS

For prismatic joints, the linear velocity Jacobian is as follows:

$$J_{v_i} = {}^0z_i. \quad (3.50)$$

The term  ${}^0z_i$  refers to the direction of the z-axis for joint  $i$  in the global, or  $0^{th}$ , Frame. Say the transformation matrix between joint  $i$  and the global frame in terms of rows and columns is

$${}^0T_i = \begin{bmatrix} {}^0T_i(1, 1) & {}^0T_i(1, 2) & {}^0T_i(1, 3) & {}^0T_i(1, 4) \\ {}^0T_i(2, 1) & {}^0T_i(2, 2) & {}^0T_i(2, 3) & {}^0T_i(2, 4) \\ {}^0T_i(3, 1) & {}^0T_i(3, 2) & {}^0T_i(3, 3) & {}^0T_i(3, 4) \\ {}^0T_i(4, 1) & {}^0T_i(4, 2) & {}^0T_i(4, 3) & {}^0T_i(4, 4) \end{bmatrix}. \quad (3.51)$$

To find  ${}^0z_i$  you use the first 3 elements of the third column of  ${}^0T_i$ :

$${}^0z_i = \left\{ \begin{array}{l} {}^0T_i(1, 3) \\ {}^0T_i(2, 3) \\ {}^0T_i(3, 3) \end{array} \right\}. \quad (3.52)$$

### 3.5.4.2 REVOLUTE JOINTS

For revolute joints, the velocity of the end-effector can be written as follows:

$$\dot{p}_e = \omega \times r. \quad (3.53)$$

The  $r$  term refers a vector describing the distance between the joint and the end-effector. The linear velocity is then

$$v = ({}^0z_i \times (p_e - {}^0O_i))\dot{q}_i. \quad (3.54)$$

The linear velocity Jacobian for revolute joints can then be written as

$$J_v = {}^0z_i \times (p_e - {}^0O_i). \quad (3.55)$$

The term  ${}^0O_i$  refers to the origin of frame  $i$ . If we know the position of the end-effector in Cartesian space ( $p_e$ ), it can be defined as

$$p_e = \begin{Bmatrix} x_p \\ y_p \\ z_p \end{Bmatrix}. \quad (3.56)$$

Combining the terms above yields the following equation for the linear velocity Jacobian for revolute joints:

$$J_{v_i} = \begin{Bmatrix} {}^0T_i(1, 3) \\ {}^0T_i(2, 3) \\ {}^0T_i(3, 3) \end{Bmatrix} \times \begin{Bmatrix} x_p - {}^0T_i(1, 4) \\ y_p - {}^0T_i(2, 4) \\ z_p - {}^0T_i(3, 4) \end{Bmatrix}. \quad (3.57)$$

### 3.5.5 Angular Velocity Jacobian

The term for the angular velocity Jacobian is  $J_\omega$  and it is also a 3 x n matrix with n columns for n joints:

$$J_\omega = \begin{bmatrix} \rho_1 z_1 & \rho_2 z_2 & \cdots & \rho_n z_n \end{bmatrix}. \quad (3.58)$$

For prismatic joints,  $\rho = 0$ . For revolute joints,  $\rho = 1$ .

### 3.5.6 Inverting the Jacobian

The inverse of the Jacobian can be used with a moving tool point with a specified tool point velocity to find the joint speed. For the general case

$$\begin{bmatrix} v \\ \omega \end{bmatrix} = J(q)\dot{q}. \quad (3.59)$$

Using the inverse of the Jacobian yields

$$\dot{q} = J^{-1}(q) \begin{bmatrix} v \\ \omega \end{bmatrix}. \quad (3.60)$$

### 3.5.7 Singularities

The inverse of the Jacobian involves using the determinant. Problems arise when the determinant is equal to 0, leading to an undefined solution. The following are reasons why a singularity may exist [22]:

- At the singularity, the manipulator loses mobility; there is a loss of a DOF;
- At a boundary/workspace singularity, the manipulator has reached the furthest it can extend;
- At internal singularities, there is an alignment of axes;
- At a joint space singularity, there may be infinite solutions for its inverse kinematics;
- At a joint space singularity, small motions in the Cartesian space require an unattainable joint velocity (infinite joint velocity).

## 3.6 STATIC FORCE

Torque at each joint can be found using the Jacobian as shown below [21]:

$$\{\tau\} = [J_v^T] \{F\} \quad (3.61)$$

where

- $\tau$  - torque at the joints;
- $J_v^T$  - linear velocity Jacobian transposed;
- $F$  - force/load applied to robot end-effector.

This is possible through the virtual work principal, which eliminates the internal forces [23].

Figure 3.6 below provides an illustration of the principal:

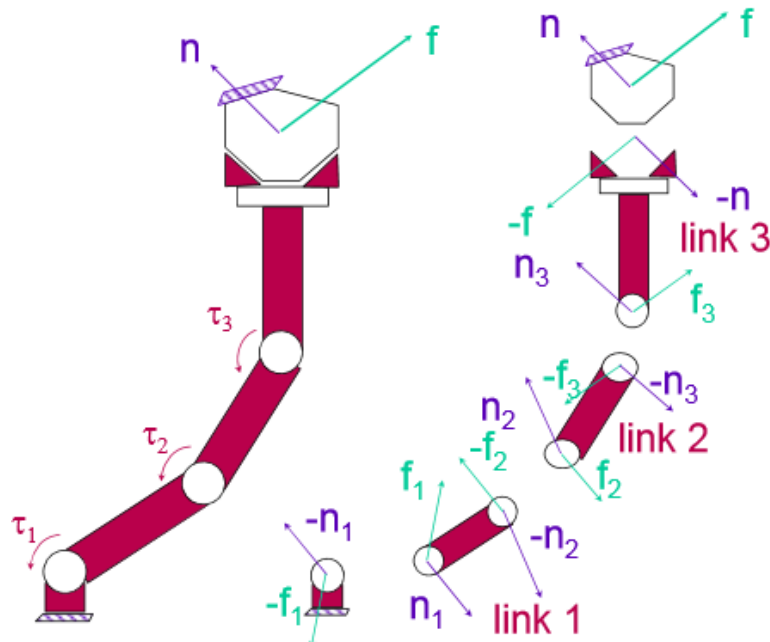


**Figure 3.6.** Virtual work principal for a manipulator. Source: Khatib, Oussama. “Jacobians: Explicit Form.” Accessed July 26, 2014. <http://cs.stanford.edu/groups/manips/images/stories/teaching/cs223a/handouts/Jacobian2-2014.pdf>.

In the case that the joint torques are known, the static force at the end-effector can be solved using the following equation:

$$\{F\} = [J_v^T]^{-1} \{\tau\}. \quad (3.62)$$

Problems may arise while solving for the force as the robot may be in a position where a singularity exists.

### 3.7 DYNAMICS

**Dynamics** allows us to find equations that relates the forces needed to produce motion. In other words, it is how the motion of a manipulator is the result of "torques applied by the actuators or ... external forces applied to the manipulator" [18:165]. There are two ways to determine the dynamics of a robot: Newton-Euler and Lagrangian. This thesis will examine dynamics using the latter.

### 3.8 LAGRANGIAN

The **Lagrangian** is another method of examining the forces and motions of an object. To find the Lagrangian, it is the difference between the kinetic energy and the potential energy. In equation form, it is as follows

$$L(q, \dot{q}) = T(q, \dot{q}) - U(q) \quad (3.63)$$

where  $T$  is the kinetic energy and  $U$  is the potential energy. For a manipulator, the Euler-Lagrange equation can be used to find the torque or force at the joints:

$$\frac{d}{dt} \left[ \frac{\partial L(q, \dot{q})}{\partial \dot{q}} \right] - \frac{\partial L(q, \dot{q})}{\partial q} = \tau. \quad (3.64)$$

Another form of Equation (3.64) is

$$\frac{d}{dt} \left[ \frac{\partial L(q, \dot{q})}{\partial \dot{q}_i} \right] - \frac{\partial L(q, \dot{q})}{\partial q_i} = \tau_i, \quad i = 1, \dots, n \quad (3.65)$$

where  $i$  corresponds to a specific joint. Sections 3.8.1 (Mass Matrix), 3.8.2 (Centrifugal and Coriolis Forces), and 3.8.3 (Gravity Forces) will go further in depth as to how we go from Equation (3.64) to Equation (3.66) below, which is the **Joint Space Dynamics Equation**:

$$M(q)\ddot{q} + C(q, \dot{q}) + G(q) = \tau. \quad (3.66)$$

The variables in the Joint Space Dynamics Equation represent the following [24]:

- $q$  - Generalized Joint Coordinates;
- $\dot{q}$  - Vector of Joint velocities;
- $\ddot{q}$  - Vector of Joint accelerations;
- $M(q)$  - Mass Matrix [see Section 3.8.1 on page 26];
- $C(q, \dot{q})$  - Centrifugal and Coriolis forces [see Section 3.8.2 on page 28];
- $G(q)$  - Gravity forces [see Section 3.8.3 on page 30];
- $\tau$  - Generalized forces.

### 3.8.1 Mass Matrix

The **mass matrix** can be determined based on the kinetic energy of the links. This is found by combining the linear kinetic energy and the kinetic energy of each link. Kinetic energy is determined by the work done on an object. Figure 3.7 illustrates the linear and angular kinetic energy of a link  $i$ .

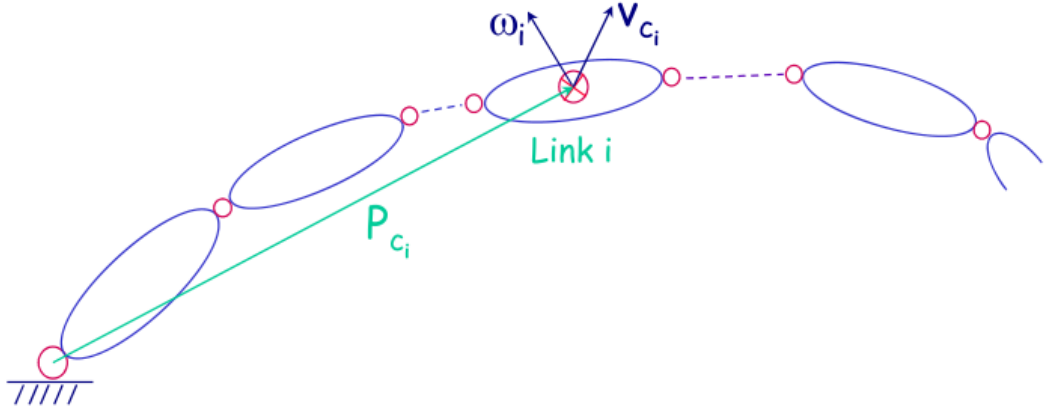


**Figure 3.7.** Kinetic energy of link  $i$ . Source: Khatib, Oussama. “Dynamics: Explicit Form.” Accessed July 26, 2014. <http://cs.stanford.edu/groups/manips/images/stories/teaching/cs223a/handouts/dynamics2-2014.pdf>.

The equation for the linear kinetic energy of a known mass  $m$  is as follows:

$$T_{linear} = \frac{1}{2}mv^2 \quad (3.67)$$

where  $v$  is velocity. And the equation for the rotational kinetic energy of a rigid body is as follows:

$$T_{rotational} = \frac{1}{2}\omega^T I_C \omega \quad (3.68)$$

where  $\omega$  is the angular velocity, and  $I_C$  is the moment of inertia at the center of mass. Just as a larger mass requires more energy to produce a linear motion, a larger moment of interia requires more energy to produce a rotation.

Combining the linear and rotational kinetic energies for link  $i$ , we can find the total kinetic energy of that particular link  $T_i$ :

$$T_i = \frac{1}{2}(m_i v_{C_i}^T v_{C_i} + \omega_i^T {}^0 I_{C_i} \omega_i). \quad (3.69)$$

The term  ${}^0 I_{C_i}$  refers to the inertia matrix of link  $i$  transformed from frame  $i$  to the global frame. It may be expanded as [25]

$${}^0 I_{c_i} = {}^0 R_i {}^i I_{c_i} {}^0 R_i^T \quad (3.70)$$

where  ${}^0 R_i$  refers to the rotation transformation between frame  $i$  and the global frame, and  ${}^i I_{c_i}$  refers to the inertia matrix of link  $i$  as seen in frame  $i$ .

To find the total kinetic energy of the entire manipulator, the equation will be

$$T = \sum_{i=1}^n T_i. \quad (3.71)$$

The mass matrix will be a symmetric matrix that represents the mass of the entire system. Since we know the total kinetic energy of the system, we can relate it to the mass matrix:

$$T = \frac{1}{2} \dot{q}^T M \dot{q}. \quad (3.72)$$

Breaking down the total kinetic energy equation further to relate to each link yields the following:

$$\frac{1}{2} \dot{q}^T M \dot{q} \equiv \frac{1}{2} \sum_{i=1}^n (m_i v_{C_i}^T v_{C_i} + \omega_i^T I_{C_i} \omega_i). \quad (3.73)$$

Using the Jacobian, we can relate the linear and angular velocities to the joint velocity using the following equations:

$$v_{C_i} = J_{v_i} \dot{q}, \quad (3.74)$$

$$\omega_{C_i} = J_{\omega_i} \dot{q}. \quad (3.75)$$

Plugging in Equations (3.74) and (3.75) into Equation (3.73) expands the equation further [26]:

$$\frac{1}{2} \dot{q}^T M \dot{q} = \frac{1}{2} \sum_{i=1}^n (m_i \dot{q}^T J_{v_i}^T J_{v_i} \dot{q} + \dot{q}^T J_{\omega_i}^T I_{C_i} J_{\omega_i} \dot{q}) \quad (3.76)$$

$$\frac{1}{2} \dot{q}^T M \dot{q} = \frac{1}{2} \dot{q}^T \left[ \sum_{i=1}^n (m_i J_{v_i}^T J_{v_i} + J_{\omega_i}^T I_{C_i} J_{\omega_i}) \right] \dot{q} \quad (3.77)$$

The equation for the mass matrix is then

$$M = \sum_{i=1}^n (m_i J_{v_i}^T J_{v_i} + J_{\omega_i}^T I_{C_i} J_{\omega_i}). \quad (3.78)$$

The mass matrix will be an  $n \times n$  matrix, whose elemental form looks like

$$M(q) = \begin{bmatrix} m_{11} & m_{12} & \cdots & m_{1n} \\ m_{21} & m_{22} & \cdots & m_{2n} \\ \vdots & \vdots & \vdots & \vdots \\ m_{n1} & m_{n2} & \cdots & m_{nn} \end{bmatrix}. \quad (3.79)$$

The diagonal elements are the perceptive inertia at each joint, while the off-diagonal elements are the result of coupling. The mass matrix is also positive definite as mass will always be a positive value. Element  $m_{nn}$  will not be a function of the last joint; instead it is a constant. And  $m_{11}$  will not be dependent of joint 1, but instead be dependent on joints 2 to  $n$ .

The equations for the linear and angular Jacobians will be similar to Equations (3.48) and (3.58), but in this instance, the vector  $p_{c_i}$  goes from the origin of the global frame to the center of mass of link  $i$ . This leads to columns  $i + 1$  to  $n$  be equal to zero in the linear and rotational Jacobians for link  $i$ . The general form of the linear and angular Jacobians for link  $i$  is then

$$J_{v_i} = \begin{bmatrix} \frac{\partial p_{c_i}}{\partial q_1} & \frac{\partial p_{c_i}}{\partial q_2} & \cdots & \frac{\partial p_{c_i}}{\partial q_i} & 0 & 0 & \cdots & 0 \end{bmatrix}, \quad (3.80)$$

$$J_{\omega_i} = \begin{bmatrix} \rho_1 z_1 & \rho_2 z_2 & \cdots & \rho_i z_i & 0 & 0 & \cdots & 0 \end{bmatrix}. \quad (3.81)$$

### 3.8.2 Centrifugal and Coriolis Forces

The **Centrifugal and Coriolis Forces** can be determined through the mass matrix. From Equation (3.72), we know the kinetic energy of the system. Plugging in Equation (3.72) into Equation (3.63) we get

$$L(q, \dot{q}) = \frac{1}{2} \dot{q}^T M(q) \dot{q} - U(q). \quad (3.82)$$

Furthermore, plugging in Equation (3.82) into Equation (3.64) yields

$$\frac{d}{dt} \left[ \frac{\partial}{\partial \dot{q}} \left[ \frac{1}{2} \dot{q}^T M(q) \dot{q} \right] \right] - \frac{\partial}{\partial \dot{q}} \left[ \frac{1}{2} \dot{q}^T M(q) \dot{q} \right] + \frac{\partial U(q)}{\partial q} = \tau. \quad (3.83)$$

The following terms can be simplified as shown below:

$$\frac{\partial}{\partial \dot{q}} \left[ \frac{1}{2} \dot{q}^T M(q) \dot{q} \right] = M(q) \dot{q} \quad (3.84)$$

$$\frac{d}{dt} \left[ \frac{\partial}{\partial \dot{q}} \left[ \frac{1}{2} \dot{q}^T M(q) \dot{q} \right] \right] = M(q) \ddot{q} + \dot{M}(q) \dot{q} \quad (3.85)$$

Equation (3.83) can then be reduced to

$$M(q)\ddot{q} + \dot{M}(q)\dot{q} - \frac{1}{2} \frac{\partial}{\partial q} \left[ \dot{q}^T M(q) \dot{q} \right] + \frac{\partial U(q)}{\partial q} = \tau. \quad (3.86)$$

The Centrifugal and Coriolis Force terms  $C(q, \dot{q})$  is

$$C(q, \dot{q}) = \dot{M}(q)\dot{q} - \frac{1}{2} \frac{\partial}{\partial q} \left[ \dot{q}^T M(q) \dot{q} \right]. \quad (3.87)$$

Another way of writing Equation (3.87) is [27]

$$C(q, \dot{q}) = \dot{M}(q)\dot{q} - \frac{1}{2} (I_n \otimes \dot{q}^T) \frac{\partial M}{\partial q} \dot{q} \quad (3.88)$$

where  $\otimes$  is the tensor product. To simplify the expression for the Centrifugal and Coriolis forces further, we can use the following substitution

$$\mathcal{U}(q, \dot{q}) \equiv (I_n \otimes \dot{q}^T) \frac{\partial M}{\partial q} \quad (3.89)$$

into Equation (3.88) to reduce it to

$$C_{m1}(q, \dot{q}) = \left[ \dot{M}(q) - \frac{1}{2} \mathcal{U}(q, \dot{q}) \right] \dot{q} \quad (3.90)$$

where  $C_{m1}$  is one way of writing  $C(q, \dot{q})$ .

The second method of writing  $C(q, \dot{q})$  involves using the following relationship for  $\dot{M}$  where

$$\dot{M}(q) = \sum_{i=1}^n \frac{\partial M}{\partial q_i} \dot{q}_i, \quad (3.91)$$

$$= \left[ \frac{\partial M}{\partial q} \right]^T (\dot{q} \otimes I_n). \quad (3.92)$$

Substituting Equation (3.92) into Equation (3.88) yields

$$C(q, \dot{q}) = \left[ \frac{\partial M}{\partial q} \right]^T (\dot{q} \otimes I_n) \dot{q} - \frac{1}{2} (I_n \otimes \dot{q}^T) \frac{\partial M}{\partial q} \dot{q}. \quad (3.93)$$

The second form of  $C(q, \dot{q})$  is then

$$C_{m2}(q, \dot{q}) = \left[ \mathcal{U}(q, \dot{q})^T - \frac{1}{2} \mathcal{U}(q, \dot{q}) \right] \dot{q}. \quad (3.94)$$

Although  $C(q, \dot{q})$  may be written in two different ways, in general,  $\dot{M} \neq \mathcal{U}^T$  and  $C_{m1} \neq C_{m2}$ .

The standard form of  $C(q, \dot{q})$  used for adaptive control and robust control algorithms incorporates components of both forms to become [27]

$$C(q, \dot{q}) = \frac{1}{2} \left( \dot{M}(q, \dot{q}) + \mathcal{U}(q, \dot{q})^T - \mathcal{U}(q, \dot{q}) \right) \dot{q}. \quad (3.95)$$

### 3.8.3 Gravity Forces

The remaining term in Equation (3.86) consists of the potential energy term. This term refers to the **gravity forces**:

$$G = \frac{\partial U(q)}{\partial q}. \quad (3.96)$$

The potential energy for link  $i$  is

$$U_i = m_i(-g^T p_{c_i}) \quad (3.97)$$

while the total potential energy of the system is

$$U = \sum_{i=1}^n U_i. \quad (3.98)$$

Taken with respect to position of joint  $j$ , the gravity vector is

$$G_j = \frac{\partial U}{\partial q_j} = - \sum_{i=1}^n (m_i g^T \frac{\partial p_{c_i}}{\partial q_j}). \quad (3.99)$$

We can then rewrite the overall gravity vector as

$$G = - \begin{pmatrix} J_{v_1}^T & J_{v_2}^T & \cdots & J_{v_n}^T \end{pmatrix} \begin{pmatrix} m_1 g \\ m_2 g \\ \vdots \\ m_n g \end{pmatrix}, \quad (3.100)$$

which can also be written as

$$G = -(J_{v_1}^T(m_1 g) + J_{v_2}^T(m_2 g) + \cdots + J_{v_n}^T(m_n g)). \quad (3.101)$$

## CHAPTER 4

### EQUIPMENT

#### 4.1 DYNAMIXEL MOTOR

##### 4.1.1 Description

Dynamixel is a line of actuators created by the company ROBOTIS, which is based in Korea. Dynamixel actuators are typically referred to as *smart* actuators as they possess a built in microprocessor. This microprocessor can "facilitate bus communication, position feedback, temperature and load monitoring" [28:1]. The actuator used for this particular robotic arm is the MX-64R, which is shown below in Figure 4.1:



**Figure 4.1.** MX-64R actuator. Source: ROBOTIS. "MX-64T / MX-64R e-Manual." Accessed July 29, 2014. <http://support.robotis.com/en/product/dynamixel/mx-series/mx-64.htm>.

The properties of the motor can be found in Table 4.1 [29].

**Table 4.1. MX-64R Specs**

Property	Value
Onboard CPU	Cortex M3 (STM32F103C8 @ 72MHz, 32 Bit)
Position Sensor	Magnetic Encoder
Motor	Maxon
Control Algorithm	PID Control
Resolution	0.088°
Weight	126 g
Dimension	40.2mm x 61.1 mm x 41 mm
Gear Reduction Ratio	200:1
Recommended Voltage	12 V
Stall Torque (@12 V)	6.0 N·m
Speed (@12 V)	63 rpm
Communication Protocol	RS-485
Default Baud Rate	57600 bps

#### 4.1.2 Wiring

Another benefit of using the Dynamixel line is the ability to "daisy-chain" the actuators. For the MX-64R, this is possible because the motors communicate using RS-485. Daisy chain is a method of connecting items in series with one another. A daisy chain is connected in a sequence, in which one device is connected to another device, which is then connected to another device, and so on. For items needing information from a central hub, instead of each device connecting to the hub individually, only one device needs to be connected, and the information will be passed along through each device until it reaches the right one.

Instead of connecting each Dynamixel motor to a controller and power source, they can be daisy-chained to one another. Even though the motors are connected to one another using this method, each can be controlled individually through information packets, in which each motor can be distinguished through a unique ID number. A general setup of Dynamixel motors and a controller is shown in Figure 4.2. To connect the multiple MX-64 motors into a daisy chain network, the proper pins must be connected to one another, otherwise the motor may become damaged. Each MX-64 motor will contain two sets of four-pin connectors as shown in Figure 4.3. The pins are not oriented the same way on both the left and right sides. A diagram showing how to properly wire the MX-64R can be found in figure 4.4.

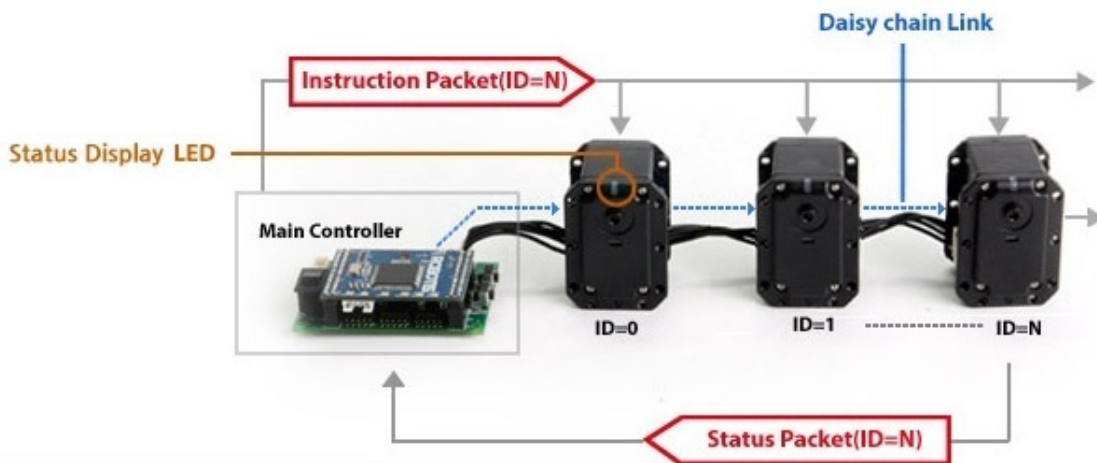


**Figure 4.2.** Daisy-chain link of Dynamixel motors connected to a controller. Source: ROBOTIS. “Dynamixel.” Accessed August 26, 2014. [http://www.robotis.com/xe/dynamixel\\_en](http://www.robotis.com/xe/dynamixel_en).

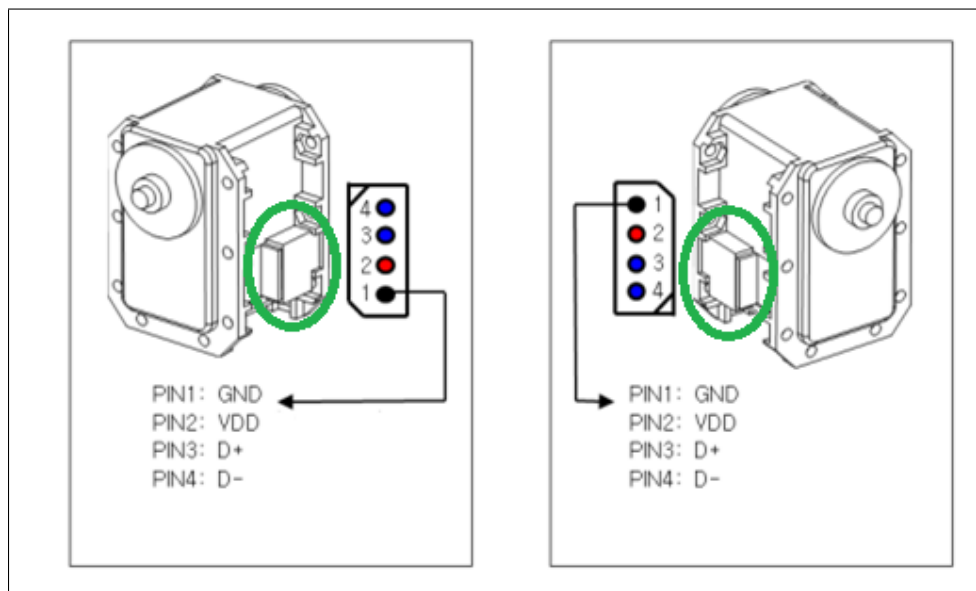


**Figure 4.3.** Two sets of 4-Pin connectors on MX-64 motor. Source: ROBOTIS. “MX Series.” Accessed August 26, 2014. [http://support.robotis.com/en/product/dynamixel/dxl\\_mx\\_main.htm](http://support.robotis.com/en/product/dynamixel/dxl_mx_main.htm).

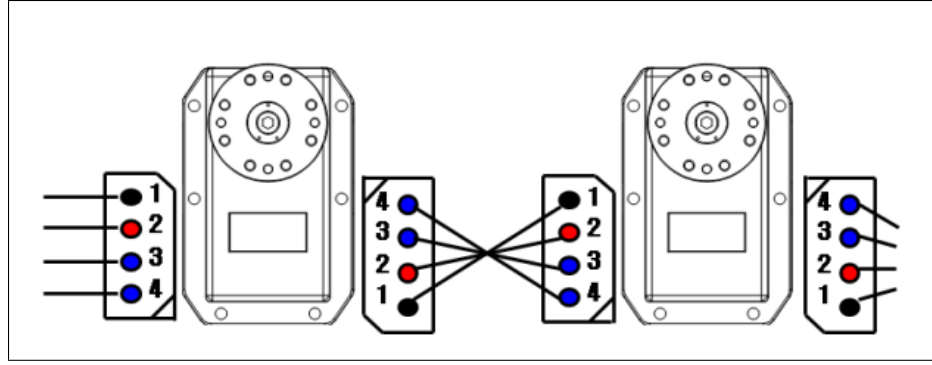


**Figure 4.4.** Matching pins on multiple MX-64 motors.

Source: ROBOTIS. “MX Series.” Accessed August 26, 2014.  
[http://support.robotis.com/en/product/dynamixel/dxl\\_mx\\_main.htm](http://support.robotis.com/en/product/dynamixel/dxl_mx_main.htm).

#### 4.1.3 Limitations

Even though the Dynamixel series is a robust brand of actuators, they still have some limitations. These include:

- stable motions at quantities much lower than stall torque;
- gear backlash;
- slow communication speeds due to half duplex UART.

##### 4.1.3.1 STALL TORQUE

For the MX-64R, the stall torque is rated as 6.0 Nm. According to the manual, the motor provides stable motions when the load applied to the motor is approximately 20% or less of the rated stall torque [29]. This means that the actual load that the actuator can withstand is much closer to 1.2 Nm. In addition, experiments have been conducted to verify the manufacturer’s claim of a max stall torque of 6.0 Nm, but the findings show that they are actually closer to half that [30].

##### 4.1.3.2 GEAR BACKLASH

The MX-64R has a gear reduction ratio of 200:1 from its internal gear box. Because of the gears however, the motor experiences backlash when commanded to remain at a fixed position. The range of the backlash in the motor is about  $1.76^\circ$ . Figure 4.5 demonstrates how different the position can be as a result of the gear backlash for the motor that articulates the humerus.

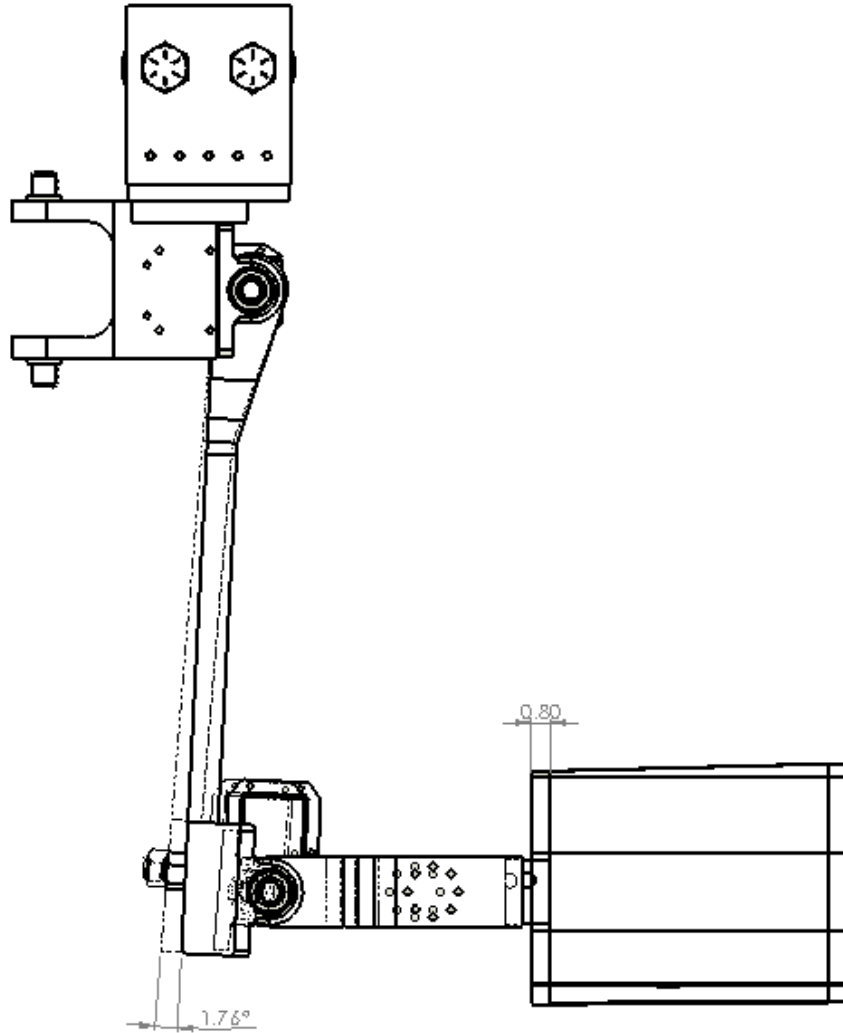


**Figure 4.5. Error in position due to gear backlash.**

In the case of Figure 4.5, link 3 and the end-effector will be offset by about 0.80 cm.

#### 4.1.3.3 HALF DUPLEX UART

The benefit of half duplex UART is that it allows for a daisy chain configuration of the actuators. But as a result, the communication speed suffers. With half duplex UART, the transfer and receiving of information with the actuators cannot take place at the same time [31]. Instead, the actuators are either receiving information from the computer, or transferring information back to the computer.

Furthermore, the communication speed between the actuator and the computer will slow down based on how many items are being transferred or received. For example, if one wants to read 200 points of data on the actuator's position, it might take about 1 second to record all that information. Now if that same person wanted to read position *and* speed, it

would take 2 seconds to read 200 points of data of both position and speed. So only the first 100 points of position data will match the previously recorded position information when only position was being recorded. Similarly, the number of motors influences the communication speed; as the number of motor increases, the communication between the motor and the computer is split accordingly [32].

## 4.2 DELSYS TRIGNO

The Delsys Trigno is a wireless electromyography (EMG) system. Electromyography is a technique used to measure muscle activity based on the electrical signals produced by the muscle. The Delsys Trigno specifically measures surface electromyography (sEMG), in which electrodes are placed on the surface of one's skin to record the electrical activity. The benefit of this method is that it is “safe, easy, and noninvasive” [33:5]. Figure 4.6 shows the base station and two sensors.



**Figure 4.6. Delsys Trigno wireless EMG system.** Source: Delsys. “Trigno Wireless System User’s Guide.” Accessed March 30, 2015. <https://www.delsys.com/Attachments.pdf/Trigno%20Wireless%20System%20Users%20Guide%20%28MAN-012-2-3%29.pdf>.

The left sensor is a view of the back, and it shows the four contact points used to detect the EMG signal. The right sensor is a view of the front, which contains an LED indicator, and the on/off switch for the sensor. The system initially comes with 16 sensors. Each sensor has 1 channel for EMG data, and 3 channels for accelerometer data (X, Y, and Z). The base station is where the sensors may be placed to be charged, and stored when not in use. More information on the features of the system can be found in Table 4.2 [34]:

**Table 4.2. Delsys Trigno Features**

Property	Value
Transmission Range	20 m
Inter-sensor Latency	< 500 $\mu$ s
Battery	Rechargeable
EMG Signal Bandwidth	20 - 450 Hz
EMG Signal Sampling Rate	2000 samples/sec
EMG Baseline Noise	< 750 nV RMS
EMG Signal Resolution	16-bit

The sensor is placed on the surface of the skin through the use of a double-sided adhesive. To get the best reading, the sensor should be placed with the arrow parallel to the direction of the muscle-fiber as seen in Figure 4.7.

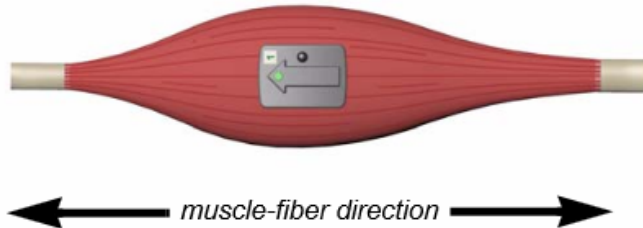


**Figure 4.7. Trigno sensor placement.**  
**Source:** Delsys. “Trigno Wireless System User’s Guide.” Accessed March 30, 2015. [https://www.delsys.com/Attachments\\_pdf/Trigno%20Wireless%20System%20Users%20Guide%20%28MAN-012-2-3%29.pdf](https://www.delsys.com/Attachments_pdf/Trigno%20Wireless%20System%20Users%20Guide%20%28MAN-012-2-3%29.pdf).

In addition, a stronger reading is possible by placing the sensor at the center of the muscle belly [34]. And to detect an EMG signal, Delsys employs a patented approach using the four contact points. Figure 4.8 is a diagram showing a top-level view of how the EMG signal is produced. The sensor works by detecting two separate EMG signals, where one set

of contact bars are used for reference, and the other set of contact bars are used for the differential EMG input signal. The end result is a single differential signal. According to the manufacturer, this approach reduces the effect of noise on the detected signal [35].

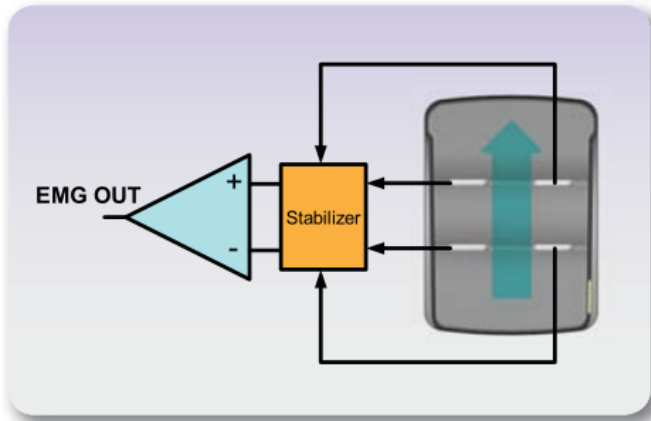


**Figure 4.8.** Trigno EMG detection. Source: Delsys. “Trigno Wireless - FAQ.” Accessed March 30, 2015. <https://www.delsys.com/Attachments.pdf/Trigno%20FAQ%20%28DOC-208-1-0%29-web.pdf>.

## CHAPTER 5

### DESIGN

#### 5.1 ROBOTIC ARM EXOSKELETON FRAME

The frame of the robotic arm exoskeleton was designed to support the weight of an average male human arm. From a study of thirteen male human cadavers, the average weight of the total arm of the sample population was 3.216 kg [36]. The frame of the robotic arm exoskeleton consists of four parts:

- base;
- link 1;
- link 2;
- link 3.

A CAD model annotated to show these different parts can be found in Figure 5.1.

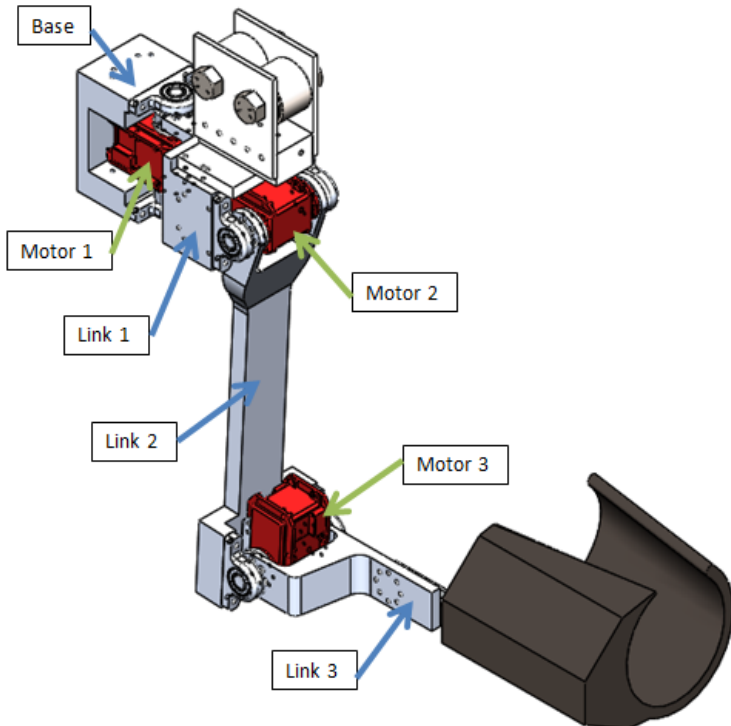


**Figure 5.1. Annotated robotic arm CAD model.**

The arm was originally going to be made out of ABS plastic through the use of a 3D printer, but the material was not strong enough to support the load of the human arm. Now, most of the arm is made out of aluminum. Sections 5.1.1 through 5.1.4 go into more depth of the properties of those components.

### 5.1.1 Base

The base of the robotic arm consists primarily of four parts: motor, base motor case, and two base mounted bearings. The base is where the first motor is used, and it is used for shoulder articulation. Figure 5.2 shows a CAD model of the base.

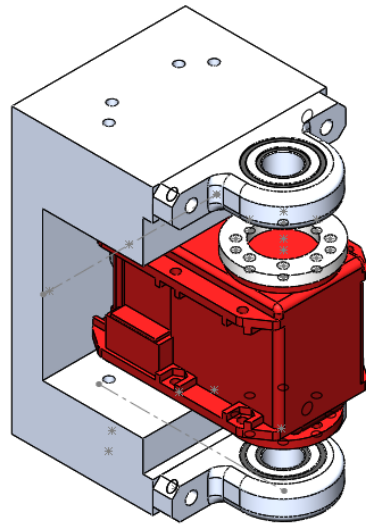


**Figure 5.2. CAD model of base.**

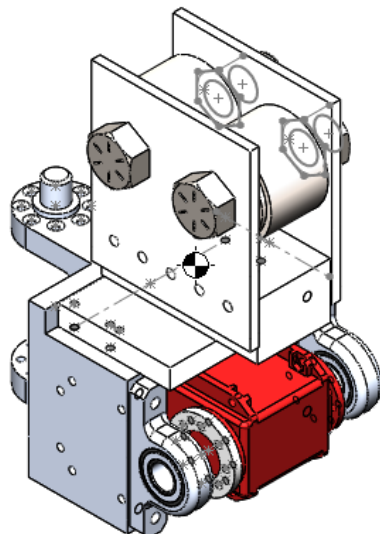
### 5.1.2 Link 1

Link 1 connects motor 1 (shoulder articulation) with motor 2 (humorous articulation). It houses motor 2, and consists of many components. The Bill of Materials (BOM) and the weight of the components can be found in Table 5.1.

**Table 5.1. Bill of Materials and Weight Comparison for Link 1**

Component	Quantity	SolidWorks Mass (kg)	Actual Mass (kg)
Base, Spring Case	1	0.073	0.073
Base Mounted Bearings	2	0.022	0.022
Bolt - 1/2" D, 2" L	1	0.070	0.062
Bolt - 1/2" D, 2.5" L	1	0.079	0.075
Constant Force Spring - 7 lb	1	0.078	0.078
Constant Force Spring - 10 lb	1	0.082	0.082
Motor	1	0.139	0.139
Mounting Plate, Spring	1	0.033	0.029
Nut - 1/2" D	2	0.017	0.016
Shoulder Motor Case	1	0.365	0.373
Side Wall, Spring Case	2	0.021	0.022
Spring Bearing	4	0.031	0.031
<b>Link 1 (Total)</b>	<b>1</b>	<b>1.161</b>	<b>1.169</b>

A CAD model showing all the components in Table 5.1 in a single assembly can be found in Figure 5.3.

**Figure 5.3. CAD model of link 1.**

The origin of link 1 can be found in Figures 5.4 and 5.5 as the red, green, and blue axes. Figure 5.4 shows the X-Y axes of the origin, and Figure 5.5 shows the X-Z axes.

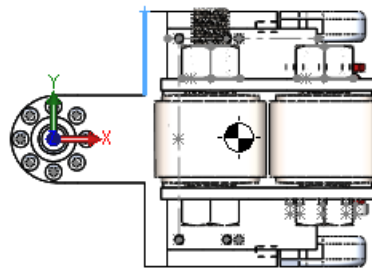


**Figure 5.4. X-Y axes for link 1.**

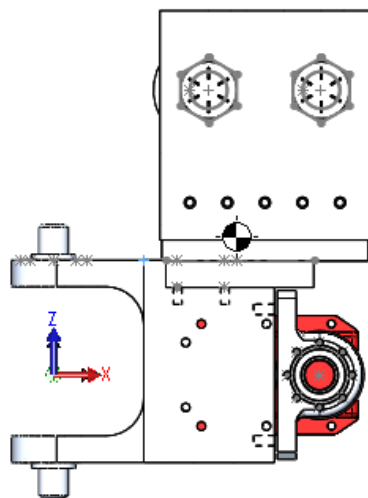


**Figure 5.5. X-Z axes for link 1.**

This CAD model and reference origin is used to calculate the center of mass (see Table 5.2) and the moment of inertia tensor (see Table 5.3) for link 1.

**Table 5.2. Center of Mass for Link 1**

Axis	Location (m)
x	0.0602000
y	0.0006171
z	0.0465900

**Table 5.3. Moment of Inertia Tensor About Axis of Rotation for Link 1**

Moment/Product of Inertia	Quantity ( $kg \cdot m^2$ )
$I_{xx}$	2.429e-03
$I_{xy}$	1.751e-06
$I_{xz}$	4.616e-04
$I_{yy}$	2.510e-03
$I_{yz}$	3.925e-05
$I_{zz}$	1.050e-03

### 5.1.3 Link 2

Link 2 connects motor 2 (humerous articulation) with motor 3 (forearm articulation). It houses motor 3, and consists of the heaviest component (aluminum humerous). The BOM and the weight of the components can be found in Table 5.4.

**Table 5.4. Bill of Materials and Weight Comparison for Link 2**

Component	Quantity	SolidWorks Mass (kg)	Actual Mass (kg)
Base Mounted Bearings	2	0.022	0.022
Bolt - 3/8" D, 1" L	1	0.020	0.018
Humerous, Aluminum	1	0.556	0.561
Motor	1	0.139	0.139
Motor Bracket	1	0.007	0.007
Nut - 3/8" D	1	0.008	0.007
<b>Link 2 (Total)</b>	<b>1</b>	<b>0.773</b>	<b>0.775</b>

A CAD model showing all the components in Table 5.4 in a single assembly can be found in Figure 5.6.

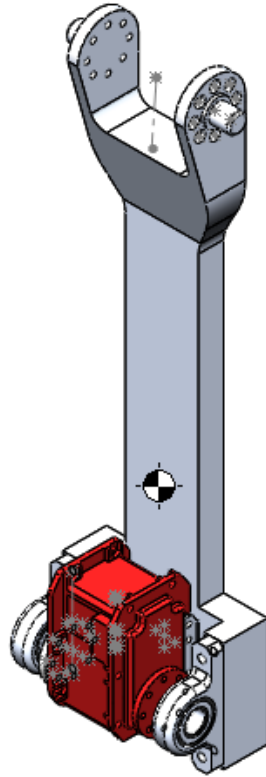


**Figure 5.6.** CAD model of link 2.

The origin of link 2 can be found in Figures 5.7 and 5.8 as the red, green, and blue axes. Figure 5.7 shows the X-Y axes of the origin, and Figure 5.8 shows the X-Z axes.

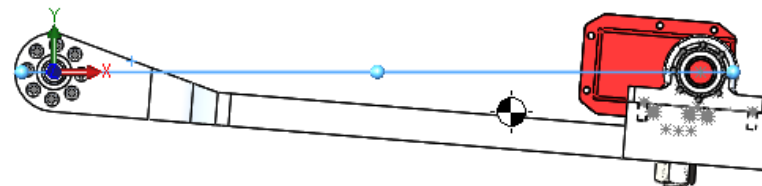


**Figure 5.7.** X-Y axes for link 2.

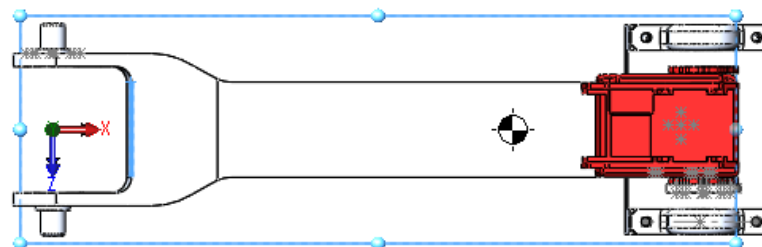


**Figure 5.8.** X-Z axes for link 2.

This CAD model and reference origin is used to calculate the center of mass (see Table 5.5) and the moment of inertia tensor (see Table 5.6) for link 2.

**Table 5.5. Center of Mass for Link 2**

Axis	Location (m)
x	0.1848000
y	-0.0161100
z	-0.0002956

**Table 5.6. Moment of Inertia Tensor About Axis of Rotation for Link 2**

Moment/Product of Inertia	Quantity ( $kg \cdot m^2$ )
$I_{xx}$	3.649e-04
$I_{xy}$	-3.887e-04
$I_{xz}$	-4.258e-06
$I_{yy}$	5.679e-03
$I_{yz}$	4.581e-07
$I_{zz}$	5.468e-03

### 5.1.4 Link 3

Link 3 connects motor 3 (forearm articulation) to the end-effector. The BOM and the weight of the components can be found in Table 5.7.

**Table 5.7. Bill of Materials and Weight Comparison for Link 3**

Component	Quantity	SolidWorks Mass (kg)	Actual Mass (kg)
Cuff	1	0.332	0.332
Forearm, Aluminum	1	0.153	0.155
<b>Link 3 (Total)</b>	<b>1</b>	<b>0.485</b>	<b>0.487</b>

A CAD model showing all the components in Table 5.7 in a single assembly can be found in Figure 5.9.

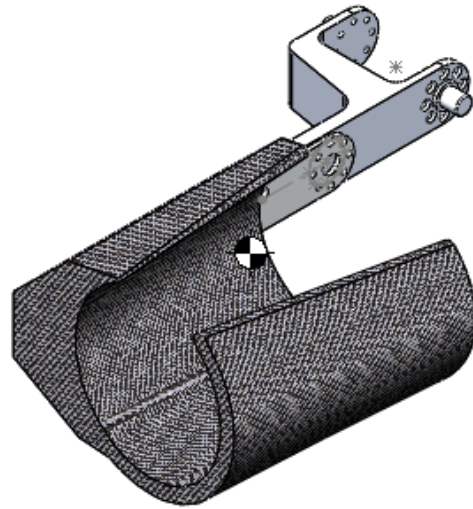


**Figure 5.9. CAD model of link 3.**

The origin of link 3 can be found in Figures 5.10 and 5.11 as the red, green, and blue axes. Figure 5.10 shows the X-Y axes of the origin, and Figure 5.11 shows the X-Z axes.

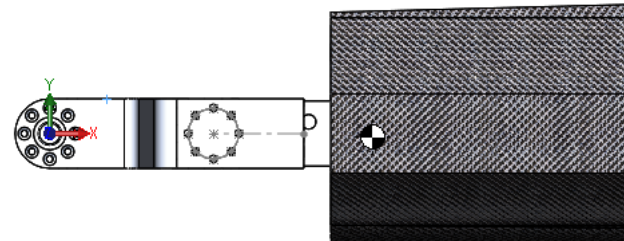


**Figure 5.10. X-Y axes for link 3.**

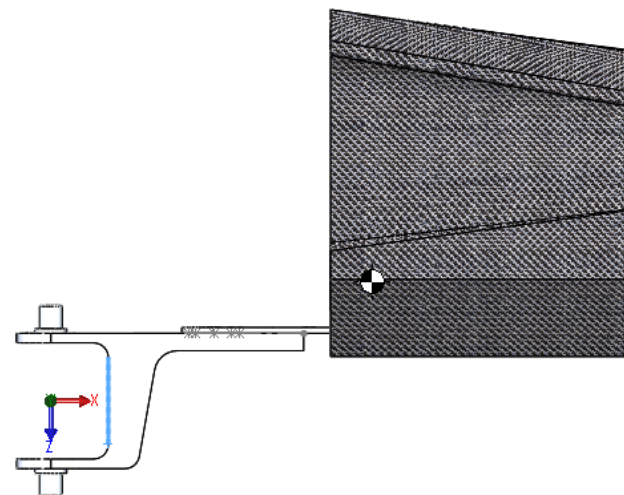


**Figure 5.11. X-Z axes for link 3.**

This CAD model and reference origin is used to calculate the center of mass (see Table 5.8) and the moment of inertia tensor (see Table 5.9) for link 3.

**Table 5.8. Center of Mass for Link 3**

Axis	Location (m)
x	0.140100
y	-0.001449
z	-0.052110

**Table 5.9. Moment of Inertia Tensor About Axis of Rotation for Link 3**

Moment/Product of Inertia	Quantity ( $kg \cdot m^2$ )
$I_{xx}$	8.178e-05
$I_{xy}$	-7.635e-08
$I_{xz}$	-5.046e-05
$I_{yy}$	2.138e-04
$I_{yz}$	3.667e-05
$I_{zz}$	9.684e-03

### 5.1.5 Hysteresis

The biggest obstacle with the robotic arm is gravity compensation. Not only does it require more torque from the actuator, it makes it hard for the actuator to move to reach the desired position. This is especially evident when the motor is moving against gravity, which leads to a greater error.

#### 5.1.5.1 MOTOR 2

Motor 2 provides the humerous articulation. As a result, it experiences the largest torque since it is attached to the largest and heaviest link. To compensate for that weight, a constant force spring is used to counteract it. Figure 5.12 shows the hysteresis in motor 2 with no spring attached.

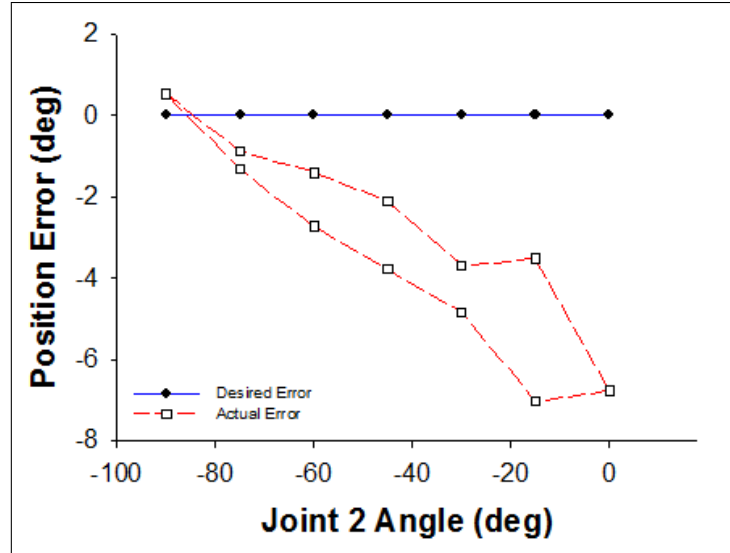


**Figure 5.12.** Hysteresis of position error for motor 2.

As motor 2 moves from  $-90^\circ$  to  $0^\circ$ , the torque experienced at the joint increases. This is the result of the horizontal distance of the load from the joint increasing. The relationship between torque and distance is

$$\tau = r \times F, \quad (5.1)$$

where  $\tau$  is the torque,  $r$  is the distance from the joint to the point where the force is applied, and  $F$  is the applied force. Because both the position error and joint torque increase with joint angle, it appears that position error increases with joint torque.

A hysteresis effect is noticeable for motor 2. When the motor moves counter-clockwise about the  $z_2$ -axis, or against gravity, the position error is noticeably larger than when the motor moves clockwise. This suggests that when the motor moves in a direction against gravity, it has a harder time reaching that position. Furthermore, when motor 2 moves from  $-90^\circ$  to  $0^\circ$ , the joint torque increases. This also suggests that position error is based on whether joint torque is increasing or decreasing.

### 5.1.5.2 MOTOR 3

Motor provides the forearm articulation. It does not require the use of a spring to counteract the gravity forces like motor 3, but it still experiences a hysteresis effect. The hysteresis of motor 3's position error will also be influenced by the position that motor 2 is at. Figure 5.13 shows the different hystereses of motor 3 based on the position of motor 2.

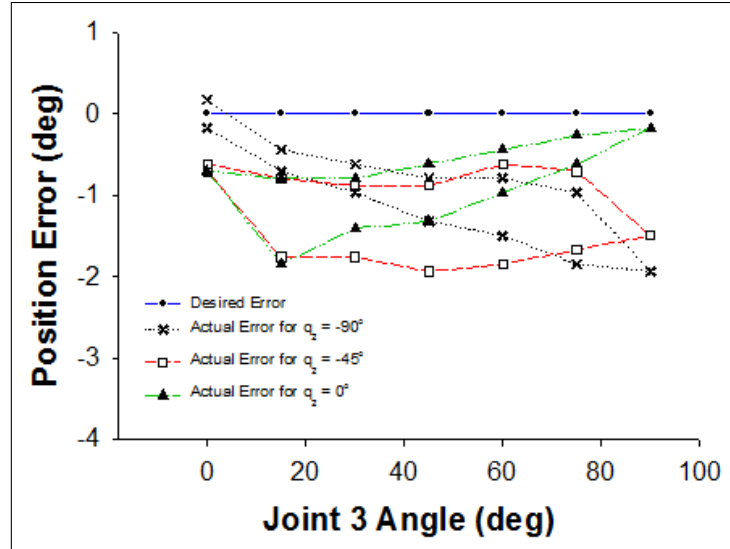


**Figure 5.13. Hysteresis of position error for motor 3.**

Figure 5.13 shows that position error is affected by the angle of joint 2. This is because the torque about joint 3 is dependent on joint angles 2 and 3. If the robotic arm were in a static position, and joint 2 position had a value of  $q_2 = 0^\circ$ , the maximum torque for joint 3 would be when  $q_3 = 90^\circ$ . The correlation of position error increasing with joint torque is verified with motor 3 as well.

A hysteresis effect occurs in motor 3. Because the joint torque about joint 3 is related to joint angles 2 and 3, there are different hysteresis observed based on the position of motor 2. The  $z_3$ -axis is parallel to the  $z_2$ -axis, and the positive direction about these axes is counter-clockwise. Like motor 2, when motor 3 moves against gravity, the motor experiences a greater position error compared to when it moves in the opposite direction. And like motor 2, whether the joint torque is increasing or decreasing, the position error changes accordingly. When joint 2 has a position of  $q_2 = 0^\circ$  and joint 3 moves from a position of  $q_3 = 0^\circ$  to  $q_3 = 90^\circ$ , the position error decreases as the joint torque decreases. Similarly, when joint 2 has a position of  $q_2 = -90^\circ$  and joint 3 moves from a position of  $q_3 = 0^\circ$  to  $q_3 = 90^\circ$ , the position error increases as the joint torque increases.

## 5.2 SAFETY

Safety is an important feature to consider when working with exoskeletons. This is because the links of the user's limbs may not always align properly with the links of the robot [37]. As a result, the robot may move to a position beyond the capability of the user, which may in turn injure the user. For this robotic arm, safety is addressed by three features: cuff design, physical stops, and stops in software. Fig. 5.14 shows the robotic arm mounted

onto the wheelchair, and a user sitting the wheelchair with his arm in the robot. The image shows the user with his forearm sittin in the cuff of link 3.



**Figure 5.14. Robotic arm attached to wheelchair with user.**

The only location of physical interaction between the user and the robot is at the cuff. The purpose of the cuff was to provide the user with an easy method to remove his or her arm if the robot ever put the user in a dangerous position. This includes the robot were moving to a position not within the physical limits of the human body. If the user's arm were attached to the robot differently, such as with straps, the user would have no way of immediately removing his or her limb from the device.

Another way to improve the safety of the robotic arm is through the use of stops. For this robotic arm, stops are in the form of physical stops, and stops in the software based on position. A physical stop is a stopper placed on the device to prevent the actuator from moving the device beyond a certain position. This particular robotic arm has physical stops designed into the links that restrict the range of motion. Table 5.10 shows the minimum and maximum joint angles of each joint.

**Table 5.10. Physical Range of Joints**

Joint	Minimum Joint Angle (deg)	Maximum Joint Angle (deg)
1	-90	90
2	-102.78	66.57
3	-20.91	100.61

Furthermore, stops are placed in the code for robotic movement. In the code, the computer gets information from the motor to determine the motor's current position. Once the software detects that the user is reaching a position beyond the user's capabilities, the computer tells the actuator to stop moving any further. This allows movement within a certain range of motion when the motors are running. The benefit of stops within the hardware is that they can be adjusted based on the user's capabilities.

### 5.3 UPPER-LIMB MOTION

The three actuators allow for six types of upper-limb motion. Figure (5.15) shows the motions motor 1 is able to provide.

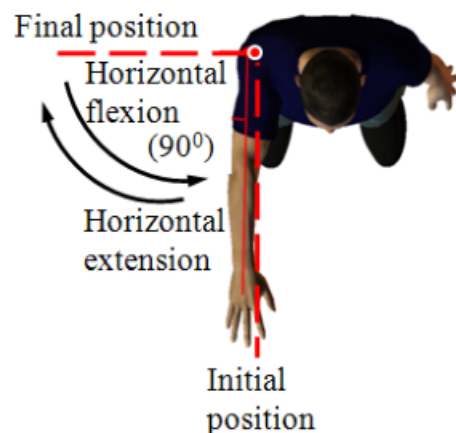


**Figure 5.15.** Arm motion due to motor 1: shoulder horizontal extension and shoulder horizontal flexion. Source: Gopura, R.A.R.C. “A Study on Human Upper-Limb Muscles Activities.” *International Journal of Bioelectromagnetism* 12, no. 2 (2010): 54-61.

These motions are horizontal extension of the shoulder and horizontal flexion of the shoulder, where both motions occur parallel to the traverse (horizontal) plane. The muscle activated for

shoulder horizontal extension is the posterior deltoid, whereas the muscle activated for shoulder horizontal flexion is the calvicular part of the pectoralis major [38].

Motor 2 provides the following motions: vertical extension of the shoulder and vertical flexion of the shoulder. Figure (5.16) is a diagram showing the motions.

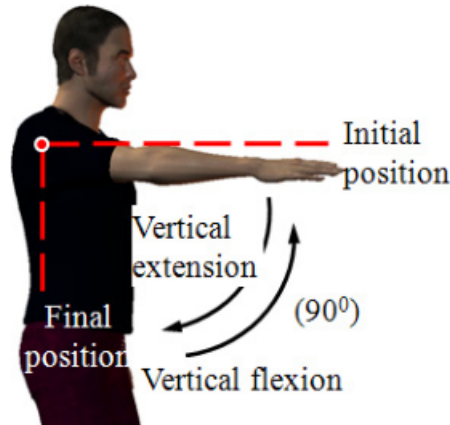


**Figure 5.16.** Arm motion due to motor 2: shoulder vertical extension and shoulder vertical flexion. Source: Gopura, R.A.R.C. “A Study on Human Upper-Limb Muscles Activities.” *International Journal of Bioelectromagnetism* 12, no. 2 (2010): 54-61.

These motions take place on the coronal (frontal) plane. The muscles activated during shoulder vertical extension are the posterior deltoid, the teres major, and the latissimus dorsi [38]. Different muscles are activated during shoulder vertical flexion, and those muscles are the coracobrachialis, the anterior deltoid, and the pectoralis major [38].

Motions provided by motor 3 are elbow extension and elbow flexion. Figure (5.17) shows the different positions of these two motions. The muscles activated during elbow extension are the anconeus and the triceps brachii [39]. The muscles activated during elbow flexion are the biceps brachii, the brachioradialis, and the brachialis [39].

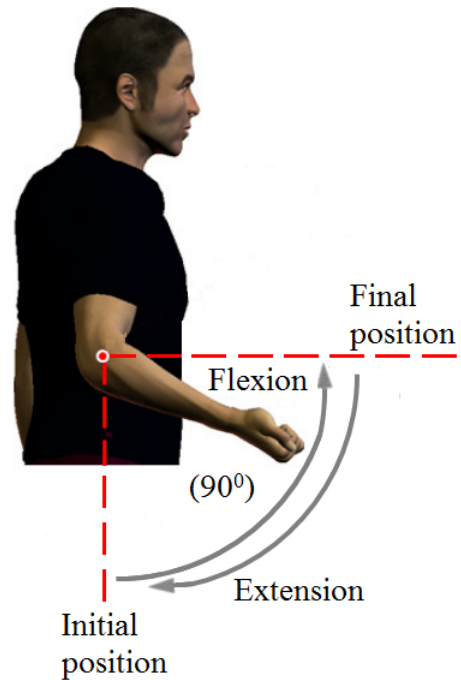


**Figure 5.17.** Arm motion due to motor 3: elbow extension and elbow flexion. Source: Gopura, R.A.R.C. "A Study on Human Upper-Limb Muscles Activities." *International Journal of Bioelectromagnetism* 12, no. 2 (2010): 54-61.

## CHAPTER 6

### KINEMATIC MODELING

#### 6.1 MODIFIED DENAVIT-HARTENBERG

As mentioned previously in Subsection 3.2.2.1, this thesis will use the Modified Denavit-Hartenberg method for the kinematic modeling. All of the link parameters for the robotic arm can be found below in Table 6.1:

**Table 6.1. Modified DH Link Parameters for Robotic Arm**

$i$	$a_{i-1}$ (cm)	$\alpha_{i-1}$ (deg)	$d_i$ (cm)	$\theta_i$ (deg)
1	0	0	0	$\theta_1$
2	8.9954	90	0	$\theta_2$
3	26.1213	0	0	$\theta_3$

Angle  $\theta_i$  is the angle between the  $x_{i-1}$ -axis and the  $x_i$ -axis. Figures 6.1 and 6.2 show the joint angles of the robotic arm.

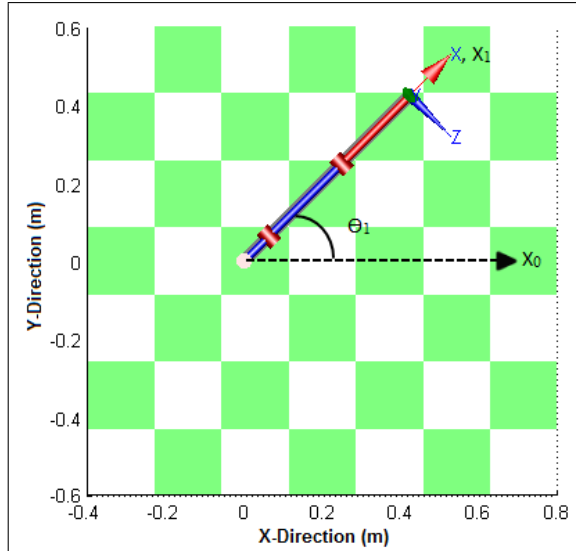


**Figure 6.1. Joint 1 angle.**

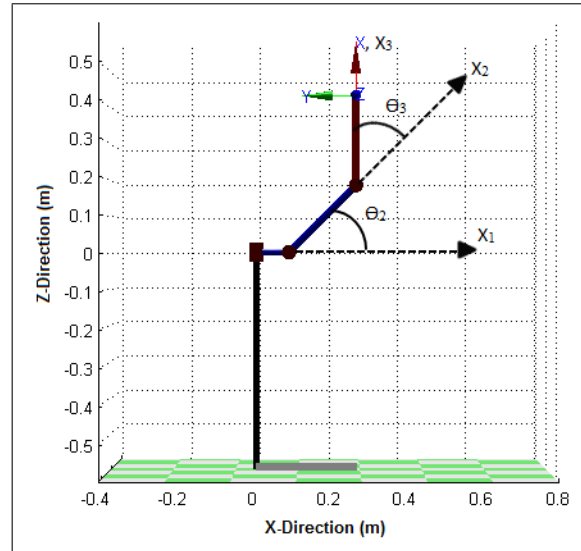


**Figure 6.2. Joint 2 and joint 3 angles.**

### 6.1.1 Link 1

To transform from the frame at link 1 to the global frame, we can plug in  $i = 1$  into Equation (3.17) to get

$${}^0T_1 = \begin{bmatrix} \cos \theta_1 & -\sin \theta_1 & 0 & a_0 \\ \sin \theta_1 \cos \alpha_0 & \cos \theta_1 \cos \alpha_0 & -\sin \alpha_0 & -\sin \alpha_0 d_1 \\ \sin \theta_1 \sin \alpha_0 & \cos \theta_1 \sin \alpha_0 & \cos \alpha_0 & \cos \alpha_0 d_1 \\ 0 & 0 & 0 & 1 \end{bmatrix}. \quad (6.1)$$

Since  $a_0$ ,  $\alpha_0$ , and  $d_1$  are all equal to zero, the transformation matrix simplifies to

$${}^0T_1 = \begin{bmatrix} \cos \theta_1 & -\sin \theta_1 & 0 & 0 \\ \sin \theta_1 & \cos \theta_1 & 0 & 0 \\ 0 & 0 & 1 & 0 \\ 0 & 0 & 0 & 1 \end{bmatrix}. \quad (6.2)$$

### 6.1.2 Link 2

To transform from the frame at link 2 to the frame at link 1, we can plug in  $i = 2$  into Equation (3.17) to get

$${}^1T_2 = \begin{bmatrix} \cos \theta_2 & -\sin \theta_2 & 0 & a_1 \\ \sin \theta_2 \cos \alpha_1 & \cos \theta_2 \cos \alpha_1 & -\sin \alpha_1 & -\sin \alpha_1 d_2 \\ \sin \theta_2 \sin \alpha_1 & \cos \theta_2 \sin \alpha_1 & \cos \alpha_1 & \cos \alpha_1 d_2 \\ 0 & 0 & 0 & 1 \end{bmatrix}. \quad (6.3)$$

Since  $\alpha_1$  and  $d_2$  are all equal to zero, the transformation matrix simplifies to

$${}^1T_2 = \begin{bmatrix} \cos \theta_2 & -\sin \theta_2 & 0 & a_1 \\ 0 & 0 & -1 & 0 \\ \sin \theta_2 & \cos \theta_2 & 0 & 0 \\ 0 & 0 & 0 & 1 \end{bmatrix}. \quad (6.4)$$

To transform from the frame at link 2 into the global frame, the following sequence may be performed:

$${}^0T_2 = {}^0T_1 {}^1T_2 \quad (6.5)$$

$$= \begin{bmatrix} \cos \theta_2 & -\sin \theta_2 & 0 & a_1 \\ 0 & 0 & -1 & 0 \\ \sin \theta_2 & \cos \theta_2 & 0 & 0 \\ 0 & 0 & 0 & 1 \end{bmatrix} \begin{bmatrix} \cos \theta_2 & -\sin \theta_2 & 0 & a_1 \\ 0 & 0 & -1 & 0 \\ \sin \theta_2 & \cos \theta_2 & 0 & 0 \\ 0 & 0 & 0 & 1 \end{bmatrix} \quad (6.6)$$

$$= \begin{bmatrix} \cos \theta_1 \cos \theta_2 & -\cos \theta_1 \sin \theta_2 & \sin \theta_1 & a_1 \cos \theta_1 \\ \sin \theta_1 \cos \theta_2 & -\sin \theta_1 \sin \theta_2 & -\cos \theta_1 & a_1 \sin \theta_1 \\ \sin \theta_2 & \cos \theta_2 & 0 & 0 \\ 0 & 0 & 0 & 1 \end{bmatrix} \quad (6.7)$$

### 6.1.3 Link 3

To transform from the frame at link 3 to the frame at link 2, we can plug in  $i = 3$  into Equation (3.17) to get

$${}^1T_2 = \begin{bmatrix} \cos \theta_3 & -\sin \theta_3 & 0 & a_2 \\ \sin \theta_3 \cos \alpha_2 & \cos \theta_3 \cos \alpha_2 & -\sin \alpha_2 & -\sin \alpha_2 d_3 \\ \sin \theta_3 \sin \alpha_2 & \cos \theta_3 \sin \alpha_2 & \cos \alpha_2 & \cos \alpha_2 d_3 \\ 0 & 0 & 0 & 1 \end{bmatrix}. \quad (6.8)$$

Since  $\alpha_2$  and  $d_3$  are all equal to zero, the transformation matrix simplifies to

$${}^2T_3 = \begin{bmatrix} \cos \theta_3 & -\sin \theta_3 & 0 & a_2 \\ \sin \theta_3 & \cos \theta_3 & 0 & 0 \\ 0 & 0 & 1 & 0 \\ 0 & 0 & 0 & 1 \end{bmatrix}. \quad (6.9)$$

To transform from the frame at link 3 into the global frame, the following sequence may be performed:

$${}^0T_3 = {}^0T_1 {}^1T_2 {}^2T_3 \quad (6.10)$$

$$= {}^0T_2 {}^2T_3 \quad (6.11)$$

$$= \begin{bmatrix} \cos \theta_1 \cos \theta_2 & -\cos \theta_1 \sin \theta_2 & \sin \theta_1 & a_1 \cos \theta_1 \\ \sin \theta_1 \cos \theta_2 & -\sin \theta_1 \sin \theta_2 & -\cos \theta_1 & a_1 \sin \theta_1 \\ \sin \theta_2 & \cos \theta_2 & 0 & 0 \\ 0 & 0 & 0 & 1 \end{bmatrix} \begin{bmatrix} \cos \theta_3 & -\sin \theta_3 & 0 & a_2 \\ \sin \theta_3 & \cos \theta_3 & 0 & 0 \\ 0 & 0 & 1 & 0 \\ 0 & 0 & 0 & 1 \end{bmatrix} \quad (6.12)$$

$$= \begin{bmatrix} c\theta_1 c\theta_2 c\theta_3 - c\theta_1 s\theta_2 s\theta_3 & -c\theta_1 c\theta_2 s\theta_3 - c\theta_1 s\theta_2 c\theta_3 & s\theta_1 & a_2 c\theta_1 c\theta_2 + a_1 s\theta_1 \\ s\theta_1 c\theta_2 c\theta_3 - s\theta_1 s\theta_2 s\theta_3 & -s\theta_1 c\theta_2 s\theta_3 - s\theta_1 s\theta_2 c\theta_3 & -c\theta_1 & a_2 s\theta_1 c\theta_2 + a_1 s\theta_1 \\ s\theta_2 c\theta_3 + c\theta_2 s\theta_3 & -s\theta_2 s\theta_3 + c\theta_2 c\theta_3 & 0 & a_2 s\theta_2 \\ 0 & 0 & 0 & 1 \end{bmatrix} \quad (6.13)$$

where  $c\theta_i$  is shorthand for  $\cos \theta_i$ , and  $s\theta_i$  is shorthand for  $\sin \theta_i$ .

### 6.1.4 End-Effector

The end-effector position is calculated by using Equation (6.13) to transform the end-effector position in the frame of joint 3 to the global frame. Equation (6.14) shows the transformation for this particular robot with 3 joints:

$${}^0r_{EE} = {}^0T_3 {}^3r_{EE} \quad (6.14)$$

where  $r_{EE}$  is the position of the end-effector.

The vector of the end-effector in the frame of joint 3 is

$${}^3r_{EE} = \begin{Bmatrix} 24.765 \\ 0 \\ 0 \\ 1 \end{Bmatrix}, \quad (6.15)$$

in which the location of the end-effector is 24.765 m away from the origin of joint 3 in the x-direction of the frame.

## 6.2 WORKSPACE

The workspace shows all the possible locations of a robot's end-effector. Knowing the limits of the joints, Equation (6.15) can be used to calculate the end-effector position at those limits. Figure 6.3 shows the workspace in the XY plane, and Figure 6.4 shows the workspace in the XZ plane.

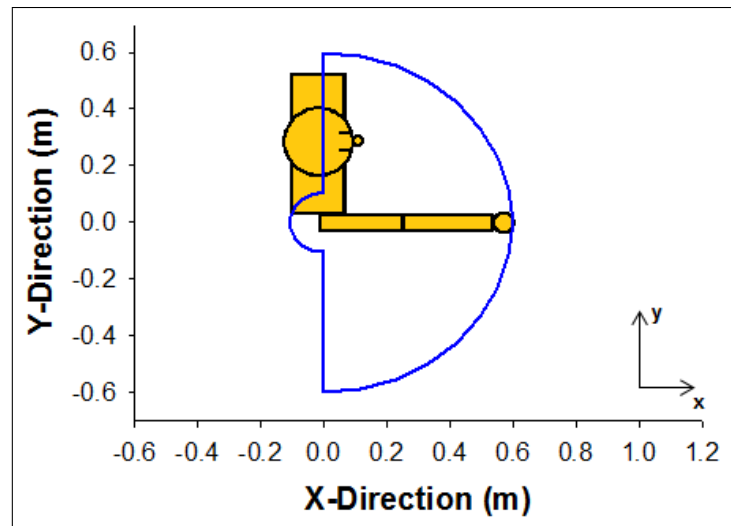


**Figure 6.3.** End-effector workspace in XY plane.

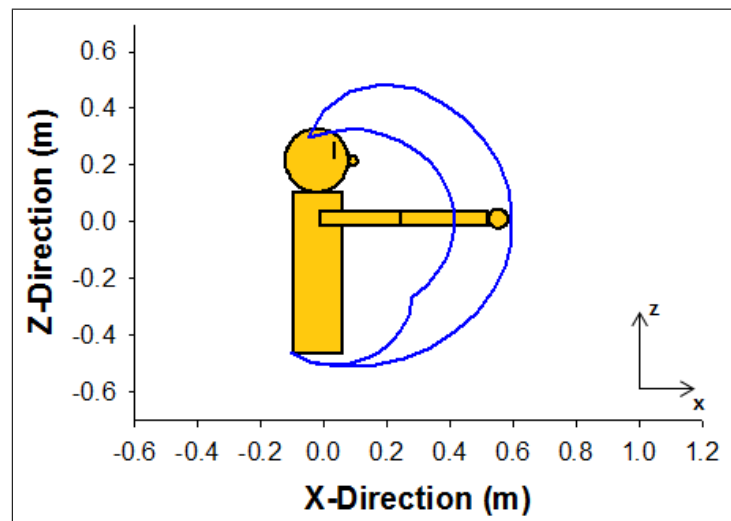


**Figure 6.4.** End-effector workspace in XZ plane.

## CHAPTER 7

### DYNAMIC MODELING

#### 7.1 TRUNCATED NOTATION

For the sake of reducing space, I will use the following notation:

- $s \rightarrow s$
- $c \rightarrow c$
- $\theta_2 + \theta_3 \rightarrow \theta_{23}$

#### 7.2 LOCATION OF CENTER OF MASS

To simplify the derivation, the location of mass will be assumed to exist on the links' x-axis only. The center of mass for all three links then become:

$$\vec{r}_{c_1} = \begin{Bmatrix} \frac{l_1}{2}c\theta_1 \\ \frac{l_1}{2}s\theta_1 \\ 0 \end{Bmatrix}, \quad (7.1)$$

$$\vec{r}_{c_2} = \begin{Bmatrix} (l_1 + \frac{l_2}{2}c\theta_2) c\theta_1 \\ (l_1 + \frac{l_2}{2}c\theta_2) s\theta_1 \\ \frac{l_2}{2}s\theta_2 \end{Bmatrix} \quad (7.2)$$

$$\vec{r}_{c_3} = \begin{Bmatrix} [l_1 + l_2c\theta_2 + \frac{l_3}{2}c\theta_{23}] c\theta_1 \\ [l_1 + l_2c\theta_2 + \frac{l_3}{2}c\theta_{23}] s\theta_1 \\ l_2s\theta_2 + \frac{l_3}{2}s\theta_{23} \end{Bmatrix}, \quad (7.3)$$

The terms  $l_1$  and  $l_2$  are equal to the values  $a_1$  and  $a_2$  from Table 6.1, respectively. The term  $l_3$  is equal to 24.765 m from Equation (6.15).

##### 7.2.1 Velocity at Link Center of Mass

The velocity of the link's center of mass is simply the time derivative of the position vector of the center of mass:

$$\vec{v}_{c_i} = \frac{d}{dt} \vec{r}_{c_i} = \sum_{i=1}^n \dot{\theta}_i \frac{d}{d\theta_i} \vec{r}_{c_i}. \quad (7.4)$$

Plugging in Equations (7.1) through (7.3) leads to:

$$\vec{v}_{c_1} = \begin{Bmatrix} -\dot{\theta}_1 \frac{l_1}{2} s\theta_1 \\ \dot{\theta}_1 \frac{l_1}{2} c\theta_1 \\ 0 \end{Bmatrix}; \quad (7.5)$$

$$\vec{v}_{c_2} = \begin{Bmatrix} -\dot{\theta}_1 \left( l_1 + \frac{l_2}{2} c\theta_2 \right) s\theta_1 - \dot{\theta}_2 \frac{l_2}{2} s\theta_2 c\theta_1 \\ \dot{\theta}_1 \left( l_1 + \frac{l_2}{2} c\theta_2 \right) c\theta_1 - \dot{\theta}_2 \frac{l_2}{2} s\theta_2 s\theta_1 \\ \dot{\theta}_2 \frac{l_2}{2} c\theta_2 \end{Bmatrix}; \quad (7.6)$$

$$\vec{v}_{c_3} = \begin{Bmatrix} -\dot{\theta}_1 \left[ l_1 + l_2 c\theta_2 + \frac{l_3}{2} c\theta_{23} \right] s\theta_1 - \dot{\theta}_2 \left[ l_2 s\theta_2 + \frac{l_3}{2} s\theta_{23} \right] c\theta_1 - \dot{\theta}_3 \frac{l_3}{2} s\theta_{23} c\theta_1 \\ \dot{\theta}_1 \left[ l_1 + l_2 c\theta_2 + \frac{l_3}{2} c\theta_{23} \right] c\theta_1 - \dot{\theta}_2 \left[ l_2 s\theta_2 + \frac{l_3}{2} s\theta_{23} \right] c\theta_1 - \dot{\theta}_3 \frac{l_3}{2} s\theta_{23} s\theta_1 \\ \dot{\theta}_2 \left( l_2 c\theta_2 + \frac{l_3}{2} c\theta_{23} \right) + \dot{\theta}_3 \frac{l_3}{2} c\theta_{23} \end{Bmatrix}. \quad (7.7)$$

## 7.3 KINETIC ENERGY

### 7.3.1 Joint 1

#### 7.3.1.1 LINEAR KINETIC ENERGY FOR JOINT 1

The linear kinetic energy of joint 1 can be calculated as follows:

$$T_{1_{linear}} = \frac{1}{2} m_1 v_{c_1}^2. \quad (7.8)$$

The term  $v_{c_1}^2$  is calculated as

$$v_{c_1}^2 = (v_{c_{1x}})^2 + (v_{c_{1y}})^2 \quad (7.9)$$

$$= \dot{\theta}_1^2 \frac{l_1^2}{4} (\sin^2 \theta_1 + \cos^2 \theta_1) \quad (7.10)$$

$$= \dot{\theta}_1^2 \frac{l_1^2}{4}, \quad (7.11)$$

where  $v_{c_{1x}}$  is the first row and  $v_{c_{1y}}$  is the second row of Equation (7.5), respectively. Plugging in Equation (7.11) into Equation (7.8) leads to

$$T_{1_{linear}} = \frac{1}{2} m_1 \dot{\theta}_1^2 \frac{l_1^2}{4}. \quad (7.12)$$

#### 7.3.1.2 ROTATIONAL KINETIC ENERGY FOR JOINT 1

The rotational kinetic energy of joint 1 can be calculated as follows:

$$T_{1_{rotational}} = \frac{1}{2} \omega_1^T {}^0 I_{c1} \omega_1 \quad (7.13)$$

The term  $\omega_1$  is

$$\omega_1 = \begin{bmatrix} 0 \\ 0 \\ \dot{\theta}_1 \end{bmatrix}. \quad (7.14)$$

And the term  ${}^0 I_{c1}$  is calculated as

$${}^0 I_{c1} = {}^0 R_1^{-1} {}^0 I_{c1} {}^0 R_1^T \quad (7.15)$$

$$= \begin{bmatrix} c\theta_1 & -s\theta_1 & 0 \\ s\theta_1 & c\theta_1 & 0 \\ 0 & 0 & 1 \end{bmatrix} \begin{bmatrix} I_{xx_1} & I_{xy_1} & I_{xz_1} \\ I_{xy_1} & I_{yy_1} & I_{yz_1} \\ I_{xz_1} & I_{yz_1} & I_{zz_1} \end{bmatrix} \begin{bmatrix} c\theta_1 & s\theta_1 & 0 \\ -s\theta_1 & c\theta_1 & 0 \\ 0 & 0 & 1 \end{bmatrix} \quad (7.16)$$

$$= \begin{bmatrix} {}^0 I_{c1}(1, 1) & {}^0 I_{c1}(1, 2) & {}^0 I_{c1}(1, 3) \\ {}^0 I_{c1}(2, 1) & {}^0 I_{c1}(2, 2) & {}^0 I_{c1}(2, 3) \\ {}^0 I_{c1}(3, 1) & {}^0 I_{c1}(3, 2) & {}^0 I_{c1}(3, 3) \end{bmatrix} \quad (7.17)$$

where

- ${}^0 I_{c1}(1, 1) = I_{xx_1} c^2 \theta_1 + I_{yy_1} s^2 \theta_1 - I_{xy_1} s(2\theta_1)$
- ${}^0 I_{c1}(1, 2) = I_{xx_1} s\theta_1 c\theta_1 + I_{xy_1} c(2\theta_1) - \frac{I_{yy_1}}{2} s(2\theta_1)$
- ${}^0 I_{c1}(1, 3) = I_{xz_1} c\theta_1 - I_{yz_1} s\theta_1$
- ${}^0 I_{c1}(2, 1) = \frac{I_{xx_1}}{2} s(2\theta_1) - \frac{I_{yy_1}}{2} s(2\theta_1) + I_{xy_1} c(2\theta_1)$
- ${}^0 I_{c1}(2, 2) = I_{xx_1} s^2 \theta_1 + I_{xy_1} s(2\theta_1) + I_{yy_1} c^2 \theta_1$
- ${}^0 I_{c1}(2, 3) = I_{xz_1} s\theta_1 + I_{yz_1} c\theta_1$
- ${}^0 I_{c1}(3, 1) = I_{xz_1} c\theta_1 - I_{yz_1} s\theta_1$
- ${}^0 I_{c1}(3, 2) = I_{yz_1} c\theta_1 + I_{xz_1} s\theta_1$
- ${}^0 I_{c1}(3, 3) = I_{zz_1}$

Plugging in Equations (7.14) and (7.17) into Equation (7.13) results in the following:

$$T_{1_{rotational}} = \frac{1}{2} \begin{bmatrix} 0 & 0 & \dot{\theta}_1 \end{bmatrix} \begin{bmatrix} {}^0 I_{c1} \end{bmatrix} \begin{bmatrix} 0 \\ 0 \\ \dot{\theta}_1 \end{bmatrix} \quad (7.18)$$

$$= \frac{1}{2} \dot{\theta}_1 I_{zz_1}. \quad (7.19)$$

### 7.3.1.3 TOTAL KINETIC ENERGY FOR JOINT 1

The total kinetic energy for joint 1 is then a matter of summing Equations (7.8) and (7.13) as follows:

$$T_1 = T_{1_{linear}} + T_{1_{rotational}} \quad (7.20)$$

$$= \frac{1}{2}m_1\dot{\theta}_1^2\frac{l_1^2}{4} + \frac{1}{2}\dot{\theta}_1^2I_{zz1}. \quad (7.21)$$

### 7.3.2 Joint 2

#### 7.3.2.1 LINEAR KINETIC ENERGY FOR JOINT 2

The linear kinetic energy of joint 2 can be calculated as follows:

$$T_{2_{linear}} = \frac{1}{2}m_2v_{c2}^2. \quad (7.22)$$

The term  $v_{c2}^2$  is calculated as

$$v_{c2}^2 = (v_{c2x})^2 + (v_{c2y})^2 + (v_{c2z})^2 \quad (7.23)$$

$$\begin{aligned} &= \left\{ \dot{\theta}_1^2 \left( l_1 + \frac{l_2}{2}c\theta_2 \right)^2 s^2\theta_1 + \dot{\theta}_2 \frac{l_2^2}{4}c^2\theta_1s^2\theta_2 + \dot{\theta}_1\dot{\theta}_2 \frac{l_2}{2} \left( l_1 + \frac{l_2}{2}c\theta_2 \right) s\theta_1c\theta_1s\theta_2 \right\} \\ &\quad + \left\{ \dot{\theta}_1^2 \left( l_1 + \frac{l_2}{2}c\theta_2 \right)^2 c^2\theta_1 + \dot{\theta}_2 \frac{l_2^2}{4}s^2\theta_1s^2\theta_2 - \dot{\theta}_1\dot{\theta}_2 \frac{l_2}{2} \left( l_1 + \frac{l_2}{2}c\theta_2 \right) s\theta_1c\theta_1s\theta_2 \right\} \end{aligned} \quad (7.24)$$

$$\begin{aligned} &+ \left\{ \dot{\theta}_2 \frac{l_2^2}{4}c^2\theta_2 \right\} \\ &= \dot{\theta}_1^2 \left( l_1 + \frac{l_2}{2}c\theta_2 \right)^2 + \dot{\theta}_2 \frac{l_2^2}{4} \end{aligned} \quad (7.25)$$

where  $v_{c2x}$  is the first row,  $v_{c2y}$  is the second row, and  $v_{c2z}$  is the third row of Equation (7.7), respectively. Plugging in Equation (7.25) into Equation (7.22) leads to

$$T_{2_{linear}} = \frac{1}{2}m_2 \left[ \dot{\theta}_1^2 \left( l_1 + \frac{l_2}{2}c\theta_2 \right)^2 + \dot{\theta}_2 \frac{l_2^2}{4} \right]. \quad (7.26)$$

#### 7.3.2.2 ROTATIONAL KINETIC ENERGY FOR JOINT 2

The rotational kinetic energy of joint 2 can be calculated as follows:

$$T_{2_{rotational}} = \frac{1}{2} \omega_2^T {}^0 I_{c_2} \omega_2 \quad (7.27)$$

The term  $\omega_2$  is

$$\omega_2 = \begin{bmatrix} \dot{\theta}_2 s\theta_1 \\ -\dot{\theta}_2 c\theta_1 \\ \dot{\theta}_1 \end{bmatrix}. \quad (7.28)$$

And the term  ${}^0 I_{c_2}$  is calculated as

$${}^0 I_{c_2} = {}^0 R_2 {}^2 I_{c_2} {}^0 R_2^T, \quad (7.29)$$

where

$${}^0 R_2 = \begin{bmatrix} c\theta_1 & -s\theta_1 & 0 \\ s\theta_1 & c\theta_1 & 0 \\ 0 & 0 & 1 \end{bmatrix} \begin{bmatrix} 1 & 0 & 0 \\ 0 & c\alpha_1 & -s\alpha_1 \\ 0 & s\alpha_1 & c\alpha_1 \end{bmatrix} \begin{bmatrix} c\theta_2 & -s\theta_2 & 0 \\ s\theta_2 & c\theta_2 & 0 \\ 0 & 0 & 1 \end{bmatrix}. \quad (7.30)$$

Plugging in  $\alpha_1 = \frac{\pi}{2}$  yields

$${}^0 R_2 = \begin{bmatrix} c\theta_1 & -s\theta_1 & 0 \\ s\theta_1 & c\theta_1 & 0 \\ 0 & 0 & 1 \end{bmatrix} \begin{bmatrix} 1 & 0 & 0 \\ 0 & 0 & -1 \\ 0 & 1 & 0 \end{bmatrix} \begin{bmatrix} c\theta_2 & -s\theta_2 & 0 \\ s\theta_2 & c\theta_2 & 0 \\ 0 & 0 & 1 \end{bmatrix} \quad (7.31)$$

$$= \begin{bmatrix} c\theta_1 c\theta_2 & -c\theta_1 s\theta_2 & s\theta_1 \\ c\theta_2 s\theta_1 & -s\theta_1 s\theta_2 & -c\theta_1 \\ s\theta_2 & c\theta_2 & 0 \end{bmatrix}. \quad (7.32)$$

Plugging in Equation (7.32) into Equation (7.29):

$${}^0 I_{c_2} = {}^0 R_2 {}^2 I_{c_2} {}^0 R_2^T \quad (7.33)$$

$$= \begin{bmatrix} c\theta_1 c\theta_2 & -c\theta_1 s\theta_2 & s\theta_1 \\ c\theta_2 s\theta_1 & -s\theta_1 s\theta_2 & -c\theta_1 \\ s\theta_2 & c\theta_2 & 0 \end{bmatrix} \begin{bmatrix} I_{xx_2} & I_{xy_2} & I_{xz_2} \\ I_{xy_2} & I_{yy_2} & I_{yz_2} \\ I_{xz_2} & I_{yz_2} & I_{zz_2} \end{bmatrix} \begin{bmatrix} c\theta_1 c\theta_2 & c\theta_2 s\theta_1 & s\theta_2 \\ -c\theta_1 s\theta_2 & -s\theta_1 s\theta_2 & c\theta_2 \\ s\theta_1 & -c\theta_1 & 0 \end{bmatrix} \quad (7.34)$$

$$= \begin{bmatrix} {}^0 I_{c_2}(1,1) & {}^0 I_{c_2}(1,2) & {}^0 I_{c_2}(1,3) \\ {}^0 I_{c_2}(2,1) & {}^0 I_{c_2}(2,2) & {}^0 I_{c_2}(2,3) \\ {}^0 I_{c_2}(3,1) & {}^0 I_{c_2}(3,2) & {}^0 I_{c_2}(3,3) \end{bmatrix} \quad (7.35)$$

where

- ${}^0I_{c_2}(1, 1) = I_{xx_2}c^2\theta_1c^2\theta_2 + I_{yy_2}c^2\theta_1s^2\theta_2 + I_{zz_2}s^2\theta_1 - 2I_{xy_2}c^2\theta_1c\theta_2s\theta_2 + 2I_{xz_2}c\theta_1c\theta_2s\theta_1 - 2I_{yz_2}c\theta_1s\theta_1s\theta_2$
- ${}^0I_{c_2}(1, 2) = I_{xx_2}c\theta_1c^2\theta_2s\theta_1 + I_{yy_2}c\theta_1s\theta_1s^2\theta_2 - I_{zz_2}c\theta_1s\theta_1 - I_{xz_2}c(2\theta_1)c\theta_2 + I_{yz_2}c(2\theta_1)s\theta_2 - 2I_{xy_2}c\theta_1c\theta_2s\theta_1s\theta_2$
- ${}^0I_{c_2}(1, 3) = I_{xx_2}c\theta_1c\theta_2s\theta_2 - I_{yy_2}c\theta_1c\theta_2s\theta_2 + I_{xy_2}c\theta_1c(2\theta_2) + I_{xz_2}s\theta_1s\theta_2 + I_{yz_2}c\theta_2s\theta_1$
- ${}^0I_{c_2}(2, 1) = I_{xx_2}c\theta_1c^2\theta_2s\theta_1 + I_{yy_2}c\theta_1s\theta_1s^2\theta_2 - I_{zz_2}c\theta_1s\theta_1 - 2I_{xy_2}c\theta_1c\theta_2s\theta_1s\theta_2 - I_{xz_2}c(2\theta_1)c\theta_2 + I_{yz_2}c(2\theta_1)s\theta_2$
- ${}^0I_{c_2}(2, 2) = I_{xx_2}c^2\theta_2s^2\theta_1 + I_{yy_2}s^2\theta_1s^2\theta_2 + I_{zz_2}c^2\theta_1 - 2I_{xy_2}c\theta_2s^2\theta_1s\theta_2 - 2I_{xz_2}c\theta_1c\theta_2s\theta_1 + 2I_{yz_2}c\theta_1s\theta_1s\theta_2$
- ${}^0I_{c_2}(2, 3) = I_{xx_2}c\theta_2s\theta_1s\theta_2 - I_{yy_2}c\theta_2s\theta_1s\theta_2 + I_{xy_2}c(2\theta_2)s\theta_1 - I_{xz_2}c\theta_1s\theta_2 - I_{yz_2}c\theta_1\theta_2$
- ${}^0I_{c_2}(3, 1) = I_{xx_2}c\theta_1c\theta_2s\theta_2 - I_{yy_2}c\theta_1c\theta_2s\theta_2 + I_{xy_2}c\theta_1c(2\theta_2) + I_{xz_2}s\theta_1s\theta_2 + I_{yz_2}c\theta_1s\theta_1$
- ${}^0I_{c_2}(3, 2) = I_{xx_2}c\theta_2s\theta_1s\theta_2 - I_{yy_2}c\theta_2s\theta_1s\theta_2 + I_{xy_2}c(2\theta_2)s\theta_1 - I_{xz_2}c\theta_1s\theta_2 - I_{yz_2}c\theta_1c\theta_2$
- ${}^0I_{c_2}(3, 3) = I_{xx_2}s^2\theta_2 + I_{yy_2}c^2\theta_2 + 2I_{xy_2}c\theta_2s\theta_2$

Plugging in Equations (7.28) and (7.35) into Equation (7.27) results in the following:

$$T_{2_{rotational}} = \frac{1}{2} \begin{bmatrix} \dot{\theta}_2s\theta_1 & -\dot{\theta}_2c\theta_1 & \dot{\theta}_1 \end{bmatrix} [{}^0I_{c_2}] \begin{bmatrix} \dot{\theta}_2s\theta_1 \\ -\dot{\theta}_2c\theta_1 \\ \dot{\theta}_1 \end{bmatrix} \quad (7.36)$$

$$= \frac{1}{2} \left[ \dot{\theta}_1^2 I_{xx_2}s^2\theta_2 + \dot{\theta}_1^2 I_{yy_2}c^2\theta_2 + \dot{\theta}_2^2 I_{zz_2} + \dot{\theta}_1^2 I_{xy_2}s(2\theta_2) + 2\dot{\theta}_1\dot{\theta}_2 I_{xz_2}s\theta_2 + 2\dot{\theta}_1\dot{\theta}_2 I_{yz_2}c\theta_2 \right] \quad (7.37)$$

### 7.3.2.3 TOTAL KINETIC ENERGY FOR JOINT 2

The total kinetic energy for joint 2 is then a matter of summing Equations (7.22) and (7.27) as follows:

$$T_2 = T_{2_{linear}} + T_{2_{rotational}} \quad (7.38)$$

$$\begin{aligned} &= \frac{1}{2}m_2 \left[ \dot{\theta}_1^2 \left( l_1 + \frac{l_2}{2}c\theta_2 \right)^2 + \dot{\theta}_2 \frac{l_2^2}{4} \right] \\ &\quad + \frac{1}{2} \left[ \dot{\theta}_1^2 I_{xx_2}s^2\theta_2 + \dot{\theta}_1^2 I_{yy_2}c^2\theta_2 + \dot{\theta}_2^2 I_{zz_2} + \dot{\theta}_1^2 I_{xy_2}s(2\theta_2) + 2\dot{\theta}_1\dot{\theta}_2 I_{xz_2}s\theta_2 + 2\dot{\theta}_1\dot{\theta}_2 I_{yz_2}c\theta_2 \right] \end{aligned} \quad (7.39)$$

### 7.3.3 Joint 3

#### 7.3.3.1 LINEAR KINETIC ENERGY FOR JOINT 3

The linear kinetic energy of joint 3 can be calculated as follows:

$$T_{3_{linear}} = \frac{1}{2}m_3v_{c3}^2 \quad (7.40)$$

The term  $v_{c3}^2$  is calculated as

$$v_{c3}^2 = (v_{c3_x})^2 + (v_{c3_y})^2 + (v_{c3_z})^2, \quad (7.41)$$

where the terms  $v_{c3_x}^2$ ,  $v_{c3_y}^2$ , and  $v_{c3_z}^2$  are calculated as follows:

$$\begin{aligned} v_{c3_x}^2 = & \left\{ \dot{\theta}_1^2 \left[ l_1 + l_2 c\theta_2 + \frac{l_3}{2} c\theta_{23} \right]^2 s^2 \theta_1 + \dot{\theta}_1 \dot{\theta}_2 \left[ l_2 s\theta_2 + \frac{l_3}{2} s\theta_{23} \right] \left[ l_1 + l_2 c\theta_2 + \frac{l_3}{2} c\theta_{23} \right] c\theta_1 s\theta_1 \right. \\ & + \dot{\theta}_1 \dot{\theta}_3 \frac{l_3}{2} \left[ l_1 + l_2 c\theta_2 + \frac{l_3}{2} c\theta_{23} \right] c\theta_1 s\theta_1 s\theta_{23} \\ & + \dot{\theta}_2^2 \left[ l_1 s\theta_2 + \frac{l_3}{2} s\theta_{23} \right]^2 c^2 \theta_1 + \dot{\theta}_1 \dot{\theta}_2 \left[ l_2 s\theta_2 + \frac{l_3}{2} s\theta_{23} \right] \left[ l_1 + l_2 c\theta_2 + \frac{l_3}{2} c\theta_{23} \right] c\theta_1 s\theta_1 \\ & + \dot{\theta}_2 \dot{\theta}_3 \frac{l_3}{2} \left[ l_2 s\theta_2 + \frac{l_3}{2} s\theta_{23} \right] c^2 \theta_1 s\theta_{23} \\ & + \dot{\theta}_3^2 \frac{l_3^2}{4} c^2 \theta_1 s^2 \theta_{23} + \dot{\theta}_1 \dot{\theta}_3 \frac{l_3}{2} \left[ l_1 + l_2 c\theta_2 + \frac{l_3}{2} c\theta_{23} \right] c\theta_1 s\theta_1 s\theta_{23} \\ & \left. + \dot{\theta}_2 \dot{\theta}_3 \frac{l_3}{2} \left[ l_2 s\theta_2 + \frac{l_3}{2} s\theta_{23} \right] c^2 \theta_1 s\theta_{23} \right\} \end{aligned} \quad (7.42)$$

$$\begin{aligned}
v_{c_{3y}}^2 = & \left\{ \dot{\theta}_1^2 \left[ l_1 + l_2 c\theta_2 + \frac{l_3}{2} c\theta_{23} \right]^2 c^2 \theta_1 - \dot{\theta}_1 \dot{\theta}_2 \left[ l_2 s\theta_2 + \frac{l_3}{2} s\theta_{23} \right] \left[ l_1 + l_2 c\theta_2 + \frac{l_3}{2} c\theta_{23} \right] c\theta_1 s\theta_1 \right. \\
& - \dot{\theta}_1 \dot{\theta}_3 \frac{l_3}{2} \left[ l_1 + l_2 c\theta_2 \frac{l_3}{2} c\theta_{23} \right] c\theta_1 s\theta_1 s\theta_{23} \\
& + \dot{\theta}_2 \left[ l_2 s\theta_2 + \frac{l_3}{2} s\theta_{23} \right]^2 s^2 \theta_1 - \dot{\theta}_1 \dot{\theta}_2 \left[ l_2 s\theta_2 + \frac{l_3}{2} s\theta_{23} \right] \left[ l_1 + l_2 c\theta_2 + \frac{l_3}{2} c\theta_{23} \right] c\theta_1 s\theta_1 \\
& + \dot{\theta}_2 \dot{\theta}_3 \frac{l_3}{2} \left[ l_2 s\theta_2 + \frac{l_3}{2} s\theta_{23} \right] s^2 \theta_1 s\theta_{23} \\
& + \dot{\theta}_3^2 \frac{l_3^2}{4} s^2 \theta_1 s^2 \theta_{23} - \dot{\theta}_1 \dot{\theta}_3 \frac{l_3}{2} \left[ l_1 + l_2 c\theta_2 + \frac{l_3}{2} c\theta_{23} \right] c\theta_1 s\theta_1 s\theta_{23} \\
& \left. + \dot{\theta}_2 \dot{\theta}_3 \frac{l_3}{2} \left[ l_2 s\theta_2 + \frac{l_3}{2} s\theta_{23} \right] s^2 \theta_1 s\theta_{23} \right\} \\
& \quad (7.43)
\end{aligned}$$

$$v_{c_{3z}}^2 = \left\{ \dot{\theta}_2^2 \left[ l_2 c\theta_2 + \frac{l_3}{2} c\theta_{23} \right]^2 + \dot{\theta}_3^2 \frac{l_3^2}{4} c^2 \theta_{23} + 2\dot{\theta}_2 \dot{\theta}_3 \frac{l_3}{2} \left[ l_2 c\theta_2 + \frac{l_3}{2} c\theta_{23} \right] c\theta_{23} \right\} \quad (7.44)$$

From Equation (7.7),  $v_{c_{3x}}$  is the first row,  $v_{c_{3y}}$  is the second row, and  $v_{c_{3z}}$  is the third row, respectively. Equations (7.42), (7.43), and (7.44) can be plugged into Equation (7.41) to get

$$\begin{aligned}
v_{c_3}^2 = & \dot{\theta}_1^2 \left( l_1^2 + l_2^2 c^2 \theta_2 + \frac{l_3^2}{4} c^2 \theta_{23} + 2l_1 l_2 c\theta_2 + l_1 l_3 c\theta_{23} + l_2 l_3 c\theta_2 c\theta_{23} \right) \\
& + \dot{\theta}_2^2 \left( l_2^2 + l_2 l_3 c\theta_3 + \frac{l_3^2}{4} \right) + \dot{\theta}_3^2 \frac{l_3^2}{4} + 2\dot{\theta}_2 \dot{\theta}_3 \frac{l_3}{2} \left( l_2 c\theta_3 + \frac{l_3}{2} \right).
\end{aligned} \quad (7.45)$$

Plugging in Equation (7.45) into Equation (7.40) leads to

$$\begin{aligned}
T_{3_{linear}} = & \frac{1}{2} m_3 \left[ \dot{\theta}_1^2 \left( l_1^2 + l_2^2 c^2 \theta_2 + \frac{l_3^2}{4} c^2 \theta_{23} + 2l_1 l_2 c\theta_2 + l_1 l_3 c\theta_{23} + l_2 l_3 c\theta_2 c\theta_{23} \right) \right. \\
& \left. + \dot{\theta}_2^2 \left( l_2^2 + l_2 l_3 c\theta_3 + \frac{l_3^2}{4} \right) + \dot{\theta}_3^2 \frac{l_3^2}{4} + 2\dot{\theta}_2 \dot{\theta}_3 \frac{l_3}{2} \left( l_2 c\theta_3 + \frac{l_3}{2} \right) \right].
\end{aligned} \quad (7.46)$$

### 7.3.3.2 ROTATIONAL KINETIC ENERGY FOR JOINT 3

The rotational kinetic energy of joint 3 can be calculated as follows:

$$T_{3_{rotational}} = \frac{1}{2} \omega_3^T I_{c_3} \omega_3 \quad (7.47)$$

The term  $\omega_3$  is

$$\omega_3 = \begin{bmatrix} (\dot{\theta}_2 + \dot{\theta}_3) s\theta_1 \\ -(\dot{\theta}_2 + \dot{\theta}_3) c\theta_1 \\ \dot{\theta}_1 \end{bmatrix}. \quad (7.48)$$

And the term  ${}^0I_{c_3}$  is calculated as

$${}^0I_{c_3} = {}^0R_3 {}^3I_{c_3} {}^0R_3^T \quad (7.49)$$

where

$${}^0R_3 = {}^0R_2 {}^2R_3 \quad (7.50)$$

$$= \begin{bmatrix} c\theta_1 c\theta_2 & -c\theta_1 s\theta_2 & s\theta_1 \\ s\theta_1 c\theta_2 & -s\theta_1 s\theta_2 & -c\theta_1 \\ s\theta_2 & c\theta_2 & 0 \end{bmatrix} \begin{bmatrix} c\theta_3 & -s\theta_3 & 0 \\ s\theta_3 & c\theta_3 & 0 \\ 0 & 0 & 1 \end{bmatrix} \quad (7.51)$$

$$= \begin{bmatrix} c\theta_1 c\theta_{23} & -c\theta_1 s\theta_{23} & s\theta_1 \\ c\theta_{23} s\theta_1 & -s\theta_{23} s\theta_1 & -c\theta_1 \\ s\theta_{23} & c\theta_{23} & 0 \end{bmatrix} \quad (7.52)$$

Plugging in Equation (7.52) into Equation (7.49):

$${}^0I_{c_3} = {}^0R_3 {}^3I_{c_3} {}^0R_3^T \quad (7.53)$$

$$= \begin{bmatrix} c\theta_1 c\theta_{23} & -c\theta_1 s\theta_{23} & s\theta_1 \\ c\theta_{23} s\theta_1 & -s\theta_{23} s\theta_1 & -c\theta_1 \\ s\theta_{23} & c\theta_{23} & 0 \end{bmatrix} \begin{bmatrix} I_{xx_3} & I_{xy_3} & I_{xz_3} \\ I_{xy_3} & I_{yy_3} & I_{yz_3} \\ I_{xz_3} & I_{yz_3} & I_{zz_3} \end{bmatrix} \begin{bmatrix} c\theta_1 c\theta_{23} & c\theta_{23} s\theta_1 & s\theta_{23} \\ -c\theta_1 s\theta_{23} & -s\theta_1 s\theta_{23} & c\theta_{23} \\ s\theta_1 & -c\theta_1 & 0 \end{bmatrix} \quad (7.54)$$

$$= \begin{bmatrix} {}^0I_{c_3}(1, 1) & {}^0I_{c_3}(1, 2) & {}^0I_{c_3}(1, 3) \\ {}^0I_{c_3}(2, 1) & {}^0I_{c_3}(2, 2) & {}^0I_{c_3}(2, 3) \\ {}^0I_{c_3}(3, 1) & {}^0I_{c_3}(3, 2) & {}^0I_{c_3}(3, 3) \end{bmatrix} \quad (7.55)$$

where

- ${}^0I_{c_3}(1, 1) = I_{xx_3} c^2 \theta_1 c^2 \theta_{23} + I_{yy_3} c^2 \theta_1 s^2 \theta_{23} + I_{zz_3} s^2 \theta_1$   
 $- 2I_{xy_3} c^2 \theta_1 c\theta_{23} s\theta_{23} + 2I_{xz_3} c\theta_1 c\theta_{23} s\theta_1 - 2I_{yz_3} c\theta_1 s\theta_1 s\theta_{23}$
- ${}^0I_{c_3}(1, 2) = I_{xx_3} c\theta_1 c^2 \theta_{23} s\theta_1 + I_{yy_3} c\theta_1 s\theta_1 s^2 \theta_{23} - I_{zz_3} c\theta_1 s\theta_1$   
 $- I_{xz_3} c(2\theta_1) c\theta_{23} + I_{yz_3} c(2\theta_1) s\theta_{23} - 2I_{xy_3} c\theta_1 c\theta_{23} s\theta_1 s\theta_{23}$

- ${}^0I_{c_3}(1, 3) = I_{xx_3}c\theta_1c\theta_{23}s\theta_{23} - I_{yy_3}c\theta_1c\theta_{23}s\theta_{23} + I_{xy_3}c\theta_1c(2\theta_{23}) + I_{xz_3}s\theta_1s\theta_{23} + I_{yz_3}c\theta_{23}s\theta_1$
- ${}^0I_{c_3}(2, 1) = I_{xx_3}c\theta_1c^2\theta_{23}s\theta_1 + I_{yy_3}c\theta_1s\theta_1s^2\theta_{23} - I_{zz_3}c\theta_1s\theta_1 - 2I_{xy_3}c\theta_1c\theta_{23}s\theta_1s\theta_{23} - I_{xz_3}c(2\theta_1)c\theta_{23} + I_{yz_3}c(2\theta_1)s\theta_{23}$
- ${}^0I_{c_3}(2, 2) = I_{xx_3}c^2\theta_{23}s^2\theta_1 + I_{yy_3}s^2\theta_1s^2\theta_{23} + I_{zz_3}c^2\theta_1 - 2I_{xy_3}c\theta_{23}s^2\theta_1s\theta_{23} - 2I_{xz_3}c\theta_1c\theta_{23}s\theta_1 + 2I_{yz_3}c\theta_1s\theta_1s\theta_{23}$
- ${}^0I_{c_3}(2, 3) = I_{xx_3}c\theta_{23}s\theta_1s\theta_{23} - I_{yy_3}c\theta_{23}s\theta_1s\theta_{23} + I_{xy_3}c(2\theta_{23})s\theta_1 - I_{xz_3}c\theta_1s\theta_{23} - I_{yz_3}c\theta_1\theta_{23}$
- ${}^0I_{c_3}(3, 1) = I_{xx_3}c\theta_1c\theta_{23}s\theta_{23} - I_{yy_3}c\theta_1c\theta_{23}s\theta_{23} + I_{xy_3}c\theta_1c(2\theta_{23}) + I_{xz_3}s\theta_1s\theta_{23} + I_{yz_3}c\theta_1s\theta_1$
- ${}^0I_{c_3}(3, 2) = I_{xx_3}c\theta_{23}s\theta_1s\theta_{23} - I_{yy_3}c\theta_{23}s\theta_1s\theta_{23} + I_{xy_3}c(2\theta_{23})s\theta_1 - I_{xz_3}c\theta_1s\theta_{23} - I_{yz_3}c\theta_1c\theta_{23}$
- ${}^0I_{c_3}(3, 3) = I_{xx_3}s^2\theta_{23} + I_{yy_3}c^2\theta_{23} + 2I_{xy_3}c\theta_{23}s\theta_{23}$

Plugging in Equations (7.48) and (7.55) into Equation (7.47) results in the following:

$$T_{3_{rotational}} = \frac{1}{2} \begin{bmatrix} (\dot{\theta}_2 + \dot{\theta}_3) s\theta_1 & -(\dot{\theta}_2 + \dot{\theta}_3) c\theta_1 & \dot{\theta}_1 \end{bmatrix} \begin{bmatrix} {}^0I_{c_2} \\ -(\dot{\theta}_2 + \dot{\theta}_3) c\theta_1 \\ \dot{\theta}_1 \end{bmatrix} \quad (7.56)$$

$$\begin{aligned} &= \frac{1}{2} \left[ \dot{\theta}_1^2 I_{xx_3} s^2 \theta_{23} + \dot{\theta}_1^2 I_{yy_3} c^2 \theta_{23} + (\dot{\theta}_2^2 + \dot{\theta}_3^2 + 2\dot{\theta}_2\dot{\theta}_3) I_{zz_3} \right. \\ &\quad \left. + \dot{\theta}_1^2 I_{xy_3} s(2\theta_{23}) + 2\dot{\theta}_1 (\dot{\theta}_2 + \dot{\theta}_3) I_{xz_3} s\theta_{23} + 2\dot{\theta}_1 (\dot{\theta}_2 + \dot{\theta}_3) I_{yz_3} c\theta_{23} \right] \end{aligned} \quad (7.57)$$

### 7.3.3.3 TOTAL KINETIC ENERGY FOR JOINT 3

The total kinetic energy for joint 3 is then a matter of summing Equations (7.40) and (7.47) as follows:

$$T_3 = T_{3_{linear}} + T_{3_{rotational}} \quad (7.58)$$

$$\begin{aligned} &= \frac{1}{2}m_3 \left[ \dot{\theta}_1^2 \left( l_1^2 + l_2^2 c^2 \theta_2 + \frac{l_3^2}{4} c^2 \theta_{23} + 2l_1 l_2 c \theta_2 + l_1 l_3 c \theta_{23} + l_2 l_3 c \theta_2 c \theta_{23} \right) \right. \\ &\quad \left. + \dot{\theta}_2^2 \left( l_2^2 + l_2 l_3 c \theta_3 + \frac{l_3^2}{4} \right) + \dot{\theta}_3^2 \frac{l_3^2}{4} + 2\dot{\theta}_2 \dot{\theta}_3 \frac{l_3}{2} \left( l_2 c \theta_3 + \frac{l_3}{2} \right) \right] \\ &+ \frac{1}{2} \left[ \dot{\theta}_1^2 I_{xx_3} s^2 \theta_{23} + \dot{\theta}_1^2 I_{yy_3} c^2 \theta_{23} + \left( \dot{\theta}_2^2 + \dot{\theta}_3^2 + 2\dot{\theta}_2 \dot{\theta}_3 \right) I_{zz_3} \right. \\ &\quad \left. + \dot{\theta}_1^2 I_{xy_3} s(2\theta_{23}) + 2\dot{\theta}_1 \left( \dot{\theta}_2 + \dot{\theta}_3 \right) I_{xz_3} s \theta_{23} + 2\dot{\theta}_1 \left( \dot{\theta}_2 + \dot{\theta}_3 \right) I_{yz_3} c \theta_{23} \right] \end{aligned} \quad (7.59)$$

### 7.3.4 Total Kinetic Energy

The total kinetic energy is calculated as the sum of Equations (7.21), (7.39), and (7.59) per Equation (3.71):

$$T = T_1 + T_2 + T_3 \quad (7.60)$$

$$\begin{aligned} &= \frac{1}{2}m_1 \dot{\theta}_1^2 \frac{l_1^2}{4} + \frac{1}{2} \dot{\theta}_1^2 I_{zz_1} + \frac{1}{2}m_2 \left[ \dot{\theta}_1^2 \left( l_1 + \frac{l_2}{2} c \theta_2 \right)^2 + \dot{\theta}_2 \frac{l_2^2}{4} \right] \\ &\quad + \frac{1}{2} \left[ \dot{\theta}_1^2 I_{xx_2} s^2 \theta_2 + \dot{\theta}_1^2 I_{yy_2} c^2 \theta_2 + \dot{\theta}_2^2 I_{zz_2} + \dot{\theta}_1^2 I_{xy_2} s(2\theta_2) + 2\dot{\theta}_1 \dot{\theta}_2 I_{xz_2} s \theta_2 + 2\dot{\theta}_1 \dot{\theta}_2 I_{yz_2} c \theta_2 \right] \\ &\quad + \frac{1}{2}m_3 \left[ \dot{\theta}_1^2 \left( l_1^2 + l_2^2 c^2 \theta_2 + \frac{l_3^2}{4} c^2 \theta_{23} + 2l_1 l_2 c \theta_2 + l_1 l_3 c \theta_{23} + l_2 l_3 c \theta_2 c \theta_{23} \right) \right. \\ &\quad \left. + \dot{\theta}_2^2 \left( l_2^2 + l_2 l_3 c \theta_3 + \frac{l_3^2}{4} \right) + \dot{\theta}_3^2 \frac{l_3^2}{4} + 2\dot{\theta}_2 \dot{\theta}_3 \frac{l_3}{2} \left( l_2 c \theta_3 + \frac{l_3}{2} \right) \right] \\ &\quad + \frac{1}{2} \left[ \dot{\theta}_1^2 I_{xx_3} s^2 \theta_{23} + \dot{\theta}_1^2 I_{yy_3} c^2 \theta_{23} + \left( \dot{\theta}_2^2 + \dot{\theta}_3^2 + 2\dot{\theta}_2 \dot{\theta}_3 \right) I_{zz_3} \right. \\ &\quad \left. + \dot{\theta}_1^2 I_{xy_3} s(2\theta_{23}) + 2\dot{\theta}_1 \left( \dot{\theta}_2 + \dot{\theta}_3 \right) I_{xz_3} s \theta_{23} + 2\dot{\theta}_1 \left( \dot{\theta}_2 + \dot{\theta}_3 \right) I_{yz_3} c \theta_{23} \right] \end{aligned} \quad (7.61)$$

## 7.4 POTENTIAL ENERGY

The total potential energy of the system is calculated as

$$-U = \sum_{i=1}^n m_i \vec{g}^T \vec{r}_{c_i}, \quad (7.62)$$

where the gravity vector,  $\vec{g}$  is

$$\vec{g} = \begin{Bmatrix} 0 \\ 0 \\ -g \end{Bmatrix}. \quad (7.63)$$

The term  $g$  refers to the gravity of Earth, which is equal to approximately  $9.81 \text{ m/s}^2$ .

Plugging in Equations (7.5), (7.6), (7.7), and (7.63) into Equation (7.62) yields

$$U = m_2 g \frac{l_2}{2} s\theta_2 + m_3 g \left( l_2 s\theta_2 + \frac{l_3}{2} s\theta_{23} \right). \quad (7.64)$$

## 7.5 LAGRANGIAN

To calculate the Lagrangian, we can plug Equations (7.61) and (7.64) into Equation (3.63):

$$\begin{aligned} L = & \frac{1}{2} m_1 \dot{\theta}_1^2 \frac{l_1^2}{4} + \frac{1}{2} \dot{\theta}_1^2 I_{zz_1} + \frac{1}{2} m_2 \left[ \dot{\theta}_1^2 \left( l_1 + \frac{l_2}{2} c\theta_2 \right)^2 + \dot{\theta}_2 \frac{l_2^2}{4} \right] \\ & + \frac{1}{2} \left[ \dot{\theta}_1^2 I_{xx_2} s^2 \theta_2 + \dot{\theta}_1^2 I_{yy_2} c^2 \theta_2 + \dot{\theta}_2^2 I_{zz_2} + \dot{\theta}_1^2 I_{xy_2} s(2\theta_2) + 2\dot{\theta}_1 \dot{\theta}_2 I_{xz_2} s\theta_2 + 2\dot{\theta}_1 \dot{\theta}_2 I_{yz_2} c\theta_2 \right] \\ & + \frac{1}{2} m_3 \left[ \dot{\theta}_1^2 \left( l_1^2 + l_2^2 c^2 \theta_2 + \frac{l_3^2}{4} c^2 \theta_{23} + 2l_1 l_2 c\theta_2 + l_1 l_3 c\theta_{23} + l_2 l_3 c\theta_2 c\theta_{23} \right) \right. \\ & \quad \left. + \dot{\theta}_2^2 \left( l_2^2 + l_2 l_3 c\theta_3 + \frac{l_3^2}{4} \right) + \dot{\theta}_3^2 \frac{l_3^2}{4} + 2\dot{\theta}_2 \dot{\theta}_3 \frac{l_3}{2} \left( l_2 c\theta_3 + \frac{l_3}{2} \right) \right] \\ & + \frac{1}{2} \left[ \dot{\theta}_1^2 I_{xx_3} s^2 \theta_{23} + \dot{\theta}_1^2 I_{yy_3} c^2 \theta_{23} + \left( \dot{\theta}_2^2 + \dot{\theta}_3^2 + 2\dot{\theta}_2 \dot{\theta}_3 \right) I_{zz_3} \right. \\ & \quad \left. + \dot{\theta}_1^2 I_{xy_3} s(2\theta_{23}) + 2\dot{\theta}_1 \left( \dot{\theta}_2 + \dot{\theta}_3 \right) I_{xz_3} s\theta_{23} + 2\dot{\theta}_1 \left( \dot{\theta}_2 + \dot{\theta}_3 \right) I_{yz_3} c\theta_{23} \right] \\ & - m_2 g \frac{l_2}{2} s\theta_2 - m_3 g \left( l_2 s\theta_2 + \frac{l_3}{2} s\theta_{23} \right) \end{aligned} \quad (7.65)$$

## 7.6 GENERAL JOINT TORQUE

To find the torque about joint  $i$ , we can use Equation (3.65). Replacing  $q$  with  $\theta$  results in the following:

$$\frac{d}{dt} \left( \frac{\partial L}{\partial \dot{\theta}_i} \right) - \frac{\partial L}{\partial \theta_i} = \tau_i \quad (7.66)$$

## 7.7 JOINT 1 TORQUE

For  $i = 1$ , Equation 7.66 becomes

$$\tau_1 = \frac{d}{dt} \left( \frac{\partial L}{\partial \dot{\theta}_1} \right) - \frac{\partial L}{\partial \theta_1} \quad (7.67)$$

$$\begin{aligned} &= \left[ \frac{d}{d\theta_1} \left( \frac{\partial L}{\partial \dot{\theta}_1} \right) \dot{\theta}_1 + \frac{d}{d\dot{\theta}_1} \left( \frac{\partial L}{\partial \dot{\theta}_1} \right) \ddot{\theta}_1 + \frac{d}{d\theta_2} \left( \frac{\partial L}{\partial \dot{\theta}_1} \right) \dot{\theta}_2 + \frac{d}{d\dot{\theta}_2} \left( \frac{\partial L}{\partial \dot{\theta}_1} \right) \ddot{\theta}_2 \right. \\ &\quad \left. + \frac{d}{d\theta_3} \left( \frac{\partial L}{\partial \dot{\theta}_1} \right) \dot{\theta}_3 + \frac{d}{d\dot{\theta}_3} \left( \frac{\partial L}{\partial \dot{\theta}_1} \right) \ddot{\theta}_3 \right] - \frac{\partial L}{\partial \theta_1} \end{aligned} \quad (7.68)$$

where

$$\begin{aligned} \frac{\partial L}{\partial \dot{\theta}_1} &= m_1 \dot{\theta}_1 \frac{l_1^2}{4} + \dot{\theta}_1 I_{zz_1} + m_2 \dot{\theta}_1 \left( l_1 + \frac{l_2}{2} c \theta_2 \right)^2 \\ &\quad + \dot{\theta}_1 I_{xx_2} s^2 \theta_2 + \dot{\theta}_1 I_{yy_2} c^2 \theta_2 + \dot{\theta}_1 I_{xy_2} s(2\theta_2) + \dot{\theta}_2 I_{xz_2} s \theta_2 + \dot{\theta}_2 I_{yz_2} c \theta_2 \\ &\quad + m_3 \dot{\theta}_1 \left( l_1^2 + l_2^2 c^2 \theta_2 + \frac{l_3^2}{4} c^2 \theta_{23} + 2l_1 l_2 c \theta_2 + l_1 l_3 c \theta_{23} + l_2 l_3 c \theta_2 c \theta_{23} \right) \\ &\quad + \dot{\theta}_1 I_{xx_3} s^2 \theta_{23} + \dot{\theta}_1 I_{yy_3} c^2 \theta_{23} + \dot{\theta}_1 I_{xy_3} s(2\theta_{23}) + (\dot{\theta}_2 + \dot{\theta}_3) I_{xz_3} s \theta_{23} + (\dot{\theta}_2 + \dot{\theta}_3) I_{yz_3} c \theta_{23}, \end{aligned} \quad (7.69)$$

$$\frac{d}{d\theta_1} \left( \frac{\partial L}{\partial \dot{\theta}_1} \right) = 0, \quad (7.70)$$

$$\begin{aligned} \frac{d}{d\dot{\theta}_1} \left( \frac{\partial L}{\partial \dot{\theta}_1} \right) &= m_1 \frac{l_1^2}{4} + I_{zz_1} + m_2 \left( l_1 + \frac{l_2}{2} c \theta_2 \right)^2 + I_{xx_2} s^2 \theta_2 + I_{yy_2} c^2 \theta_2 + I_{xy_2} s(2\theta_2) \\ &\quad + m_3 \left( l_1^2 + l_2^2 c^2 \theta_2 + \frac{l_3^2}{4} c^2 \theta_{23} + 2l_1 l_2 c \theta_2 + l_1 l_3 c \theta_{23} + l_2 l_3 c \theta_2 c \theta_{23} \right) \\ &\quad + I_{xx_3} s^2 \theta_{23} + I_{yy_3} c^2 \theta_{23} + I_{xy_3} s(2\theta_{23}), \end{aligned} \quad (7.71)$$

$$\begin{aligned} \frac{d}{d\theta_2} \left( \frac{\partial L}{\partial \dot{\theta}_1} \right) &= -m_2 \dot{\theta}_1 l_2 \left( l_1 + \frac{l_2}{2} c \theta_2 \right) s \theta_2 + 2\dot{\theta}_1 I_{xx_2} c \theta_2 s \theta_2 - 2\dot{\theta}_1 I_{yy_2} c \theta_2 s \theta_2 \\ &\quad + 2\dot{\theta}_1 I_{xy_2} c 2 \theta_2 + \dot{\theta}_2 I_{xz_2} c \theta_2 - \dot{\theta}_2 I_{yz_2} s \theta_2 \\ &\quad + m_3 \dot{\theta}_1 \left[ -2l_2^2 c \theta_2 s \theta_2 - \frac{l_3^2}{4} c \theta_{23} s \theta_{23} - 2l_1 l_2 s \theta_2 - l_1 l_3 s \theta_{23} - l_2 l_3 s(2\theta_2 + \theta_3) \right] \\ &\quad + 2\dot{\theta}_1 I_{xx_3} c \theta_{23} s \theta_{23} - 2\dot{\theta}_1 I_{yy_3} c \theta_{23} s \theta_{23} + 2\dot{\theta}_1 I_{xy_3} c(2\theta_{23}) \\ &\quad + (\dot{\theta}_2 + \dot{\theta}_3) I_{xz_3} c \theta_{23} - (\dot{\theta}_2 + \dot{\theta}_3) I_{yz_3} s \theta_{23}, \end{aligned} \quad (7.72)$$

$$\frac{d}{d\dot{\theta}_2} \left( \frac{\partial L}{\partial \dot{\theta}_1} \right) = I_{xz_2} s\theta_2 + I_{yz_2} c\theta_2 + I_{xz_3} s\theta_{23} + I_{yz_3} c\theta_{23}, \quad (7.73)$$

$$\begin{aligned} \frac{d}{d\theta_3} \left( \frac{\partial L}{\partial \dot{\theta}_1} \right) = & -m_3 \dot{\theta}_1 \left( \frac{l_3^2}{2} c\theta_{23} s\theta_{23} + l_1 l_3 s\theta_{23} + l_2 l_3 c\theta_2 s\theta_{23} \right) + 2\dot{\theta}_1 I_{xx_3} c\theta_{23} s\theta_{23} \\ & - 2\dot{\theta}_1 I_{yy_3} c\theta_{23} s\theta_{23} + 2\dot{\theta}_1 I_{xy_3} c(2\theta_{23}) + (\dot{\theta}_2 + \dot{\theta}_3) I_{xz_3} c\theta_{23} - (\dot{\theta}_2 + \dot{\theta}_3) I_{yz_3} s\theta_{23}, \end{aligned} \quad (7.74)$$

$$\frac{d}{d\theta_3} \left( \frac{\partial L}{\partial \dot{\theta}_1} \right) = I_{xz_3} s\theta_{23} + I_{yz_3} c\theta_{23}, \quad (7.75)$$

$$\frac{\partial L}{\partial \theta_1} = 0. \quad (7.76)$$

Plugging in Equations (7.70) through (7.76) into Equation (7.68) solves the joint 1 torque as

$$\begin{aligned} \tau_1 = & \ddot{\theta}_1 \left[ m_1 \frac{l_1^2}{4} + I_{zz_1} + m_2 \left( l_1 + \frac{l_2}{2} c\theta_2 \right)^2 + I_{xx_2} s^2\theta_2 + I_{yy_2} c^2\theta_2 + I_{xy_2} s(2\theta_2) \right. \\ & + m_3 \left( l_1^2 + l_2^2 c^2\theta_2 + \frac{l_3^2}{4} c^2\theta_{23} + 2l_1 l_2 c\theta_2 + l_1 l_3 c\theta_{23} + l_2 l_3 c\theta_2 c\theta_{23} \right) \\ & \left. + I_{xx_3} s^2\theta_{23} + I_{yy_3} c^2\theta_{23} + I_{xy_3} s(2\theta_{23}) \right] \\ & + \dot{\theta}_2 \left\{ -m_2 \dot{\theta}_1 l_2 \left( l_1 + \frac{l_2}{2} c\theta_2 \right) s\theta_2 + 2\dot{\theta}_1 I_{xx_2} c\theta_2 s\theta_2 - 2\dot{\theta}_1 I_{yy_2} c\theta_2 s\theta_2 \right. \\ & + 2\dot{\theta}_1 I_{xy_2} c2\theta_2 + \dot{\theta}_2 I_{xz_2} c\theta_2 - \dot{\theta}_2 I_{yz_2} s\theta_2 \\ & + m_3 \dot{\theta}_1 \left[ -2l_2^2 c\theta_2 s\theta_2 - \frac{l_3^2}{4} c\theta_{23} s\theta_{23} - 2l_1 l_2 s\theta_2 - l_1 l_3 s\theta_{23} - l_2 l_3 s(2\theta_2 + \theta_3) \right] \\ & + 2\dot{\theta}_1 I_{xx_3} c\theta_{23} s\theta_{23} - 2\dot{\theta}_1 I_{yy_3} c\theta_{23} s\theta_{23} + 2\dot{\theta}_1 I_{xy_3} c(2\theta_{23}) \\ & \left. + (\dot{\theta}_2 + \dot{\theta}_3) I_{xz_3} c\theta_{23} - (\dot{\theta}_2 + \dot{\theta}_3) I_{yz_3} s\theta_{23} \right\} \\ & + \ddot{\theta}_2 [I_{xz_2} s\theta_2 + I_{yz_2} c\theta_2 + I_{xz_3} s\theta_{23} + I_{yz_3} c\theta_{23}] \\ & + \dot{\theta}_3 \left[ -m_3 \dot{\theta}_1 \left( \frac{l_3^2}{2} c\theta_{23} s\theta_{23} + l_1 l_3 s\theta_{23} + l_2 l_3 c\theta_2 s\theta_{23} \right) + 2\dot{\theta}_1 I_{xx_3} c\theta_{23} s\theta_{23} \right. \\ & \left. - 2\dot{\theta}_1 I_{yy_3} c\theta_{23} s\theta_{23} + 2\dot{\theta}_1 I_{xy_3} c(2\theta_{23}) + (\dot{\theta}_2 + \dot{\theta}_3) I_{xz_3} c\theta_{23} - (\dot{\theta}_2 + \dot{\theta}_3) I_{yz_3} s\theta_{23} \right] \\ & + \ddot{\theta}_3 [I_{xz_3} s\theta_{23} + I_{yz_3} c\theta_{23}]. \end{aligned} \quad (7.77)$$

## 7.8 JOINT 2 TORQUE

For  $i = 2$ , Equation 7.66 becomes

$$\tau_2 = \frac{d}{dt} \left( \frac{\partial L}{\partial \dot{\theta}_2} \right) - \frac{\partial L}{\partial \theta_2} \quad (7.78)$$

$$\begin{aligned} &= \left[ \frac{d}{d\theta_1} \left( \frac{\partial L}{\partial \dot{\theta}_2} \right) \dot{\theta}_1 + \frac{d}{d\dot{\theta}_1} \left( \frac{\partial L}{\partial \dot{\theta}_2} \right) \ddot{\theta}_1 + \frac{d}{d\theta_2} \left( \frac{\partial L}{\partial \dot{\theta}_2} \right) \dot{\theta}_2 + \frac{d}{d\dot{\theta}_2} \left( \frac{\partial L}{\partial \dot{\theta}_2} \right) \ddot{\theta}_2 \right. \\ &\quad \left. + \frac{d}{d\theta_3} \left( \frac{\partial L}{\partial \dot{\theta}_2} \right) \dot{\theta}_3 + \frac{d}{d\dot{\theta}_3} \left( \frac{\partial L}{\partial \dot{\theta}_2} \right) \ddot{\theta}_3 \right] - \frac{\partial L}{\partial \theta_2} \end{aligned} \quad (7.79)$$

where

$$\begin{aligned} \frac{\partial L}{\partial \dot{\theta}_2} &= m_2 \dot{\theta}_2 \frac{l_2^2}{4} + \dot{\theta}_2 I_{zz_2} + \dot{\theta}_1 I_{xz_2} s\theta_2 + \dot{\theta}_1 I_{yz_2} c\theta_2 \\ &\quad + \frac{1}{2} m_3 \left[ 2\dot{\theta}_2 \left( l_2^2 + l_2 l_3 c\theta_3 + \frac{l_3^2}{4} \right) + \dot{\theta}_3 l_3 \left( l_2 c\theta_3 + \frac{l_3}{2} \right) \right] \\ &\quad + (\dot{\theta}_2 + \dot{\theta}_3) I_{zz_3} + \dot{\theta}_1 I_{xz_3} s\theta_{23} + \dot{\theta}_1 I_{yz_3} c\theta_{23}, \end{aligned} \quad (7.80)$$

$$\frac{d}{d\theta_1} \left( \frac{\partial L}{\partial \dot{\theta}_2} \right) = 0, \quad (7.81)$$

$$\frac{d}{d\dot{\theta}_1} \left( \frac{\partial L}{\partial \dot{\theta}_2} \right) = I_{xz_2} s\theta_2 + I_{yz_2} c\theta_2 + I_{xz_3} s\theta_{23} + I_{yz_3} c\theta_{23}, \quad (7.82)$$

$$\frac{d}{d\theta_2} \left( \frac{\partial L}{\partial \dot{\theta}_2} \right) = \dot{\theta}_1 I_{xz_2} c\theta_2 - \dot{\theta}_1 I_{yz_2} s\theta_2 + \dot{\theta}_1 I_{xz_3} c\theta_{23} - \dot{\theta}_1 I_{yz_3} s\theta_{23}, \quad (7.83)$$

$$\frac{d}{d\dot{\theta}_2} \left( \frac{\partial L}{\partial \dot{\theta}_2} \right) = m_2 \frac{l_2^2}{4} + m_3 \left( l_2^2 + l_2 l_3 c\theta_3 + \frac{l_3^2}{4} \right) + I_{zz_2} + I_{zz_3}, \quad (7.84)$$

$$\frac{d}{d\theta_3} \left( \frac{\partial L}{\partial \dot{\theta}_2} \right) = -\frac{1}{2} m_3 l_2 l_3 s\theta_3 (2\dot{\theta}_2 + \dot{\theta}_3) + \dot{\theta}_1 I_{xz_3} c\theta_{23} - \dot{\theta}_1 I_{yz_3} s\theta_{23}, \quad (7.85)$$

$$\frac{d}{d\dot{\theta}_3} \left( \frac{\partial L}{\partial \dot{\theta}_2} \right) = \frac{1}{2} m_3 l_3 \left( l_2 c\theta_2 + \frac{l_3}{2} \right) + I_{zz_3}, \quad (7.86)$$

$$\begin{aligned}
\frac{\partial L}{\partial \theta_2} = & -m_2 \dot{\theta}_1 \frac{l_2}{2} \left( l_1 + \frac{l_2}{2} c\theta_2 \right) s\theta_2 + \dot{\theta}_1^2 I_{xx_2} c\theta_2 s\theta_2 - \dot{\theta}_1^2 I_{yy_2} c(2\theta_2) s\theta_2 \\
& + \dot{\theta}_1^2 I_{xy_2} c(2\theta_2) + \dot{\theta}_1 \dot{\theta}_2 I_{xz_2} c\theta_2 - \dot{\theta}_1 \dot{\theta}_2 I_{yz_2} s\theta_2 \\
& - \frac{1}{2} m_3 \dot{\theta}_1^2 \left[ 2l_2^2 c\theta_2 s\theta_2 + \frac{l_3^2}{2} c\theta_{23} s\theta_{23} + 2l_1 l_2 s\theta_2 + l_1 l_3 s\theta_{23} + l_2 l_3 s(2\theta_2 + \theta_3) \right] \\
& + \dot{\theta}_1^2 I_{xx_3} c\theta_{23} s\theta_{23} + \dot{\theta}_1^2 I_{yy_3} c\theta_{23} s\theta_{23} + \dot{\theta}_1^2 I_{xy_3} c(2\theta_{23}) \\
& + \dot{\theta}_1 (\dot{\theta}_2 + \dot{\theta}_3) I_{xz_3} c\theta_{23} - \dot{\theta}_1 (\dot{\theta}_2 + \dot{\theta}_3) I_{yz_3} s\theta_{23} - m_2 g \frac{l_2}{2} c\theta_2 - m_3 g \left( l_2 c\theta_2 + \frac{l_3}{2} c\theta_{23} \right).
\end{aligned} \tag{7.87}$$

Plugging in Equations (7.81) through (7.87) into Equation (7.79) solves the joint 2 torque as

$$\begin{aligned}
\tau_2 = & \ddot{\theta}_1 [I_{xz_2} s\theta_2 + I_{yz_2} c\theta_2 + I_{xz_3} s\theta_{23} + I_{yz_3} c\theta_{23}] \\
& + \dot{\theta}_2 [\dot{\theta}_1 I_{xz_2} c\theta_2 - \dot{\theta}_1 I_{yz_2} s\theta_2 + \dot{\theta}_1 I_{xz_3} c\theta_{23} - \dot{\theta}_1 I_{yz_3} s\theta_{23}] \\
& + \ddot{\theta}_2 \left[ m_2 \frac{l_2^2}{4} + m_3 \left( l_2^2 + l_2 l_3 c\theta_3 + \frac{l_3^2}{4} \right) + I_{zz_2} + I_{zz_3} \right] \\
& + \dot{\theta}_3 \left[ -\frac{1}{2} m_3 l_2 l_3 s\theta_3 (2\dot{\theta}_2 + \dot{\theta}_3) + \dot{\theta}_1 I_{xz_3} c\theta_{23} - \dot{\theta}_1 I_{yz_3} s\theta_{23} \right] \\
& + \ddot{\theta}_3 \left[ \frac{1}{2} m_3 l_3 \left( l_2 c\theta_2 + \frac{l_3}{2} \right) + I_{zz_3} \right] \\
& + m_2 \dot{\theta}_1 \frac{l_2}{2} \left( l_1 + \frac{l_2}{2} c\theta_2 \right) s\theta_2 - \dot{\theta}_1^2 I_{xx_2} c\theta_2 s\theta_2 + \dot{\theta}_1^2 I_{yy_2} c(2\theta_2) s\theta_2 \\
& - \dot{\theta}_1^2 I_{xy_2} c(2\theta_2) - \dot{\theta}_1 \dot{\theta}_2 I_{xz_2} c\theta_2 + \dot{\theta}_1 \dot{\theta}_2 I_{yz_2} s\theta_2 \\
& + \frac{1}{2} m_3 \dot{\theta}_1^2 \left[ 2l_2^2 c\theta_2 s\theta_2 + \frac{l_3^2}{2} c\theta_{23} s\theta_{23} + 2l_1 l_2 s\theta_2 + l_1 l_3 s\theta_{23} + l_2 l_3 s(2\theta_2 + \theta_3) \right] \\
& - \dot{\theta}_1^2 I_{xx_3} c\theta_{23} s\theta_{23} + \dot{\theta}_1^2 I_{yy_3} c\theta_{23} s\theta_{23} - \dot{\theta}_1^2 I_{xy_3} c(2\theta_{23}) \\
& - \dot{\theta}_1 (\dot{\theta}_2 + \dot{\theta}_3) I_{xz_3} c\theta_{23} + \dot{\theta}_1 (\dot{\theta}_2 + \dot{\theta}_3) I_{yz_3} s\theta_{23} + m_2 g \frac{l_2}{2} c\theta_2 + m_3 g \left( l_2 c\theta_2 + \frac{l_3}{2} c\theta_{23} \right).
\end{aligned} \tag{7.88}$$

## 7.9 JOINT 3 TORQUE

For  $i = 3$ , Equation 7.66 becomes

$$\tau_3 = \frac{d}{dt} \left( \frac{\partial L}{\partial \dot{\theta}_3} \right) - \frac{\partial L}{\partial \theta_3} \quad (7.89)$$

$$\begin{aligned} &= \left[ \frac{d}{d\theta_1} \left( \frac{\partial L}{\partial \dot{\theta}_3} \right) \dot{\theta}_1 + \frac{d}{d\dot{\theta}_1} \left( \frac{\partial L}{\partial \dot{\theta}_3} \right) \ddot{\theta}_1 + \frac{d}{d\theta_2} \left( \frac{\partial L}{\partial \dot{\theta}_3} \right) \dot{\theta}_2 + \frac{d}{d\dot{\theta}_2} \left( \frac{\partial L}{\partial \dot{\theta}_3} \right) \ddot{\theta}_2 \right. \\ &\quad \left. + \frac{d}{d\theta_3} \left( \frac{\partial L}{\partial \dot{\theta}_3} \right) \dot{\theta}_3 + \frac{d}{d\dot{\theta}_3} \left( \frac{\partial L}{\partial \dot{\theta}_3} \right) \ddot{\theta}_3 \right] - \frac{\partial L}{\partial \theta_3} \end{aligned} \quad (7.90)$$

where

$$\frac{\partial L}{\partial \dot{\theta}_3} = m_3 \left[ \dot{\theta}_3 \frac{l_3^2}{4} + \dot{\theta}_2 \frac{l_3}{2} \left( l_2 c\theta_3 + \frac{l_3}{2} \right) \right] + (\dot{\theta}_2 + \dot{\theta}_3) I_{zz3} + \dot{\theta}_1 I_{xz3} s\theta_{23} + \dot{\theta}_1 I_{yz3} c\theta_{23}, \quad (7.91)$$

$$\frac{d}{d\theta_1} \left( \frac{\partial L}{\partial \dot{\theta}_3} \right) = 0, \quad (7.92)$$

$$\frac{d}{d\dot{\theta}_1} \left( \frac{\partial L}{\partial \dot{\theta}_3} \right) = I_{xz3} s\theta_{23} + I_{yz3} c\theta_{23}, \quad (7.93)$$

$$\frac{d}{d\theta_2} \left( \frac{\partial L}{\partial \dot{\theta}_3} \right) = \dot{\theta}_1 I_{xz3} c\theta_{23} - \dot{\theta}_1 I_{yz3} s\theta_{23}, \quad (7.94)$$

$$\frac{d}{d\dot{\theta}_2} \left( \frac{\partial L}{\partial \dot{\theta}_3} \right) = m_3 \frac{l_3}{2} \left( l_2 c\theta_2 + \frac{l_3}{2} \right) + I_{zz3}, \quad (7.95)$$

$$\frac{d}{d\theta_3} \left( \frac{\partial L}{\partial \dot{\theta}_3} \right) = -m_3 \dot{\theta}_2 l_2 \frac{l_3}{2} s\theta_3 + \dot{\theta}_1 I_{xz3} c\theta_{23} - \dot{\theta}_1 I_{yz3} s\theta_{23}, \quad (7.96)$$

$$\frac{d}{d\dot{\theta}_3} \left( \frac{\partial L}{\partial \dot{\theta}_3} \right) = m_3 \frac{l_3^2}{4} + I_{zz3}, \quad (7.97)$$

$$\begin{aligned} \frac{\partial L}{\partial \theta_1} &= -\frac{1}{2} m_3 \left[ \dot{\theta}_1^2 \left( \frac{l_3^2}{2} c\theta_{23} s\theta_{23} + l_1 l_3 s\theta_{23} + l_2 l_3 c\theta_{23} s\theta_{23} \right) + \dot{\theta}_2^2 l_2 l_3 s\theta_3 + \dot{\theta}_2 \dot{\theta}_3 l_2 l_3 s\theta_3 \right] \\ &\quad + \dot{\theta}_1^2 I_{xx3} c\theta_{23} s\theta_{23} - \dot{\theta}_1^2 I_{yy3} c\theta_{23} s\theta_{23} + \dot{\theta}_1^2 I_{xy3} c(2\theta_{23}) \\ &\quad + \dot{\theta}_1 (\dot{\theta}_2 + \dot{\theta}_3) I_{xz3} c\theta_{23} - \dot{\theta}_1 (\dot{\theta}_2 + \dot{\theta}_3) I_{yz3} s\theta_{23} - m_3 g \frac{l_3}{2} c\theta_{23}. \end{aligned} \quad (7.98)$$

Plugging in Equations (7.92) through (7.98) into Equation (7.90) solves the joint 3 torque as

$$\begin{aligned}
\tau_3 = & \ddot{\theta}_1 [I_{xz_3} s\theta_{23} + I_{yz_3} c\theta_{23}] \\
& + \dot{\theta}_2 \left[ \dot{\theta}_1 I_{xz_3} c\theta_{23} - \dot{\theta}_1 I_{yz_3} s\theta_{23} \right] + \ddot{\theta}_2 \left[ m_3 \frac{l_3}{2} \left( l_2 c\theta_2 + \frac{l_3}{2} \right) + I_{zz_3} \right] \\
& + \dot{\theta}_3 \left[ -m_3 \dot{\theta}_2 l_2 \frac{l_3}{2} s\theta_3 + \dot{\theta}_1 I_{xz_3} c\theta_{23} - \dot{\theta}_1 I_{yz_3} s\theta_{23} \right] + \ddot{\theta}_3 \left[ m_3 \frac{l_3^2}{4} + I_{zz_3} \right] \\
& + \frac{1}{2} m_3 \left[ \dot{\theta}_1^2 \left( \frac{l_3^2}{2} c\theta_{23} s\theta_{23} + l_1 l_3 s\theta_{23} + l_2 l_3 c\theta_2 s\theta_{23} \right) + \dot{\theta}_2^2 l_2 l_3 s\theta_3 + \dot{\theta}_2 \dot{\theta}_3 l_2 l_3 s\theta_3 \right] \\
& - \dot{\theta}_1^2 I_{xx_3} c\theta_{23} s\theta_{23} + \dot{\theta}_1^2 I_{yy_3} c\theta_{23} s\theta_{23} - \dot{\theta}_1^2 I_{xy_3} c(2\theta_{23}) \\
& - \dot{\theta}_1 (\dot{\theta}_2 + \dot{\theta}_3) I_{xz_3} c\theta_{23} + \dot{\theta}_1 (\dot{\theta}_2 + \dot{\theta}_3) I_{yz_3} s\theta_{23} + m_3 g \frac{l_3}{2} c\theta_{23}.
\end{aligned} \tag{7.99}$$

## CHAPTER 8

### PID CONTROLLER

#### 8.1 LINEARIZATION AND STATE-SPACE

The Euler-Lagrange [see Equation (3.64)] is used to find the torque at joint  $i$ . For this particular robotic arm, the joint torques are as follows:

- $\tau_1$  - Equation (7.77);
- $\tau_2$  - Equation (7.88);
- $\tau_3$  - Equation (7.99).

The torque calculated using the Euler-Lagrange will give the results in the form of a non-linear model. For PID (proportional-integral-derivative) control, the equations for joint torques need to be linearized and placed into state-space form.

The first step is to isolate the  $\ddot{\theta}_i$  terms. To do this, the joint torque equations are written into matrix form such that it matches Equation (3.66). A vector of the  $\ddot{\theta}_i$  terms can then be found by performing the following:

$$\ddot{\theta} = M^{-1} [\tau - C(\theta, \dot{\theta}) - G(\theta)] \quad (8.1)$$

For this system, there are three degrees of freedom, so  $\ddot{\theta}_i$  in this instance becomes

$$\ddot{\theta}_i = f(\theta_1, \theta_2, \theta_3, \dot{\theta}_1, \dot{\theta}_2, \dot{\theta}_3, \tau_1, \tau_2, \tau_3). \quad (8.2)$$

To linearize Equation (8.2), an equilibrium point is chosen to be the state at which the robotic arm comes to rest as time goes to infinity. The equilibrium point,  $x^*$  is

$$x^* = \begin{Bmatrix} \theta_{1eq} \\ \theta_{2eq} \\ \theta_{3eq} \\ \dot{\theta}_{1eq} \\ \dot{\theta}_{2eq} \\ \dot{\theta}_{3eq} \end{Bmatrix} = \begin{Bmatrix} 0 \\ -\frac{\pi}{2} \\ 0 \\ 0 \\ 0 \\ 0 \end{Bmatrix}. \quad (8.3)$$

The linearized form of Equation (8.2) is the Taylor Series Expansion where the high order terms drop out:

$$\ddot{\theta}_{i_{lin}} = \ddot{\theta}_i(x^*) + \frac{d\ddot{\theta}_i}{dx}(x - x^*), \text{ where } x = \begin{Bmatrix} \theta_1 \\ \theta_2 \\ \theta_3 \\ \dot{\theta}_1 \\ \dot{\theta}_2 \\ \dot{\theta}_3 \end{Bmatrix} \quad (8.4)$$

After solving Equation (8.4) for  $\ddot{\theta}_{1_{lin}}$ ,  $\ddot{\theta}_{2_{lin}}$ , and  $\ddot{\theta}_{3_{lin}}$ , the three equations can be placed into state-space form. For this system, the state-space form is

$$\dot{\bar{x}} = [A]\bar{x} + [B]\tau \quad (8.5)$$

$$y = [C]\bar{x} + [D]\tau \quad (8.6)$$

where  $\bar{x} = x - x^*$ . The terms  $[C]$  and  $[D]$  are chosen such that

$$y = \begin{Bmatrix} \theta_1 \\ \theta_2 + \frac{\pi}{2} \\ \theta_3 \\ 0 \\ 0 \\ 0 \end{Bmatrix}. \quad (8.7)$$

For this system, the linearized state-space form of Equation (8.5) is

$$\begin{Bmatrix} \dot{\theta}_1 \\ \dot{\theta}_2 \\ \dot{\theta}_3 \\ \ddot{\theta}_1 \\ \ddot{\theta}_2 \\ \ddot{\theta}_3 \end{Bmatrix} = \begin{bmatrix} 0 & 0 & 0 & 1 & 0 & 0 \\ 0 & 0 & 0 & 0 & 1 & 0 \\ 0 & 0 & 0 & 0 & 0 & 1 \\ 0 & -0.0955 & 0.7283 & 0 & 0 & 0 \\ 0 & -52.5498 & 62.9780 & 0 & 0 & 0 \\ 0 & 83.5340 & -270.7207 & 0 & 0 & 0 \end{bmatrix} \begin{Bmatrix} \theta_1 \\ \theta_2 + \frac{\pi}{2} \\ \theta_3 \\ \dot{\theta}_1 \\ \dot{\theta}_2 \\ \dot{\theta}_3 \end{Bmatrix} + \begin{Bmatrix} 0 & 0 & 0 \\ 0 & 0 & 0 \\ 0 & 0 & 0 \\ 71.3072 & 0.3689 & -1.6052 \\ 0.3689 & 51.7315 & -158.6295 \\ -1.6052 & -158.6295 & 618.1473 \end{Bmatrix} \begin{Bmatrix} \tau_1 \\ \tau_2 \\ \tau_3 \end{Bmatrix} \quad (8.8)$$

## 8.2 VERIFICATION OF LINEAR MODEL

To verify that the linear model appropriately describes the system, the linear model is compared to the non-linear model using an ordinary differential equation (ODE) solver.

### 8.2.1 Joint 2 Released from Non-Equilibrium Position

We will first look at the results of all three joint angles when the robotic arm is released from a non-equilibrium position for joint 2 with no joint torques. For two different cases, the initial joint 2 position will be  $5^\circ$  and  $10^\circ$ . The remaining initial conditions of the system are as follows:

- $\theta_1 = 0$ ;
- $\theta_3 = 0$ ;
- $\dot{\theta}_1 = 0$ ;
- $\dot{\theta}_2 = 0$ ;
- $\dot{\theta}_3 = 0$ .

Figures 8.1 and 8.2 shows the response for joint 1 for an initial angle of 5 degrees and 10 degrees, respectively. Figures 8.3 and 8.4 shows the response for joint 2 for an initial angle of 5 degrees and 10 degrees, respectively. And Figures 8.5 and 8.6 shows the response for joint 3 for an initial angle of 5 degrees and 10 degrees, respectively.

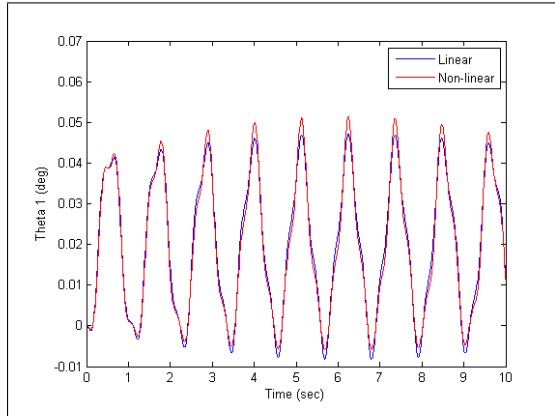


**Figure 8.1.** Response of joint 1 due to a non-equilibrium initial joint 2 angle of 5 degrees.

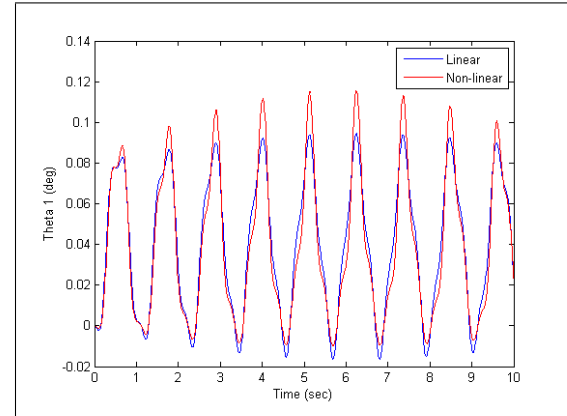


**Figure 8.2.** Response of joint 1 due to a non-equilibrium initial joint 2 angle of 10 degrees.

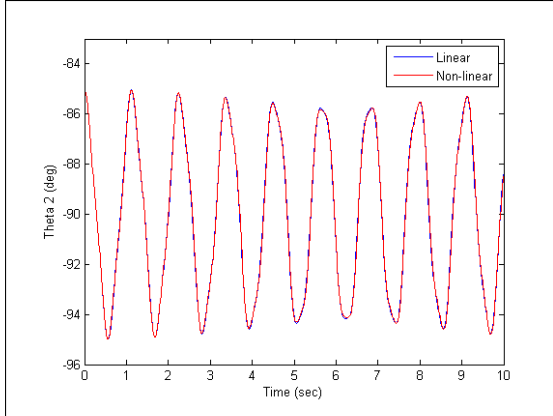


**Figure 8.3. Response of joint 2 due to a non-equilibrium initial joint 2 angle of 5 degrees.**

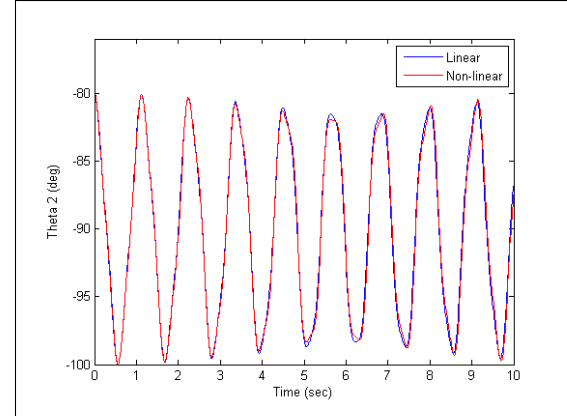


**Figure 8.4. Response of joint 2 due to a non-equilibrium initial joint 2 angle of 10 degrees.**

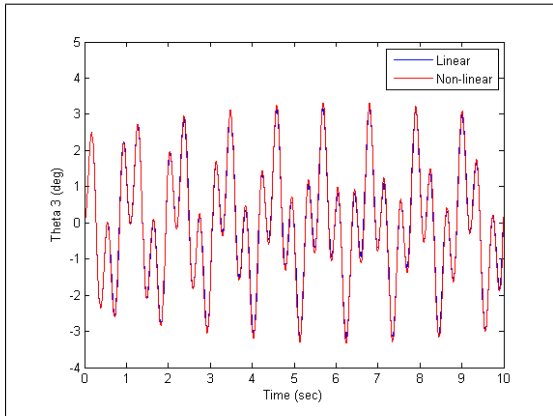


**Figure 8.5. Response of joint 3 due to a non-equilibrium initial joint 2 angle of 5 degrees.**

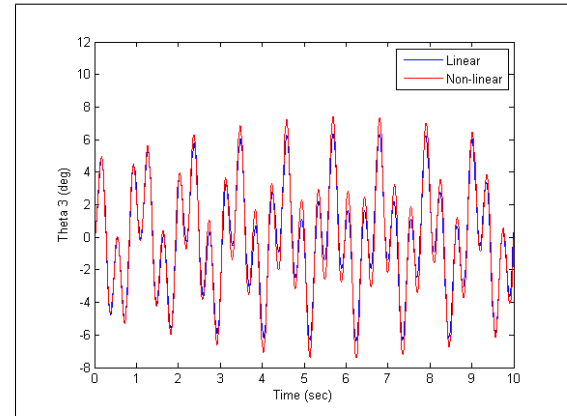


**Figure 8.6. Response of joint 3 due to a non-equilibrium initial joint 2 angle of 10 degrees.**

An increase of initial joint 2 angle lead to a decrease in model accuracy. For joint 1, a decrease in model accuracy is seen with a larger peak for the non-linear model in Figure 8.2 relative to the linear model in Figure 8.1. Truncation of peaks were also found for joint 3 as seen in Figures 8.5 and 8.6. For joint 2, an increase in initial joint 2 angle also lead to a shortening of peaks, but it is at a much lower magnitude in comparison to joints 1 and 3.

### 8.2.2 Joint 3 Released from Non-Equilibrium Position

We will also look at the results of all three joint angles when the robotic arm is released from a non-equilibrium position for joint 3 with no joint torques. Like the cases for a non-equilibrium position for joint 2, the initial joint 3 position will be  $5^\circ$  and  $10^\circ$  from its equilibrium point. The remaining initial conditions of the system are as follows:

- $\theta_1 = 0$ ;
- $\theta_2 = 0$ ;
- $\dot{\theta}_1 = 0$ ;
- $\dot{\theta}_2 = 0$ ;
- $\dot{\theta}_3 = 0$ .

Figures 8.7 and 8.8 shows the response for joint 1 for an initial angle of 5 degrees and 10 degrees, respectively. Figures 8.9 and 8.10 shows the response for joint 2 for an initial angle of 5 degrees and 10 degrees, respectively. And Figures 8.11 and 8.12 shows the response for joint 3 for an initial angle of 5 degrees and 10 degrees, respectively.

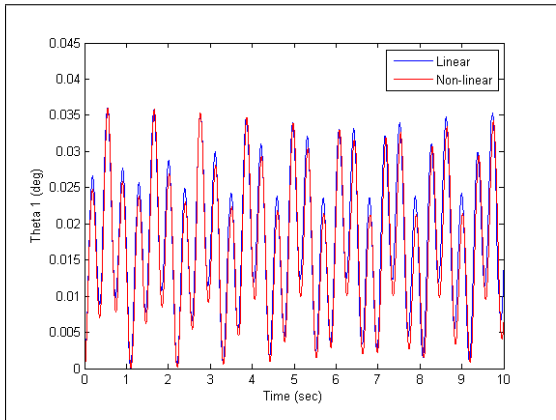


**Figure 8.7. Response of joint 1 due to a non-equilibrium initial joint 3 angle of 5 degrees.**

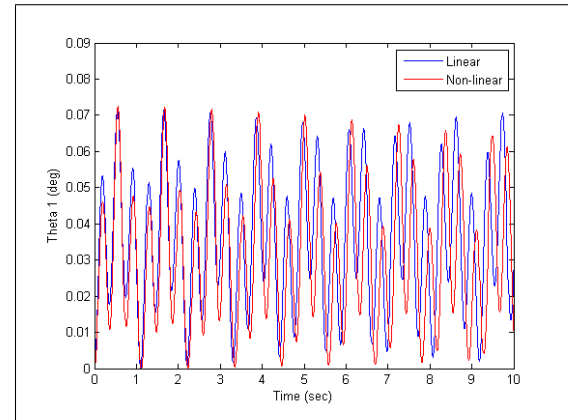


**Figure 8.8. Response of joint 1 due to a non-equilibrium initial joint 3 angle of 10 degrees.**

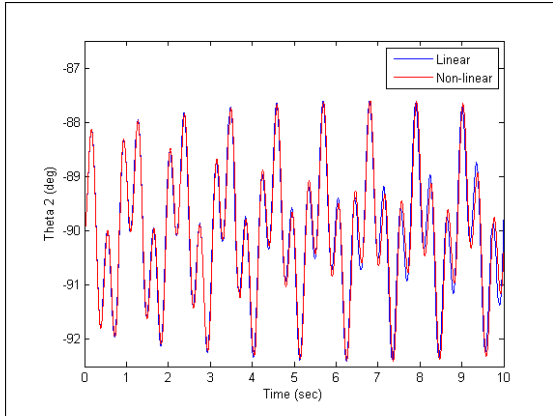


**Figure 8.9. Response of joint 2 due to a non-equilibrium initial joint 3 angle of 5 degrees.**

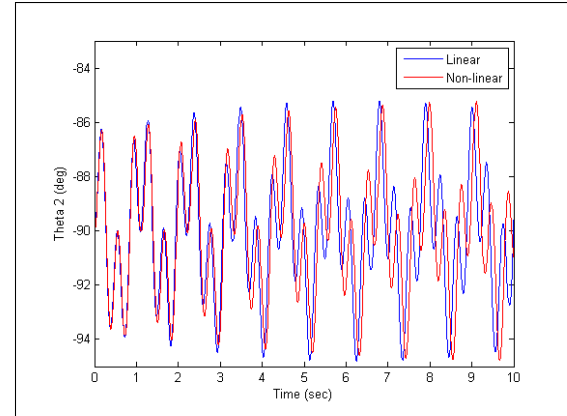


**Figure 8.10. Response of joint 2 due to a non-equilibrium initial joint 3 angle of 10 degrees.**

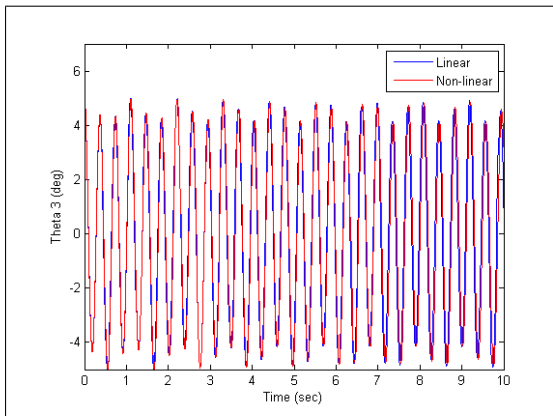


**Figure 8.11. Response of joint 3 due to a non-equilibrium initial joint 3 angle of 5 degrees.**

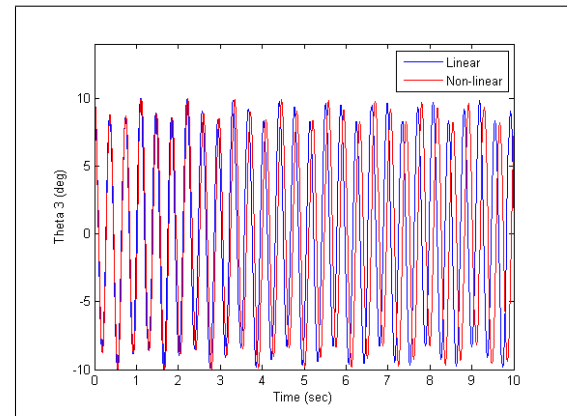


**Figure 8.12. Response of joint 3 due to a non-equilibrium initial joint 3 angle of 10 degrees.**

An increase of initial joint angle for joint 3 lead to an overall decrease in model accuracy. The most noticeable change when increasing the initial joint angle for joint 3 is the response of the linear model becoming out of phase with the non-linear model for all three joints. When the initial joint 3 angle is  $5^\circ$ , the linear and non-linear responses mostly stay in phase during the time window. For an initial joint 3 angle of  $10^\circ$ , the linear and non-linear models get noticeably out of phase at about 2 seconds. And as time increases, the responses get increasingly out of phase.

### 8.3 INDIVIDUAL PID CONTROLLER

The control for this wearable robot is done through an individual PID controller for each actuator. A block diagram of the PID controller can be found in Fig. 8.13.

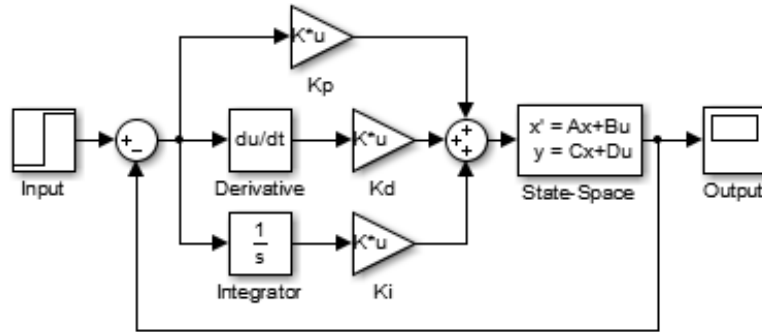


**Figure 8.13. Block diagram of PID controller.**

For this system, the input is the torque,  $\tau$ . This is also reflected in Equations (8.5) through (8.6). To implement PID, the input is transformed as follows [18]

$$\tau = K_D \dot{E} + K_P E + K_i \int E dt, \quad (8.9)$$

where  $E = \theta_{desired} - \theta_{actual}$ .

The gain values for each individual PID controller were tuned based on desired response, and gain ratios. The desired response for all three joints needed to meet the following criteria for the theoretical system in Simulink:

- rise time,  $t_r$ , is less than 0.5 seconds ( $t_r < 0.5 s$ );
- overshoot,  $\%OS$ , is less than 10% ( $\%OS < 10$ );
- settling time,  $t_s$ , is less than 1 second ( $t_s < 1 s$ ).

The rise time is calculated as the time it takes to go from 10% of the step response to 90% of the step response, and settling time is calculated as the time it takes from the start of the response to when the system reaches 5% of steady-state. In addition, the following gain ratios need to also be met the following criteria:

- integral gain,  $K_I$ , is independent of the proportional and derivative gain values;
- proportional gain,  $K_P$ , is between 20-60% of integral gain ( $0.2K_I \leq K_P \leq 0.6K_I$ );
- derivative gain,  $K_D$ , is between 0-20% of integral gain ( $0 \leq K_D \leq 0.2K_I$ ).

Figure 8.14 shows the tuned response for motor 1. Because motor 1 is independent of gravity, an integral term is not necessary. Instead, the controller for motor 1 is simply a PD (proportional-derivative) controller. The gain values for motor 1 are  $K_P = 4$ ,  $K_D = 0.3$ .

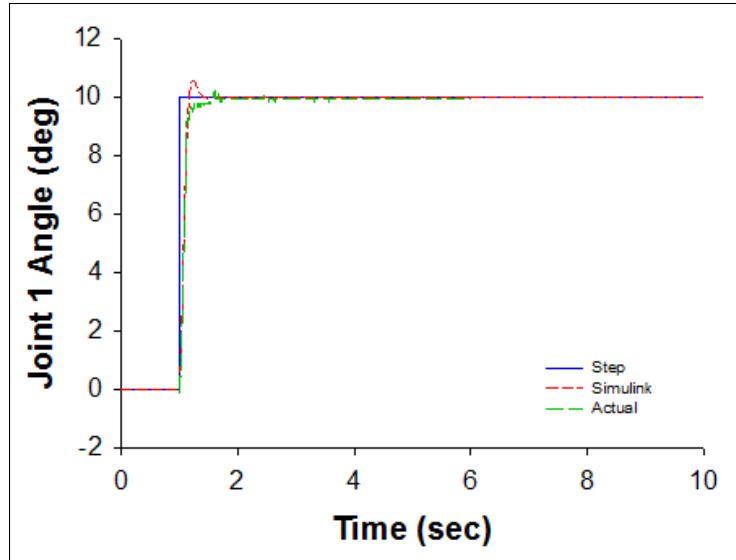


**Figure 8.14. Comparison of theoretical response and actual response for motor 1.**

The characteristics of the theoretical and actual response for motor 1 can be found in Table 8.1.

**Table 8.1. Characteristics of Motor 1 Response**

Response	Rise Time (s)	Overshoot (%)	Settling Time (s)	Steady-State (deg)
Theoretical	0.1645	5.76	0.2762	10.000
Actual	0.1252	0	0.1653	9.944

The actual steady-state value for motor 1 has a 0.56% error in comparison to the theoretical steady-state. The main takeaways when comparing the theoretical response with the actual response from Table 8.1 are that the actual response does not overshoot, and the actual response has a shorter settling time. These two items may be an indication that the theoretical model is underdamped.

Figure 8.15 shows the tuned response for motor 2. Unlike motor 1, motor 2 is affected by gravity, so a complete PID controller is needed. The gain values for motor 2 are  $K_P = 2.5$ ,  $K_I = 9.766$ ,  $K_D = 0.8$ . The proportional gain is 25.6% of the integral gain, and the derivative gain is 8.2% of the integral gain.

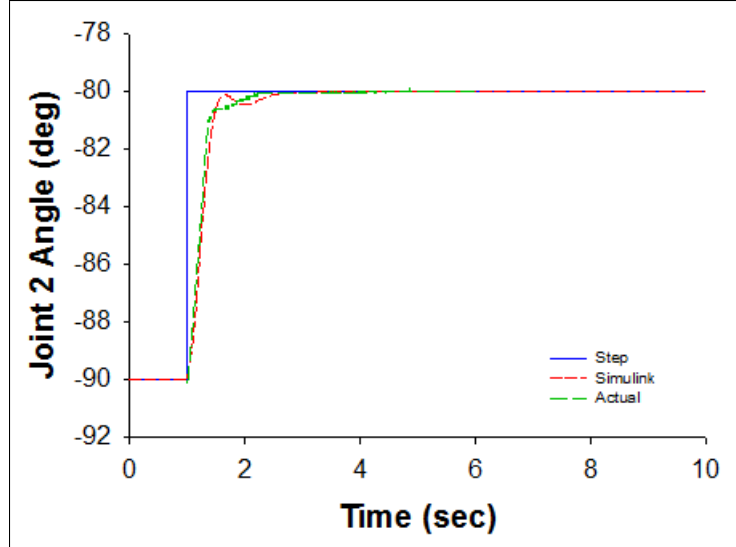


**Figure 8.15. Comparison of theoretical response and actual response for motor 2.**

The characteristics of the theoretical and actual response for motor 2 can be found in Table 8.2.

**Table 8.2. Characteristics of Motor 2 Response**

Response	Rise Time (s)	Overshoot (%)	Settling Time (s)	Steady-State (deg)
Theoretical	0.3799	0	0.5118	-80.000
Actual	0.3106	0	0.7815	-79.992

The actual steady-state value for motor 2 has a 0.01% error in comparison to the theoretical steady-state. Like the response for motor 1, motor 2 appears to be underdamped. This is because the theoretical response has more noticeable oscillations than the actual response. The results for the actual response also show that the actual system may be overdamped, as the actual response does not overshoot the desired response. Instead, it appears that the derivative gain drives the actual response to the desired step signal by reducing the offset.

Figure 8.16 shows the tuned response for motor 3. Like motor 2, motor 3 is also affected by gravity, so a complete PID controller is necessary. The gain values for motor 3 are  $K_P = 5$ ,  $K_I = 9.766$ ,  $K_D = 0.128$ . The proportional gain is 51.2% of the integral gain, and the derivative gain is 1.3% of the integral gain.

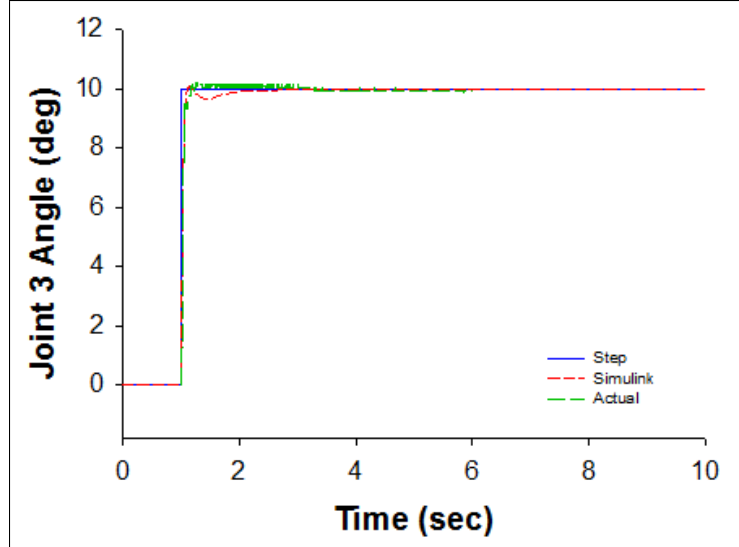


**Figure 8.16. Comparison of theoretical response and actual response for motor 3.**

The characteristics of the theoretical and actual response for motor 3 can be found in Table 8.3.

**Table 8.3. Characteristics of Motor 3 Response**

Response	Rise Time (s)	Overshoot (%)	Settling Time (s)	Steady-State (deg)
Theoretical	0.0651	1.006	0.0867	10.000
Actual	0.0551	1.012	0.1152	9.944

The actual steady-state value for motor 3 has a 0.56% error in comparison to the theoretical steady-state. Unlike motor 1 and motor 2, the actual response for motor 3 overshoots the desired value. There also appears to be a lot of noise for the actual response in the time frame between 1 second and 3 seconds. This may be an indication of a high derivative gain.

Overall, it appears that an individual PID controller for each actuator works well as far as driving the actuator to a desired position. All responses had an error less than or equal to 0.56%. For motors 1 and 2, there is no overshoot in the first peak for the actual response. Instead, it appears that the derivative gain drives the response to the desired signal, decreasing the offset to zero. Motor 3 on the other hand does have overshoot at its first peak, and some noise afterwards until it reaches steady state 2.2788 seconds after the time of input. The model as it is right now does not take into account friction. And the linearized model does not have any velocity terms, so there is no damping whatsoever.

The lack of friction and damping may explain why the simulated model appears to be underdamped in comparison to the actual model. Further discrepancies between the simulated and actual responses may be due to simplifying the location of the center of mass. The actual center of mass for each link can be found in the following tables: Table 5.2 for link 1, Table 5.5 for link 2, and Table 5.8 for link 3. Instead, we assume that the center of mass for link  $i$  is located on the  $x_i$ -axis only at a point exactly halfway between joint  $i$  and joint  $i + 1$ .

## CHAPTER 9

### GRAVITY COMPENSATION

#### 9.1 NO COMPENSATION

One component of a robotic arm exoskeleton is being able to compensate for the torque needed to hold the human limb and the robot in place, as well as move both of them together. Figure 9.1 is a free body diagram showing the forces acting about joint 2 while the robot is in a static position.

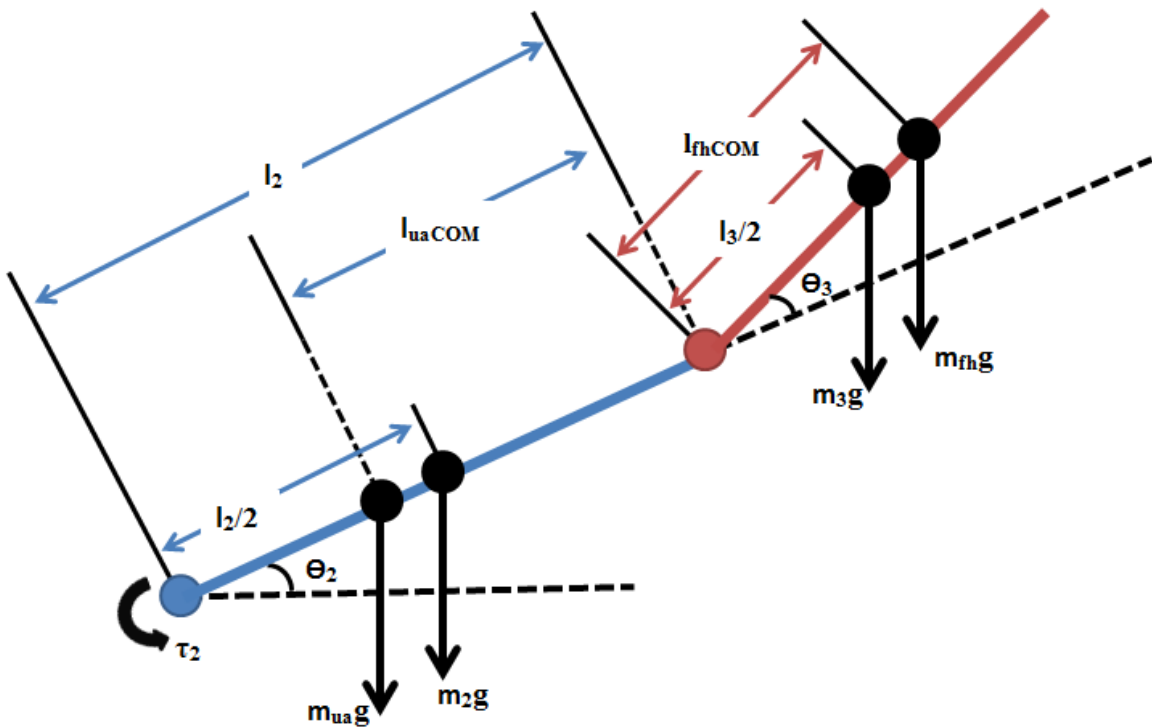


**Figure 9.1. Free body diagram about joint 2 for a static position.**

The forces that are applied on link 2 are the mass of the upper arm, as well as the mass of the link itself. As for link 3, the applied forces are the combined mass of the forearm and the hand, as well as the mass of link 3. By summing the torques about joint 2, we can find the static torque about joint 2 as

$$\begin{aligned}\tau_2 = & m_{ua}g(l_2 - l_{uaCOM})\cos\theta_2 + m_2g\frac{l_2}{2}\cos\theta_2 \\ & + m_3g\left(l_2\cos\theta_2 + \frac{l_3}{2}\cos(\theta_2 + \theta_3)\right) + m_{fh}g\left(l_2\cos\theta_2 + l_{fhCOM}\cos(\theta_2 + \theta_3)\right).\end{aligned}\quad (9.1)$$

Information on the properties of the upper arm, including the mass and center of mass, can be found in Table 9.1 [36]:

**Table 9.1. Properties of Upper Arm**

Property	Value
Mass	1.73 kg
Center of Mass from Acromion (Shoulder)	17.13 cm
Location of Center of Mass as a Ratio of Segment Size	51.30

For the combination of the robot and the human arm, the elbow is assumed to be aligned at joint 3. Thus, the distance for the upper arm center of mass used in Equation 9.1 is the difference between the length of link 2 and the distance between the center of mass of the upper arm to the elbow. Using the properties of Table 9.1, the distance from joint 2 to the upper arm center of mass is found to be 9.9113cm. Similarly, the information on the properties of the forearm and hand can be found in Table 9.2 [36]:

**Table 9.2. Properties of Forearm and Hand**

Property	Value
Mass	1.483 kg
Center of Mass from Radiale (Elbow)	16.21 cm
Location of Center of Mass as a Ratio of Segment Size	62.58

In the case of no human limb in the robotic arm, and with the use of the information taken from Tables 5.4, 5.7, and 6.1, Equation 9.1 is used to find the static torque about joint 2 with only the weights of the links themselves for different angles of joint 2 and a fixed joint 3 angle of zero. The results are plotted in Figure 9.2. The area highlighted in yellow is the recommended torque range of the Dynamixel MX-64R motor, which is  $\pm 1.2Nm$ . At  $\theta_2 = -66^\circ$  and  $\theta_3 = 0^\circ$ , the motor reaches approximately  $1.2Nm$ . The minimum desired range of motor 2 is between  $-90^\circ$  and  $0^\circ$ . So without any human arm and no gravity compensation, the robotic arm is only able to utilize less than a third of the desired range.

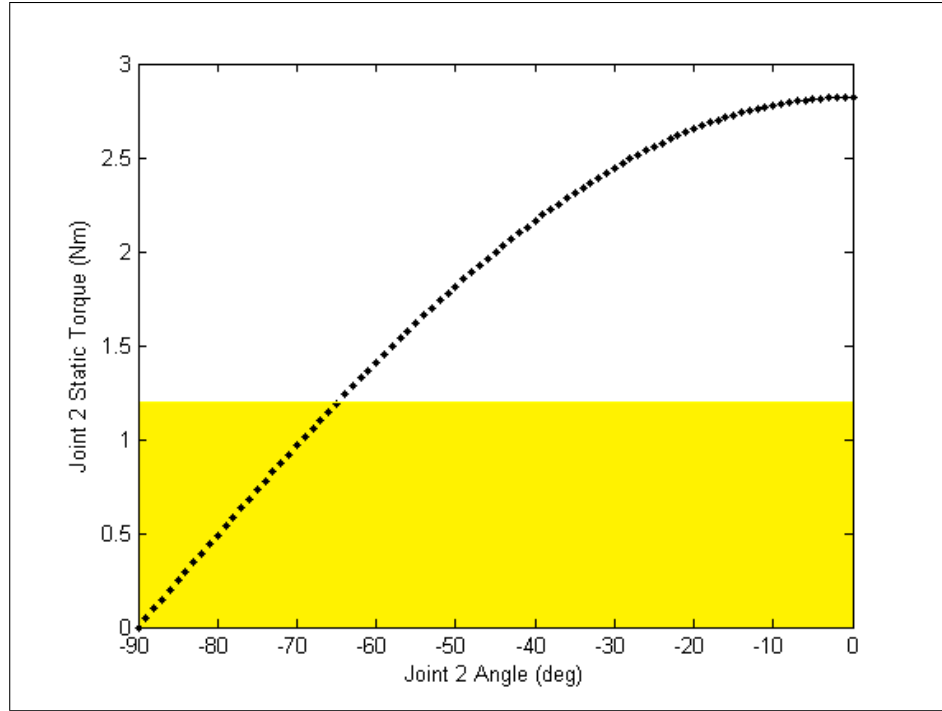


**Figure 9.2. Static joint 2 torque with no limb. Area highlighted in yellow shows recommended torque range for motor.**

## 9.2 CONSTANT FORCE SPRING

The method explored to compensate for gravity is the use of a constant force spring. A constant force spring is a radial spring that produces a constant force no matter the extended length of the spring. As a result, the constant force is similar to a counterweight system attached to a pulley. Figure 9.3 shows a constant force spring attached to the robotic arm, in which the force is applied to link 2 at a known distance.



**Figure 9.3. Side view and front view of robotic arm with constant force spring attached.**

To account for the constant force spring, an upward force is added to link 2. Figure 9.4 is an updated force body diagram.

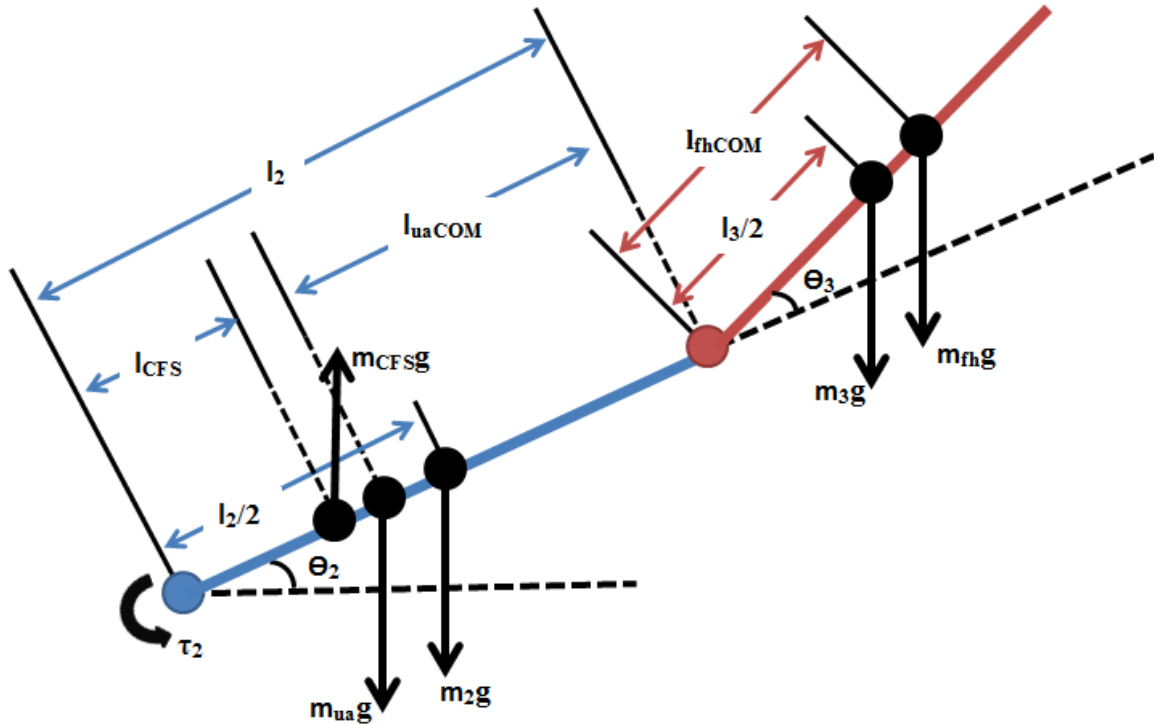


**Figure 9.4. Free body diagram about joint 2 for a static position with a constant force spring applied along link 2.**

With the additional force due to the constant force spring, the sum of the torques equation becomes

$$\begin{aligned}\tau_2 = & -m_{CFS}l_{CFS} \cos \theta_2 + m_{uag}(l_2 - l_{uaCOM}) \cos \theta_2 + m_2g \frac{l_2}{2} \cos \theta_2 \\ & + m_3g \left( l_2 \cos \theta_2 + \frac{l_3}{2} \cos(\theta_2 + \theta_3) \right) + m_{fhg} \left( l_2 \cos \theta_2 + l_{fhCOM} \cos(\theta_2 + \theta_3) \right).\end{aligned}\quad (9.2)$$

Different spring options include the following equivalent counterweight mass:

- 7 lb;
- 10.6 lb;
- 14 lb;
- 24.8 lb.

Using Equation 9.2, assuming no human arm, for a  $\theta_2$  range of  $-90^\circ$  to  $0^\circ$  and a fixed  $\theta_3$  of  $0^\circ$  leads to the results found in Figure 9.5.

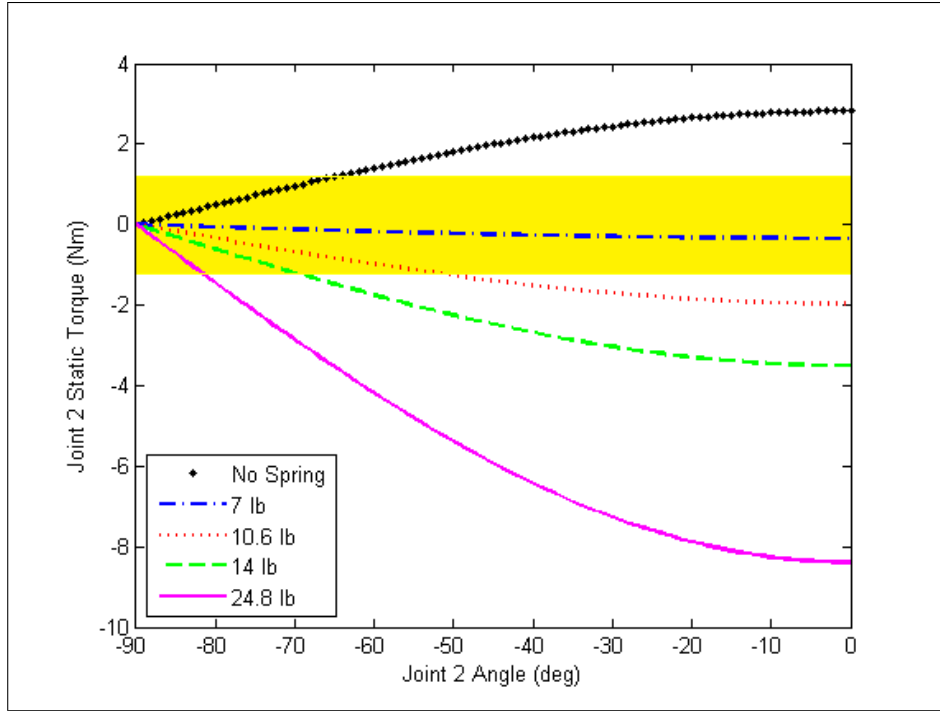


**Figure 9.5.** Static joint 2 torque with no limb for various constant force springs. Area highlighted in yellow shows recommended torque range for motor.

The best result for gravity compensation came from the use of the 7 lb constant force spring. The largest joint 2 torque for the 7 lb constant force spring was  $-0.3423\text{Nm}$  when  $\theta_2 = 0^\circ$ . A negative value of torque means that the arm is working in the same direction as gravity as the spring overcompensates for the masses. These results are however only valid for the case when the robotic arm does not have a human arm utilizing it.

Utilizing Tables 9.1 and 9.2 for the properties of the human arm with Equation 9.2, the static torque at joint 2 can be found for various arm positions. Figure 9.6 shows the results of no spring and the various springs for  $\theta_2$  range of  $-90^\circ$  to  $0^\circ$ , and a fixed joint 3 angle of  $0^\circ$ . The results show that the only constant force spring capable of compensating for the additional weight of the human arm is the 24.8 lb spring. As link 2 moves from  $-90^\circ$  to  $0^\circ$ , the motor does less work against the spring as the torque due to the masses of the links and of the human arm increases. Figure 9.7 shows the results of  $\theta_2$  fixed at  $0^\circ$ , and  $\theta_3$  with a range of  $0^\circ$  to  $90^\circ$ . In this instance, the 24.8 lb constant force spring overcompensates for gravity at  $\theta_3 = 38^\circ$  at which point the motor will fail. The results of Figures 9.6 and 9.7 show that this combination of springs and motors are not enough to make a lightweight exoskeleton at joint 2.

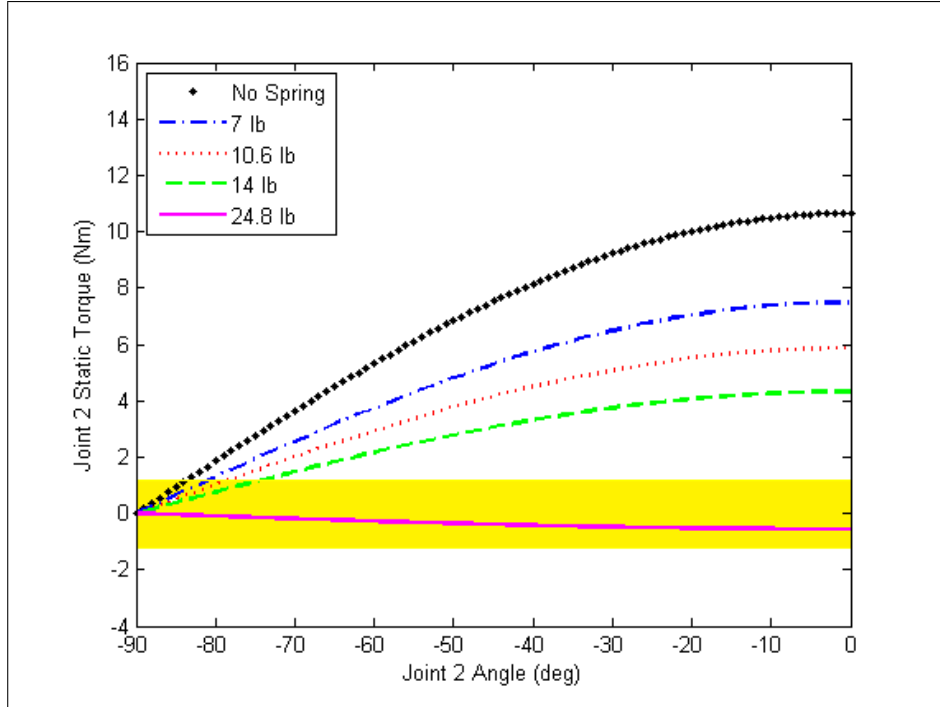


**Figure 9.6.** Static joint 2 torque with limb for joint 3 angle fixed at zero. Area highlighted in yellow shows recommended torque range for motor.

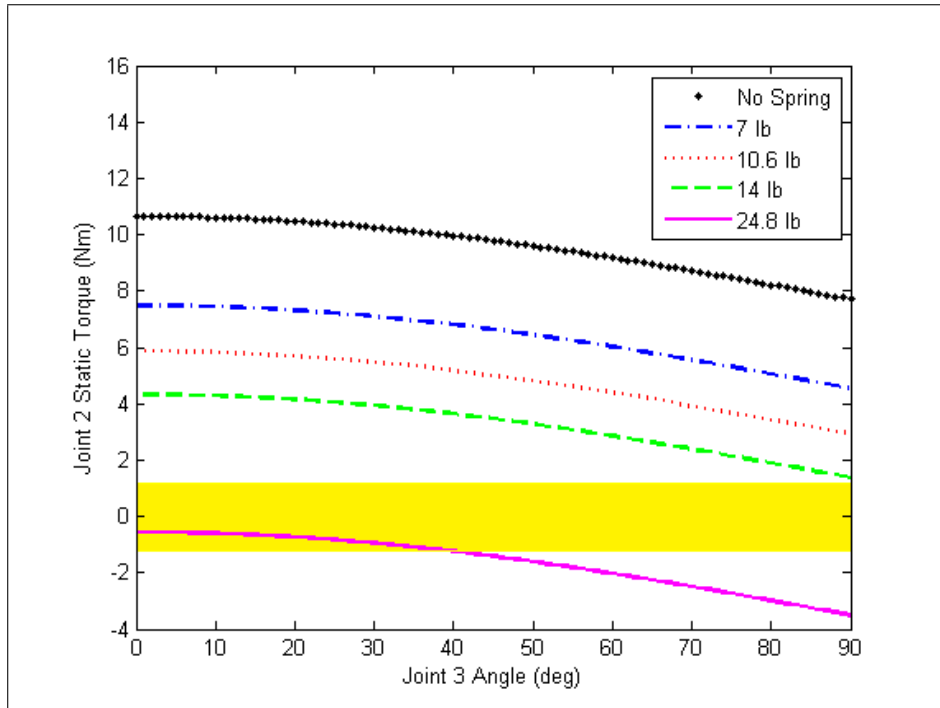


**Figure 9.7.** Static joint 2 torque with limb for joint 2 angle fixed at zero. Area highlighted in yellow shows recommended torque range for motor.

## CHAPTER 10

### DETERMINATION OF USER INTENT

#### 10.1 TORQUE FEEDBACK

One of the features of the ROBOTIS Dynamixel line of actuators is its ability to provide load information. The actuator does not provide a value of the actual applied torque however, but instead provides an inferred value [29]. To see how useful the load reading could be, various weights were hung from the motor at a set distance. Fig. 10.1 shows load information in units of *counts*, a dimensionless load value, versus applied torque in *Nm*.

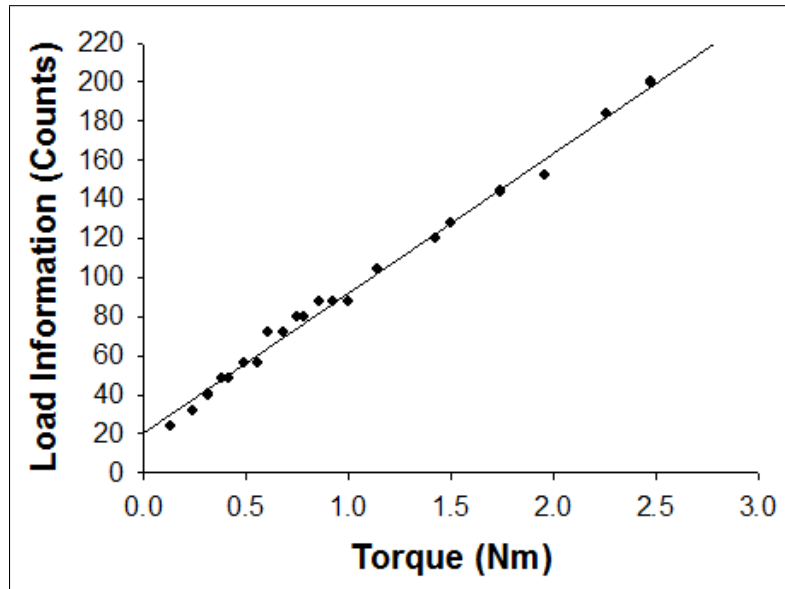


**Figure 10.1.** Torque sensor calibration.

A linear fit was performed for the points of Fig. 10.1 to get the following equation to convert the motor reading in counts to a value of applied torque:

$$y = 71.88x + 20.01. \quad (10.1)$$

The input  $x$  is in units of *counts*, and the output  $y$  is in units of *Nm*. The R-squared value for the linear fit is 0.9922, which shows a strong fit.

To test the accuracy of the load information, motor 3 and link 3 were removed from the robot to reduce it to a 2DOF system. The reason for reducing the number of DOFs to two

is to lower the number of variables affecting the torques about joints 1 and 2. Figure 10.2 is a CAD model of the simplified system.

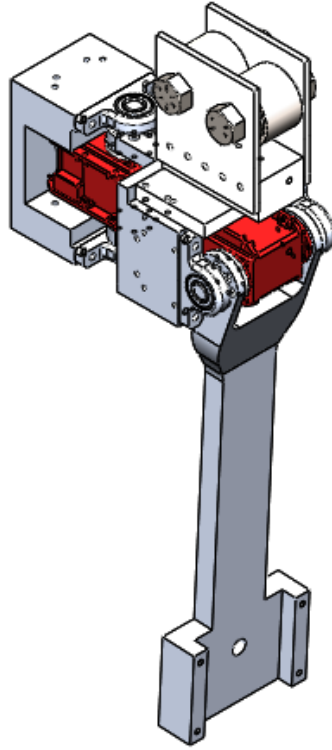


**Figure 10.2. Model of 2DOF system.**

In addition, the static torque will be used to verify the torque sensor.

By using the static torque values, the system has no motion, so there is no kinetic energy. Equation (3.63) then reduces to

$$L = -U. \quad (10.2)$$

Using Equations (3.97) and (3.98), the total potential energy of the system becomes

$$U = -m_1 \vec{g}^T \vec{r}_{c_1} - m_2 \vec{g}^T \vec{r}_{c_2}. \quad (10.3)$$

In general, the center of mass for link 1 in frame 1 is

$${ }^1 r_{c_1} = \begin{Bmatrix} L_{1COM_x} \\ L_{1COM_y} \\ L_{1COM_z} \\ 1 \end{Bmatrix}. \quad (10.4)$$

Using Equations (6.2) and (10.4), we can find the center of mass for link 1 in the global frame as

$${}^0r_{c_1} = {}^0T_1 {}^0\vec{r}_{c_1} \quad (10.5)$$

$$= \begin{bmatrix} \cos \theta_1 & -\sin \theta_1 & 0 & 0 \\ \sin \theta_1 & \cos \theta_1 & 0 & 0 \\ 0 & 0 & 1 & 0 \\ 0 & 0 & 0 & 1 \end{bmatrix} \begin{Bmatrix} L_{1COM_x} \\ L_{1COM_y} \\ L_{1COM_z} \\ 1 \end{Bmatrix} \quad (10.6)$$

$$= \begin{Bmatrix} L_{1COM_x} \cos \theta_1 - L_{1COM_y} \sin \theta_1 \\ L_{1COM_x} \sin \theta_1 + L_{1COM_y} \cos \theta_1 \\ L_{1COM_z} \\ 1 \end{Bmatrix}. \quad (10.7)$$

Table 5.2 can be used as reference for the location of the center of mass for link 1.

For link 2, the general vector for the center of mass in frame 2 is

$${}^2r_{c_2} = \begin{Bmatrix} L_{2COM_x} \\ L_{2COM_y} \\ L_{2COM_z} \\ 1 \end{Bmatrix}. \quad (10.8)$$

Using Equations (6.7) and (10.8), we can find the center of mass for link 1 in the global frame as

$${}^0r_{c_1} = {}^0T_1 {}^0\vec{r}_{c_1} \quad (10.9)$$

$$= \begin{bmatrix} \cos \theta_1 \cos \theta_2 & -\cos \theta_1 \sin \theta_2 & \sin \theta_1 & a_1 \cos \theta_1 \\ \sin \theta_1 \cos \theta_2 & -\sin \theta_1 \sin \theta_2 & -\cos \theta_1 & a_1 \sin \theta_1 \\ \sin \theta_2 & \cos \theta_2 & 0 & 0 \\ 0 & 0 & 0 & 1 \end{bmatrix} \begin{Bmatrix} L_{2COM_x} \\ L_{2COM_y} \\ L_{2COM_z} \\ 1 \end{Bmatrix} \quad (10.10)$$

$$= \begin{Bmatrix} L_{2COM_x} c\theta_1 c\theta_2 - L_{2COM_y} c\theta_1 s\theta_2 + L_{2COM_z} s\theta_1 + a_1 c\theta_1 \\ L_{2COM_x} s\theta_1 c\theta_2 - L_{2COM_y} s\theta_1 s\theta_2 - L_{2COM_z} c\theta_1 + a_1 s\theta_1 \\ L_{2COM_x} s\theta_2 + L_{2COM_z} c\theta_2 \\ 1 \end{Bmatrix}. \quad (10.11)$$

The center of mass for link 2 will be in a different location from that previously determined in Chapter 5. The mass of link 2 in this configuration is 0.556 kg. And the center of mass for link 2 for this configuration can be found in Table 10.1.

**Table 10.1. Center of Mass of Link 2 for 2DOF Configuration**

Axis	Location (m)
x	0.159185
y	-0.020642
z	0.000007

Plugging in Equations (10.7) and (10.11) into Equation (10.3) will lead to the total potential energy of the 2DOF system:

$$U = -m_1 [0 \ 0 \ -g] \begin{Bmatrix} L_{1COM_x} \cos \theta_1 - L_{1COM_y} \sin \theta_1 \\ L_{1COM_x} \sin \theta_1 + L_{1COM_y} \cos \theta_1 \\ L_{1COM_z} \end{Bmatrix} \quad (10.12)$$

$$- m_2 [0 \ 0 \ -g] \begin{Bmatrix} L_{2COM_x} c\theta_1 c\theta_2 - L_{2COM_y} c\theta_1 s\theta_2 + L_{2COM_z} s\theta_1 + a_1 c\theta_1 \\ L_{2COM_x} s\theta_1 c\theta_2 - L_{2COM_y} s\theta_1 s\theta_2 - L_{2COM_z} c\theta_1 + a_1 s\theta_1 \\ L_{2COM_x} s\theta_2 + L_{2COM_z} c\theta_2 \end{Bmatrix}$$

$$= -m_1 [(-g)L_{1COM_z}] - m_2 [(-g)(L_{2COM_x} s\theta_2 + L_{2COM_y} c\theta_2)] \quad (10.13)$$

$$= m_1 g L_{1COM_z} + m_2 g (L_{2COM_x} s\theta_2 + L_{2COM_y} c\theta_2) \quad (10.14)$$

The Euler-Lagrange Equation, Equation (3.65), can then be used to find the torques for joint 1 and joint 2. Because there is motion in the system, the following terms become zero:

$$\frac{\partial L}{\partial \dot{\theta}_1} = \frac{\partial L}{\partial \dot{\theta}_2} = 0. \quad (10.15)$$

The general equation for the static joint torques becomes

$$\tau_i = -\frac{\partial L}{\partial \theta_i} \quad (10.16)$$

$$= \frac{\partial}{\partial \theta_i} \left[ m_1 g L_{1COM_z} + m_2 g (L_{2COM_x} s\theta_2 + L_{2COM_y} c\theta_2) \right]. \quad (10.17)$$

For  $i = 1$ , Equation (10.17) is

$$\tau_1 = \frac{\partial}{\partial \theta_1} \left[ m_1 g L_{1COM_z} + m_2 g (L_{2COM_x} s\theta_2 + L_{2COM_y} c\theta_2) \right] \quad (10.18)$$

$$= 0. \quad (10.19)$$

For  $i = 2$ , Equation (10.17) is

$$\tau_2 = \frac{\partial}{\partial \theta_2} \left[ m_1 g L_{1COM_z} + m_2 g \left( L_{2COM_x} s\theta_2 + L_{2COM_y} c\theta_2 \right) \right] \quad (10.20)$$

$$= m_2 g \left( L_{2COM_x} c\theta_2 - L_{2COM_y} s\theta_2 \right). \quad (10.21)$$

Figure 10.3 presents a comparison between the expected joint torque and the actual joint torque for motor 1.

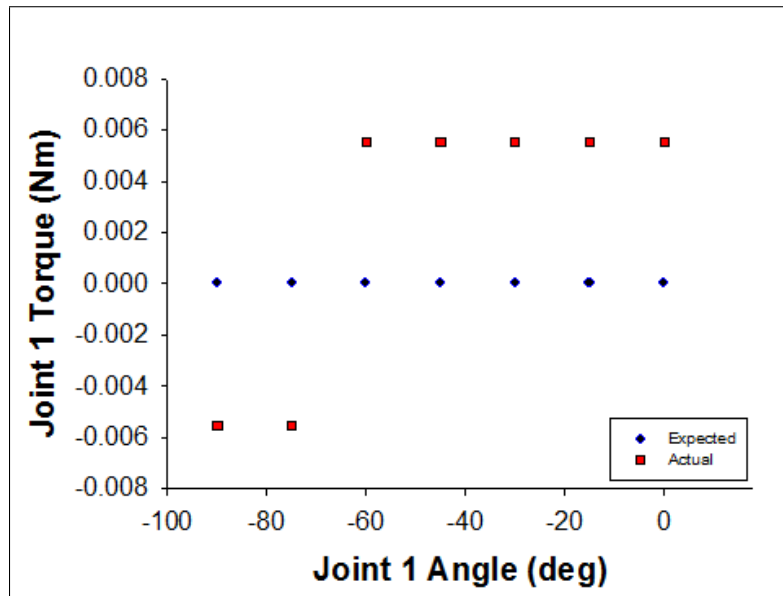


**Figure 10.3. Comparison of theoretical joint torque and actual joint torque for motor 1.**

As this joint is not affected by gravity directly, the expected joint torque is zero while the robot is not in motion. The actual joint torque do not match exactly, but are approximately  $\pm 0.0056 Nm$ .

The comparison between the expected joint torque and the actual joint torque for motor 2 can be found in Figure 10.4. The actual torque values do not match the theoretical torque values in Figure 10.4. They do however, match the pattern of an increase in torque as the arm moves to a higher joint angle. But as the torque increases, the error increases as well. Because of the discrepancy between the expected value and the actual value, the load information does not appear to be reliable.

Instead the load information appears to be much more closely related to position error. Position error is simply the actual position value in counts subtracted by the desired position

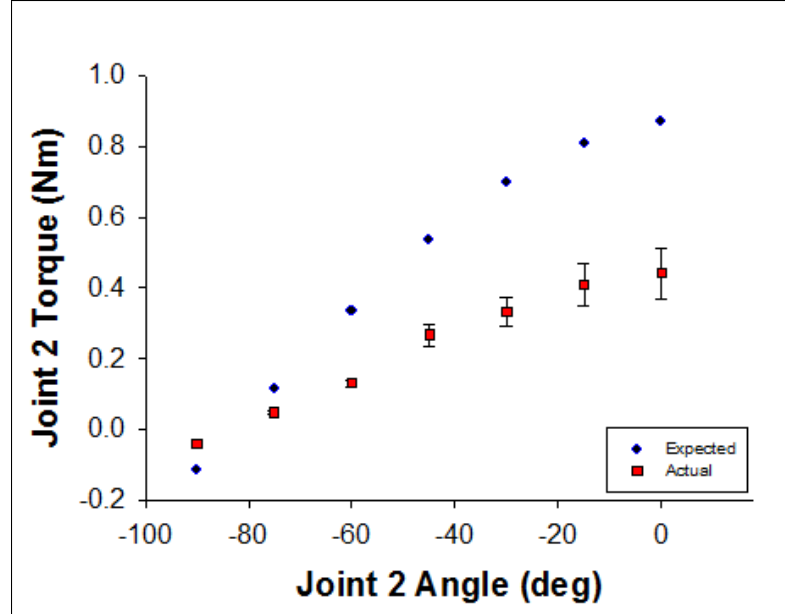


**Figure 10.4.** Comparison of theoretical joint torque and actual joint torque for motor 2.

value in counts. Figure 10.5 is a plot with the load information plotted against the left y-axis scale, and the position error plotted against the right y-axis scale for motor 1.

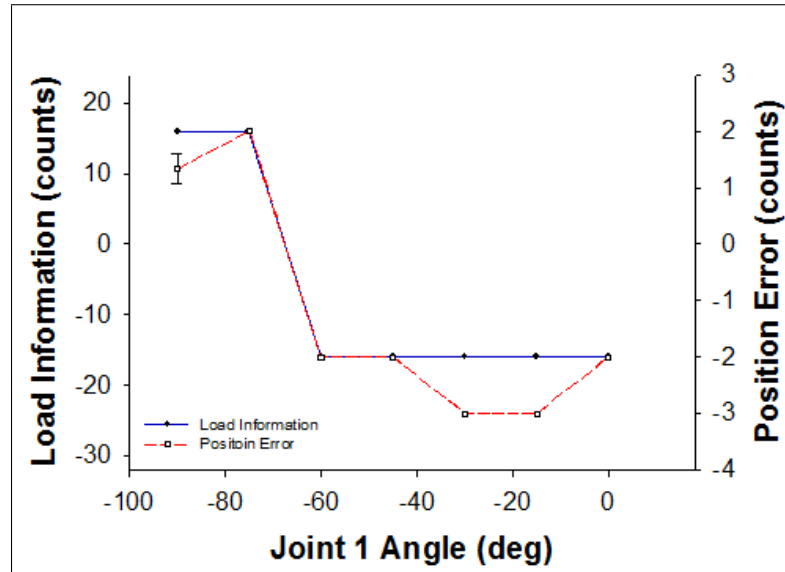


**Figure 10.5.** Load information compared to position error for motor 1.

There is a similar pattern between the load information and the position error, where there is an 8:1 ratio between the two. The resolution of the load information is 8 counts.

Because the position error is small, where 1 count is approximately  $0.088^\circ$ , it is hard to make any conclusions based on the results of motor 1 alone.

Figure 10.6 is a plot with the load information plotted against the left y-axis scale, and the position error plotted against the right y-axis scale for motor 2.

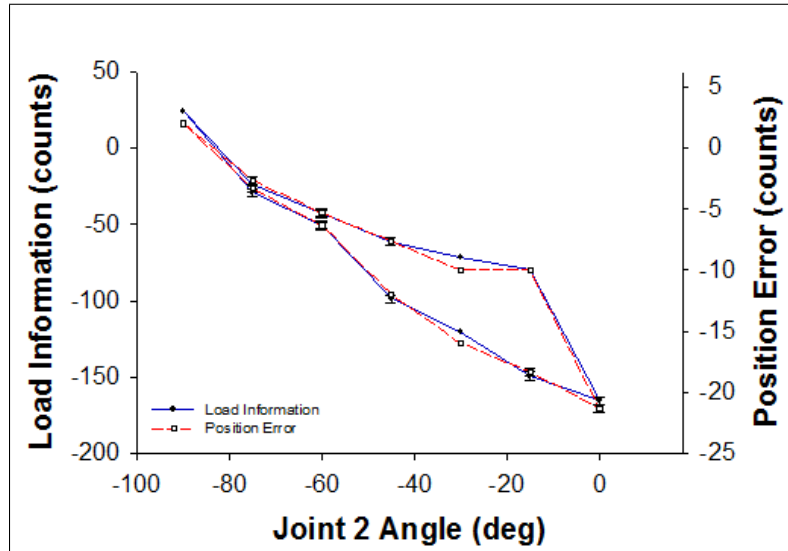


**Figure 10.6. Load information compared to position error for motor 2.**

The similarity in pattern is much more evident for motor 2. Because the position error is much larger, it is much easier to get a value for load information that is eight times the position error. Previously, motor 2 was found to have hysteresis when it came to position error for the 3DOF system as seen in Figure 5.12. Similarly, motor 2 has a hysteresis of position error for the 2DOF system. Because the load information is closely correlated to position error, the torque has hysteresis as well. This further shows how unreliable the load information is, as solving for the static torque for different joint angles should consistently produce the same value, regardless of the direction the motor is moving to before stopping.

## 10.2 ELECTROMYOGRAPHY FEEDBACK

Another method of determining user intent would be to use the user's biosignals. In this case, sEMG data recorded from the surface of the user's skin would drive the robot's movements using the Delsys Trigno system. As a proof of concept, only motor 3 was actuated by the sEMG information, in which electrodes were placed on the user's forearm to record muscle activity for two different wrist motions: flexion of the wrist and extension of the wrist. These motions primarily use forearm muscles to produce the movement.

Figure 10.7 shows a man performing wrist flexion, in which the wrist is bent such that the palms are bending toward the forearm. The muscles used for this action include the flexor carpi radialis, and the flexor carpi ulnaris [40].



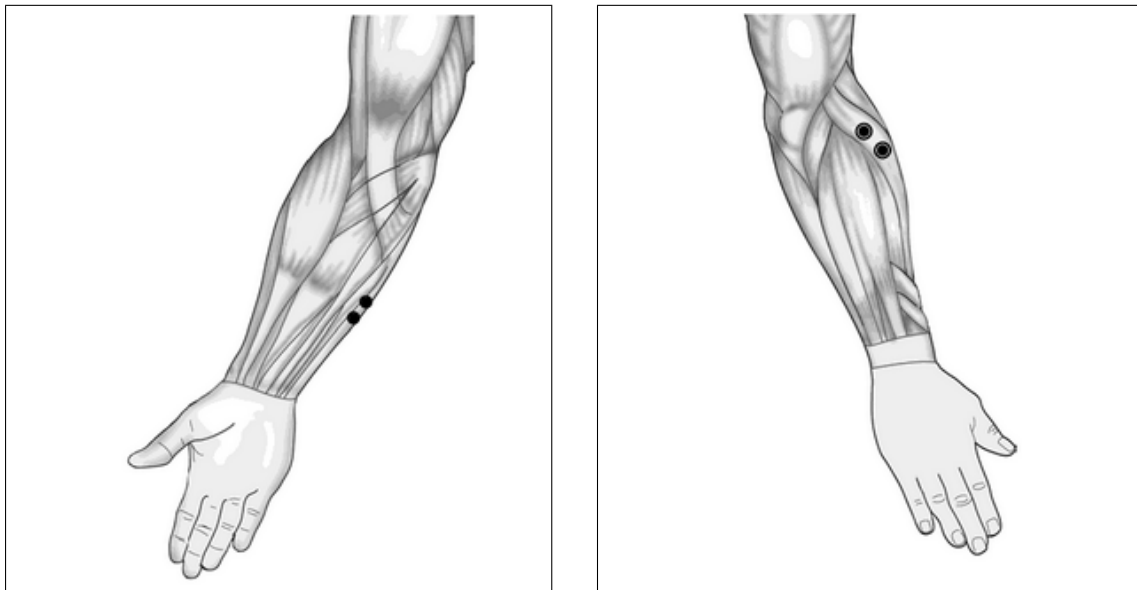
**Figure 10.7. Wrist flexion.** Source: University of Michigan. “Movements of the Upper Limb.” *Learning Modules - Medical Gross Anatomy*. Ann Arbor, 2002.

Figure 10.8 shows the same man performing wrist extension, in which the wrist is bent such that the palms are bending away from the forearm. The muscles used to produce this motion include the extensor carpi radialis, and the extensor carpi ulnaris [40].



**Figure 10.8. Wrist extension.** Source: University of Michigan. “Movements of the Upper Limb.” *Learning Modules - Medical Gross Anatomy*. Ann Arbor, 2002.

The muscle chosen to determine when flexion of the wrist occurs is the flexor carpi ulnaris, and the muscle used to determine when extension of the wrist occurs will be the extensor carpi ulnaris. Figures 10.9 and 10.10 show where the electrodes should be placed for both muscles [41].



**Figure 10.9.** Electrode placement for flexor carpi ulnaris. Source: Cram, Jeffrey, Glenn Kasman, and Jonathan Holtz. “Atlas for Electrode Placement.” In *Cram’s Introduction to Surface Electromyography*, edited by Eleanor Criswell, 245-383. Sudbury: Jones and Bartlett Publishers, 2011.

**Figure 10.10.** Electrode placement for extensor carpi ulnaris. Source: Cram, Jeffrey, Glenn Kasman, and Jonathan Holtz. “Atlas for Electrode Placement.” In *Cram’s Introduction to Surface Electromyography*, edited by Eleanor Criswell, 245-383. Sudbury: Jones and Bartlett Publishers, 2011.

The raw EMG data is not very useful information on its own. Instead, the data must be processed such that information can be used to determine what is going on in the muscle. In this case, the raw EMG signal is squared to bring all the data points onto the positive side of zero, and to magnify instances of muscle activity. Figure 10.11 shows the raw EMG during wrist flexion, and Figure 10.12 shows the raw EMG squared for wrist flexion. The region highlighted in yellow is the time frame in which wrist flexion takes place.

In Figure 10.11, there seems to be a little crosstalk in the extensor carpi ulnaris muscle during wrist flexion. Crosstalk is when electrical activity of one muscle travels through another muscle [33]. There appears to be crosstalk as the frequency increases during the time frame of wrist flexion. Otherwise, the amplitude does not increase noticeably. The amplitude does increase quite noticeably for the flexor carpi ulnaris during flexion of the wrist. Although

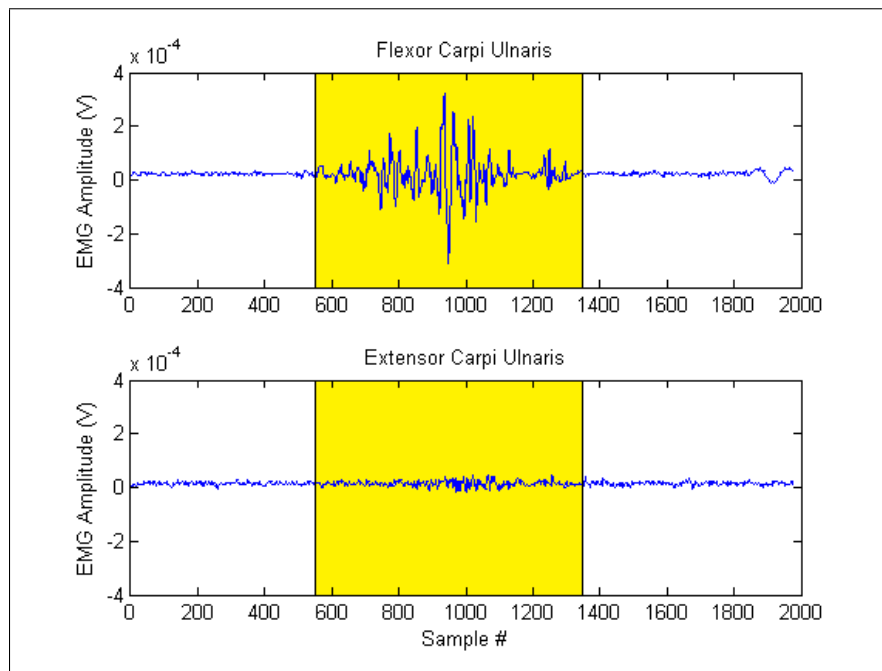


**Figure 10.11.** Raw EMG of flexor carpi ulnaris and extensor carpi ulnaris muscles during wrist flexion. Area highlighted in yellow is when wrist flexion takes place.

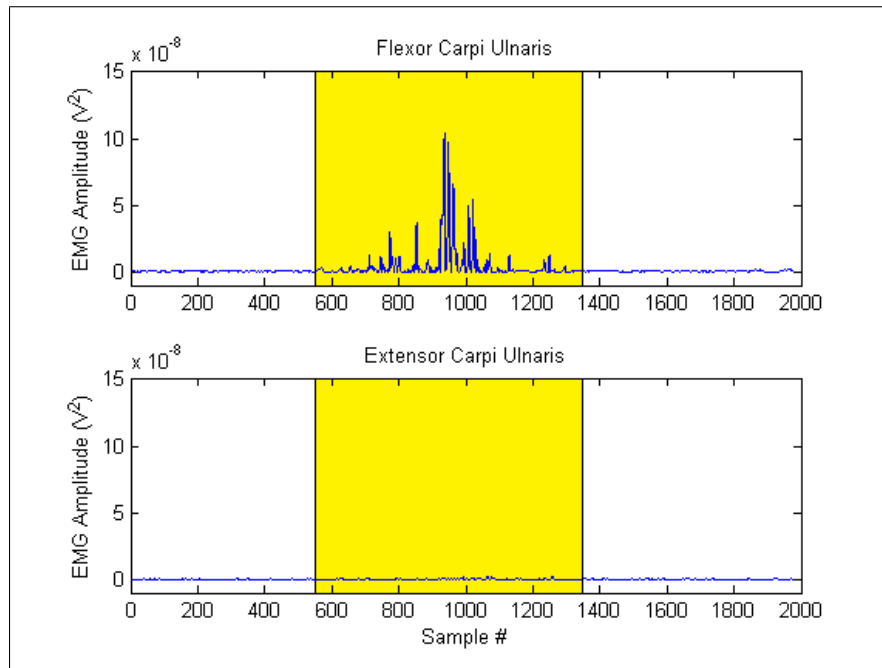


**Figure 10.12.** Squared EMG of flexor carpi ulnaris and extensor carpi ulnaris muscles during wrist flexion. Area highlighted in yellow is when wrist flexion takes place.

it appears quite evident when the motion occurs, it is much easier to determine once the signal is squared. The maximum of the flexor carpi ulnaris squared signal is  $2.3693e-9 V^2$ , while the maximum of the extensor carpi ulnaris squared signal is  $1.0462e-7 V^2$ . The difference in magnitude between the two signals is approximately 1.645. This shows that the two muscles are virtually independent of one another during wrist flexion.

For wrist extension, Figure 10.13 shows the raw EMG signal, and Figure 10.14 shows the squared EMG signal. The area highlighted in yellow is the time frame in which wrist extension occurs.

Unlike the extensor carpi ulnaris during flexion of the wrist, crosstalk does not seem to occur for the flexor carpi ulnaris during extension of the wrist. Similarly to the flexor carpi ulnaris during wrist flexion, the extensor carpi ulnaris during wrist extension shows more activity. This becomes even more apparent once the signals are squared. The maximum of the flexor carpi ulnaris squared signal is  $1.2072e-9 V^2$ , while the maximum of the extensor carpi ulnaris squared signal is  $2.1867e-8 V^2$ . The difference between the two signals of the muscle is a magnitude of approximately 1.258. Like flexion of the wrist, the two muscles appear to be independent of each other during extension of the wrist as well.

As the two muscles appear to be independent of one another during both flexion of the wrist and extension of the wrist, the electrical activity of each muscle became the input for moving motor 3 in the robotic arm. To move the motor in the counter-clockwise direction, the user would perform flexion of the wrist. If the squared signal passed a threshold value of  $5e-8 V^2$ , that would trigger the motor to start moving. To stop the motor from moving in the counter-clockwise direction, the user would perform wrist extension. If the squared signal passed a threshold value of  $1e-8 V^2$ , the motor would stop moving. The threshold values carried over to rotating the motor clockwise, which is initiated by extension of the wrist. To stop the motor from moving clockwise, the user would perform flexion of the wrist.

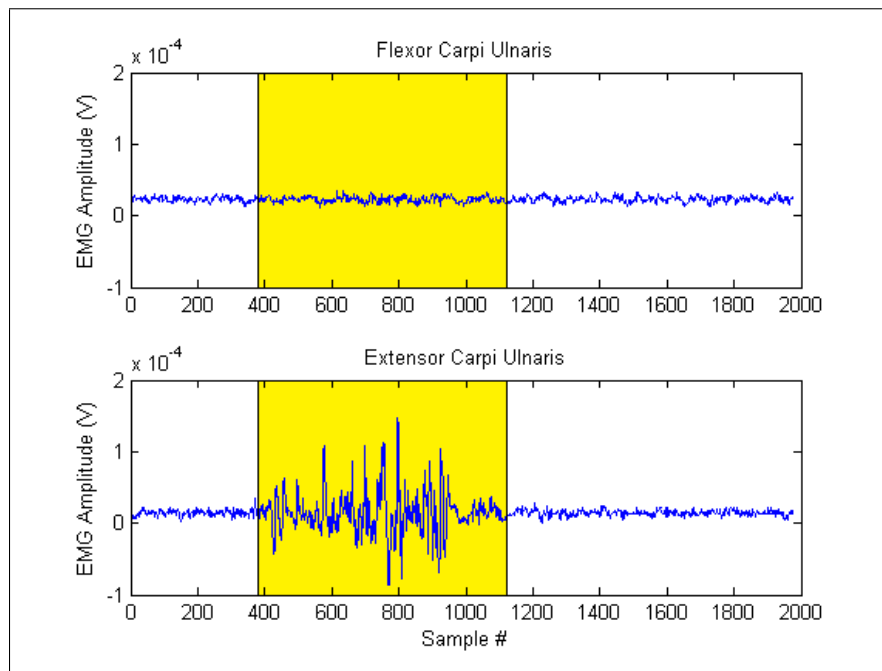


**Figure 10.13. Raw EMG of flexor carpi ulnaris and extensor carpi ulnaris muscles during wrist extension. Area highlighted in yellow is when wrist extension takes place.**

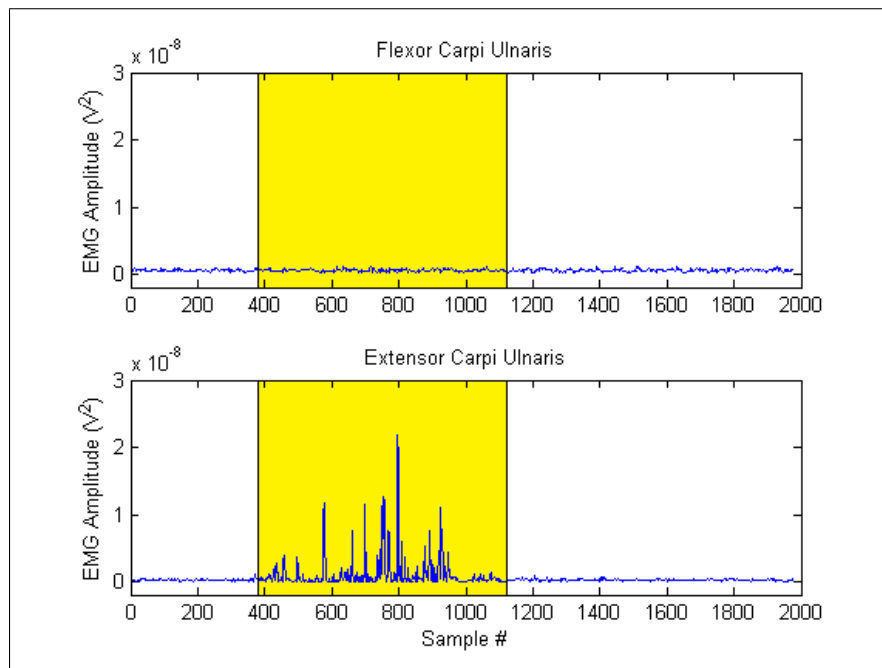


**Figure 10.14. Squared EMG of flexor carpi ulnaris and extensor carpi ulnaris muscles during wrist extension. Area highlighted in yellow is when wrist extension takes place.**

## CHAPTER 11

### CONCLUSION

There is a growing need for robots in the healthcare industry. One way in which robots have helped people medically, is in the form of exoskeletons and prosthetics. Robots taking these forms increase the usefulness of a user's limb, either by restoring functionality that was lost due to injury or disease, or by replacing the limb altogether.

The purpose of this research is to design a lightweight exoskeleton device that restores function to the user's upper arm. This exoskeleton is attached to a wheelchair, and is to be portable. With a lightweight device, there is a tradeoff between size and weight for torque. The actuators used were Dynamixel MX-64R which have a holding torque of  $6\text{Nm}$ . The recommended torque however is 25% of the holding torque, or  $1.2\text{Nm}$ . With such strict restrictions on torque, a constant force spring was used to compensate for the forces applied to joint 2. Various constant force springs were examined, but none were enough to compensate for the minimum range of joint 2 and joint 3 angles.

The microcontroller for each motor allows for individual PID controllers. These controllers worked well, as the actual response for all three motors were within 1% of the theoretical value. More can be done to improve the results though, as the theoretical model appears underdamped. Furthermore, the results are best when working near the equilibrium point. The further away the links move from the equilibrium point, the more torque the motors experience, leading to increased inaccuracy in position control.

As far as determining user intent, the built-in feedback for load information of the Dynamixel was shown not to be accurate enough to determine joint torque. Instead, load information provided by the motor appears to be more a function of position error. An alternative means to determining user intent is to use biosignals, such as EMG. This method was shown to be effective for flexion and extension of the wrist; two separate sensors captured muscles whose electrical activity were virtually independent of one another for those movements.

## CHAPTER 12

### FUTURE WORK

Although the results of the PID controller were excellent, more can be done to improve the theoretical model. One item not addressed in the research was the existence of friction in the system. Friction was not accounted for due to difficulty measuring it, as well as the difficulty that comes with accounting for all the factors that affect it. Some factors that affect friction include temperature, material of contacting bodies, and lubrication [42]. Furthermore, friction is mostly a non-linear phenomenon [43]. The approach taken in this thesis was to use a linearized model for the PID controller which resulted in no damping terms. If the non-linear model did have friction, linearization would eliminate most of the friction terms. Two different approaches could be taken to improve the control of the output response while accounting for friction: PID controller for the non-linear model and adaptive control.

Another aspect of the model not taken into account were actuator dynamics. For this research, the dynamic model of the robotic arm is a set of second-order, non-linear differential equations. But if actuator dynamics are to be accounted for in the dynamic model, the system becomes a set of third-order differential equations [44]. The incorporation of actuator dynamics into the system model results in a trade-off: higher model accuracy at the expense of controller simplicity [45].

As far as designing a lightweight robotic arm exoskeleton, there is a tradeoff when it comes to size and torque; the larger the output torque, the larger the size. The motor was sufficient in only select positions, especially with a human arm and a constant force spring to balance the weight of the limb and the links. One way of improving the system is to use a larger motor. A possible choice would be one of the motors in the Dynamixel Pro series, such as the H54-200-S500-R, which is capable of a continuous torque of 44.2 Nm [46]. With a small form factor and large torque rating comes a steep price as it currently costs almost three thousand dollars.

By measuring the biosignals of two muscles whose electrical activity were virtually independent of one another, motion of the wrist was able to determine user intent. This only controls one motor however. Because the results showed great promise, the scope can easily be widened to have the EMG sensors work for six separate muscles to control all three degrees-of-freedom. Problems that may arise due to the shortcomings of sEMG include same muscle movements being expressed by different muscle group, as well as crosstalk [33].

## REFERENCES

- [1] Bogue, Robert. "Robots in healthcare." *Industrial Robot: An International Journal* 38, no. 3 (2011): 218-223.
- [2] Rosen, Jacob, and Joel Perry. "Upper Limb Powered Exoskeletons." *International Journal of Humanoid Robotics* 12, no. 4 (2007): 529-548.
- [3] Bogue, Robert. "Exoskeletons and robotic prosthetics: a review of recent developments." *Industrial Robot: An International Journal* 36, no. 5 (2009): 421-427.
- [4] Nof, Shimon F. Preface to *Handbook of Industrial Robots*, edited by Shimon F. Nof, xvii-xviii. New York: John Wiley & Sons, 1999.
- [5] Altschuler, Eric Lewin, et. al. "Linguistic evidence supports date for Homeric epics." *BioEssays* 35, no. 5 (2013): 417-420.
- [6] Nocks, Lisa. *The Robot: The Life Story of a Technology*. Westport: Greenwood Publishing Group, Inc, 2007.
- [7] Engelberger, Joseph F. "Historical Perspective of Industrial Robotics." In *Handbook of Industrial Robots*, edited by Shimon F. Nof, xvii-xviii. New York: John Wiley & Sons, 1985.
- [8] Pons, J.L., Ceres R., and L. Calderon. Introduction to *Wearable Robotics: Biomechatronic Exoskeletons*, edited by J.L. Pons, 1-16. Madrid: John Wiley & Sons, Ltd, 2008.
- [9] E. Guizzo, Erico, and H. Goldstein. "The Rise of the Body Bots," *IEEE Spectrum* 2, no. 10 (2005): 50-56.
- [10] Sankai, Yoshiyuki. "Leading Edge of Cybernics: Robot Suit HAL." Paper presented at the 2006 SICE-ICASE International Joint Conference, Busan, South Korea, October 18-21, 2006.
- [11] Nef, Tobias, and Robert Riener. "ARMin - Design of a Novel Arm Rehabilitation Robot." Paper presented at the 9th International Conference on Rehabilitation Robotics, Chicago, Illinois, June 28-July 1, 2005.
- [12] R. Reiner et al., "Robot-aided neurorehabilitation of the upper extremities," *Medical & Biological Engineering & Computing* 43, no. 1 (2005): 2-10.
- [13] T. Nef et al., "ARMin - Exoskeleton for Arm Therapy in Stroke Patients." Paper presented at the 10th International Conference on Rehabilitation Robotics, Noordwijk, Netherlands, June 13-15, 2007.
- [14] Guizzo, Erico. "Dean Kamen's 'Luke Arm' Prosthesis Receives FDA Approval." Last modified May 13, 2014. Accessed January 6, 2015.  
<http://spectrum.ieee.org/automaton/biomedical/bionics/dean-kamen-luke-arm-prosthesis-receives-fda-approval>.

- [15] Resnik, Linda, and Matthew Borgia. "User ratings of prosthetic usability and satisfaction in VA study to optimize DEKA Arm." *Journal of Rehabilitation Research & Development* 51, no. 1 (2014): 15-26.
- [16] Siciliano, Bruno, et. al. *Robotics: Modelling, Planning and Control*. London: Springer, 2009.
- [17] Jazar, Reza. *Theory of Applied Robotics: Kinematics, Dynamics and Control*. New York: Springer, 2010.
- [18] Craig, John J. *Introduction to Robotics: Mechanics and Control*. 3rd ed. Upper Saddle River: Prentice Hall, 2004.
- [19] Khatib, Oussama. "Forward Kinematics 1." Accessed July 1, 2014.  
[http://cs.stanford.edu/groups/manips/images/stories/teaching/cs223a/handouts/kinematics-2\\_2014.pdf](http://cs.stanford.edu/groups/manips/images/stories/teaching/cs223a/handouts/kinematics-2_2014.pdf).
- [20] Niku, Saeed. *Introduction to Robotics: Analysis, Control, Applications*. Hoboken: John Wiley & Sons, Inc, 2011.
- [21] Milford, Michael and Gordon Wyeth. "Velocity, Force and the Jacobian." Last modified August 11, 2011. Accessed October 05, 2014.  
[http://www.youtube.com/watch?v=g\\_Nl4iPd1jI&feature=c4-overview-vl&list=PLB46C8B9857C32201](http://www.youtube.com/watch?v=g_Nl4iPd1jI&feature=c4-overview-vl&list=PLB46C8B9857C32201).
- [22] Allen, Peter. "CS 4733 Class Notes: Kinematic Singularities and Jacobians." Accessed January 7, 2015. <http://www1.cs.columbia.edu/allen/F14/NOTES/jacobians.pdf>.
- [23] Khatib, Oussama. "Jacobians: Explicit Form." Accessed July 26, 2014.  
<http://cs.stanford.edu/groups/manips/images/stories/teaching/cs223a/handouts/Jacobian2-2014.pdf>.
- [24] Khatib, Oussama. "Dynamics: Acceleration and Inertia." Accessed July 26, 2014.  
<http://cs.stanford.edu/groups/manips/images/stories/teaching/cs223a/handouts/dynamics1-2014.pdf>.
- [25] Richter, Hanz. "MCE/EEC 647/747 - Robot Dynamics and Control." Accessed October 16, 2014. [http://academic.csuohio.edu/richter\\_h/courses/mce647/mce647\\_10\\_hand.pdf](http://academic.csuohio.edu/richter_h/courses/mce647/mce647_10_hand.pdf).
- [26] Khatib, Oussama. "Dynamics: Explicit Form." Accessed July 26, 2014.  
<http://cs.stanford.edu/groups/manips/images/stories/teaching/cs223a/handouts/dynamics2-2014.pdf>.
- [27] Lewis, Frank. *Robot Manipulator Control Theory and Practice*. 2nd ed. New York: Marcel Dekker, 2004.
- [28] Trossen Robotics. "Trossen Robotics Dynamixel Guide." Accessed August 26, 2014.  
[http://www.ic0nstrux.com/download/documents/servos/dynamixel\\_guide.pdf](http://www.ic0nstrux.com/download/documents/servos/dynamixel_guide.pdf).
- [29] ROBOTIS. "MX-64T / MX-64R e-Manual." Accessed July 29, 2014.  
[http://support.robotis.com/en/product/dynamixel/mx\\_series/mx-64.htm](http://support.robotis.com/en/product/dynamixel/mx_series/mx-64.htm).

- [30] Halvorsen, Kare. "Testing the MX-64T." Last modified May 7, 2014. Accessed September 9, 2014. <http://forums.trossenrobotics.com/showthread.php?6922-Testing-the-MX-64T&p=64028#post64028>.
- [31] ROBOTIS. Overview of Communication. Accessed September 9, 2014. [http://support.robotis.com/en/product/dynamixel/dxl\\_communication.htm](http://support.robotis.com/en/product/dynamixel/dxl_communication.htm).
- [32] Emami, Shervin. "Controlling Dynamixel Motors through USB." Last modified October 27, 2009. Accessed September 9, 2014. <http://www.shervinemami.info/dynamixels.html>.
- [33] Cram, Jeffrey, and Glenn Kasman. "The Basics of Surface Electromyography." In *Cram's Introduction to Surface Electromyography*, edited by Eleanor Criswell, 1-171. Sudbury: Jones and Bartlett Publishers, 2011.
- [34] Delsys. "Trigno Wireless System User's Guide." Accessed March 30, 2015. <https://www.delsys.com/Attachments.pdf/Trigno%20Wireless%20System%20Users%20Guide%20%28MAN-012-2-3%29.pdf>.
- [35] Delsys. "Trigno Wireless - FAQ." Accessed March 30, 2015. <https://www.delsys.com/Attachments.pdf/Trigno%20FAQ%20%28DOC-208-1-0%29-web.pdf>.
- [36] Clauser, Charles, John McConville, and J.W. Young. *Weight, Volume, and Center of Mass of Segments of the Human Body*. Wright-Patterson Air Force Base, Ohio: Aerospace Medical Research Laboratory, 1969.
- [37] Rocon, E., A.F. Ruiz, R Raya, A. Schiele, and J.L. Pons. "Human-robot physical interaction." In *Wearable Robots: Biomechatronic Exoskeletons*, edited by J.L. Pons, 127-163. Madrid: John Wiley & Sons, Ltd, 2008.
- [38] Gopura, R.A.R.C. "A Study on Human Upper-Limb Muscles Activities." *International Journal of Bioelectromagnetism* 12, no. 2 (2010): 54-61.
- [39] Martini, Frederic, Michael Timmons, and Robert Tallitsch. *Human Anatomy*. 7th ed. Glenview: Pearson Education, Inc, 2012.
- [40] University of Michigan. "Movements of the Upper Limb." *Learning Modules - Medical Gross Anatomy*. Ann Arbor, 2002.
- [41] Cram, Jeffrey, Glenn Kasman, and Jonathan Holtz. "Atlas for Electrode Placement." In *Cram's Introduction to Surface Electromyography*, edited by Eleanor Criswell, 245-383. Sudbury: Jones and Bartlett Publishers, 2011.
- [42] Kelly, Rafael, Jesus Llamas, and Ricardo Campa. "A Measurement Procedure for Viscous and Coulomb Friction." *IEEE Transactions on Instrumentation and Measurement* 49, no. 4 (2000): 857-861.
- [43] Marton, Lorinc, and Bela Lantos. "Friction and backlash measurement and identification method for robotic arms." Paper presented at the 14th International Conference on Advanced Robotics, Munich, Germany, June 22-26, 2009.

- [44] Tarn, Tzyh-John, Antal Bejczy, Xiaoping Yun, and Zuofeng Li. "Effect of Motor Dynamics on Nonlinear Feedback Robot Arm Control." *IEEE Transactions on Robotics and Automation* 7, no. 1 (1991): 114-122.
- [45] ElDeeb, Yasser, and W.H. ElMaraghy. "Robust Adaptive Control of a Robotic Manipulator Including Motor Dynamics." *Journal of Robotic Systems* 15, no. 11 (1998): 661-669.
- [46] ROBOTIS. "Dynamixel Pro Key Specifications." Accessed June 10, 2015.  
[http://support.robotis.com/en/product/dynamixel\\_pro/dynamixelpro/hardware\\_specifications.htm](http://support.robotis.com/en/product/dynamixel_pro/dynamixelpro/hardware_specifications.htm).